NTNU

Norwegian University of
Science and Technology

Catalytic Conversion of Kerogen in Enhanced Oil Production from Shales

Tor Erik Sørensen

Chemical Engineering and Biotechnology
Submission date: June 2016
Supervisor: De Chen, IKP

Norwegian University of Science and Technology
Department of Chemical Engineering

NTNU

Norwegian University of Science and Technology

Faculty of Natural Science and Technology

Department of Chemical Engineering

Catalytic Conversion of Kerogen in Enhanced Oil Production from Shales

by

Tor Erik Sørensen

Supervisor for the project:

Professor De Chen

June 10, 2016

Abstract

Low oil prices, limited oil reserves and an anticipated increase in global energy demand calls for alternative sources of energy. Oil production from shales is an unconventional hydrocarbon source which is currently too expensive to utilize, and research in catalytic conversion may help reduce production cost. In this work, the catalytic effect of transition metal chloride salts on thermal upgrading of kerogen from Green River Formation oil shale has been investigated by TGA, SEM-EDS, XRF, EGA and pyrolysis-GC/MS. Catalytic performance has been observed as a reduction in the temperature for maximum conversion (T_{max}) by evolved gas analysis (EGA). Of the metal chlorides tested zinc ($ZnCl_2$) proved most effective, and by optimization based on reduction in T_{max} an optimal Zn^{2+} loading of 10 wt% on decarbonated kerogen was determined, with a resulting T_{max} reduction of 35 °C. Qualitative and quantitative analysis by Pyrolysis-GC/MS determined a catalytic cracking effect, reducing the amount of hydrocarbon chains longer than C_{22} and increasing C_{10}-C_{16}. Pyrolysis product composition was found to be 65.7 % olefinic. Liquefaction was performed to reduce the amount of olefins in the product. Three hydrogen-donating liquefaction solvents were tested (isopropanol, tetralin and decalin). Tetralin displayed the highest solid conversion of 85.55 % at 400 °C and contained 75.0 % paraffins in the liquid product. Soluble catalysts were found to be effective, improving solid conversion and significantly altering product composition. Insoluble, impregnated catalysts displayed a detrimental effect on solid conversion. Isopropanol with zinc catalyst displayed a solid conversion of 76.11 % at a low reaction temperature of 330 °C. Isopropanol with potassium hydroxide as a catalyst displayed a lower solid conversion of 60.76 %; however, produced a liquid product with the highest paraffin ratio of 79.4 %.

Keywords: Oil shale; Kerogen; Catalytic upgrading; Pyrolysis; Liquefaction

Sammendrag

Grunnet lave oljepriser, begrensede fossile ressurser og en forventet økning i globalt energibehov må alternative ressurser for energi undersøkes. Produksjon av olje fra oljeskifer er en ukonvensjonell kilde til hydrokarboner som med dagens teknologi ikke er økonomisk mulig å utføre, dermed kan forskning innen katalytisk konversjon delta på å redusere produksjonskostnader. I arbeidet utført for denne rapporten blir katalytisk effekt av overgangsmetall klorider på oppgradering av kerogen fra Green River Formation oljeskifer undersøkt ved bruk av TGA, SEM-EDS, XRF, EGA og pyrolysis-GC/MS. Den katalytiske prestasjonen blir observert som en reduksjon i temperaturen for maksimal konversjon (T_{max}) ved EGA. Sink klorid viste best ytelse for EGA, og optimalisering av mengde katalysator ble bestemt basert på T_{max} til 10 vektprosent på basis av decarbonated kerogen, som resulterte i en reduksjon av T_{max} på 35 °C. Kvalitativ og kvantitativ analyse ved pyrolysis-GC/MS beviste en katalytisk cracking effekt som reduserte mengden hydrokarboner lengre enn C_{22} og økte mengden av C_{10}-C_{16}. Produktet ved pyrolyse bestod av 65.7 % olefiner. Liquefaction ble utført for å redusere mengden olefiner i produktet. Tre forskjellige hydrogen-donerende løsemidler ble testet (isopropanol, tetralin og decalin). Tetralin viste best konversjon av fast stoff på 85.55 % ved 400 °C og produktet bestod av 75.0 % parafiner. Løselige katalysatorer ble bevist effektive, med økning i konversjon av fast stoff og større endringer av produktsammensetning. Uløselige, impregnerte katalysatorer hadde negativ påvirkning på konversjon av fast stoff. Isopropanol med sink katalysator viste en konversjon av fast stoff på 76.11 % ved en lav reaksjonstemperatur på 330 °C. Isopropanol med kaliumhydroksid som katalysator viste en lavere konversjon av fast stoff, men væsken som ble produsert hadde den høyeste mengden parafiner, 79.4 %.

Acknowledgement

Gratitude must be expressed to Prof. De Chen for supervising the project and maintaining great counseling throughout the project work, providing exceptional new pathways for the project to progress.

Thanks are also given to PhD student Isaac Yeboah for his continued guidance and assistance through the project work. His knowledge of the project was invaluable.

Appreciation is also given to Statoil for funding this project.

Finally, gratitude is expressed to the Department of Chemical Engineering for providing analytical facilities, and in particular Cristian Ledesma Rodrigues for assisting in the use of equipment and organizing equipment training.

Table of Contents

List of Figures

List of Tables

Abbreviations

Py-GC/MS	Pyrolysis-Gas Chromatography/Mass Spectrometer.
EGA	Evolved Gas Analysis
OM	Organic matter
TOC	Total organic carbon
ICP	Inductively Coupled Plasma
SEM	Scanning Electron Microscopy
EDS	Energy-Dispersive X-ray Spectroscopy
XRF	X-Ray Fluorescence
TGA/DSC	Thermal Gravimetric Analysis/Differential Scanning Calorimetry
FTIR	Fourier Transform Infrared Spectrometry
HI	Hydrogen Index
OI	Oxygen Index
DCM	Dichloromethane

1. Introduction

1.1 Motivation

Global energy consumption is expected to increase by 34 % between 2014 and 2035[1]. Most of the growth (96 %) is in non-OECD countries. The increase is largely based on population growth, and the rate of growth is lower than previously (from 2.3 % p.a. in 2000-2014 to 1.4 % p.a. between 2015 and 2035).

World energy consumption is still largely dependent on fossil fuels, with oil, natural gas and coal covering 86.3 % of global energy consumption in 2014[2]. While renewable energy sources are expected to increase, fossil fuels will still remain dominant in 2035 at 80 % share[1]. Among the fossil fuels, gas is the fastest growing at 1.8 % p.a. while oil retains a steady growth at 0.9 % p.a. The growth of coal is projected to have a sharp decline, down to 0.5 % p.a., causing it to be replaced by gas as the second-largest source of fuel.

To cover for the increasing energy demand, there is a need to consider alternative sources of oil production. One unconventional source of hydrocarbon production is oil shale. Kerogen in oil shale can be upgraded to crude oil, known as shale oil or tight oil. This oil can be further upgraded in existing refineries to produce fuel for transportation.

Upgrading of kerogen from oil shales has been estimated to require an oil price of $70-95 per barrel to support mining and surface retorting processes in 2005[3]. Low oil prices fluctuating between $30-60 per barrel for Brent crude oil in 2015-2016[4] calls for further research to reduce processing costs of oil shale. Of particular interest is the use of catalysts, as surface retorting applies high temperatures to upgrade kerogen. Reduction in energy costs as well as higher selectivity for desired products may improve profitability of kerogen upgrading processes.

Catalytic upgrading of kerogen is a largely unexplored area, and so fundamental research is of primary interest.

1.2 Objectives

The main objectives for this project work are to improve the knowledge of catalytic upgrading of kerogen and develop better techniques to analyze catalytic performance. The objectives can be summarized as:

- Analyze the catalytic performance of metal chlorides as catalysts for thermal upgrading of kerogen by use of EGA and pyrolysis-GC/MS

- Optimize catalyst loading by EGA
- Perform liquefaction processes to improve product quality, particularly focusing on paraffin-to-olefin ratio, varying conditions such as liquefaction solvent and temperature
- Analyze catalyst performance for liquefaction processes
- Use TGA, EGA and pyrolysis-GC/MS to analyze the performance of liquefaction processes
- Use SEM-EDS, TGA, EGA, XRF and pyrolysis-GC/MS to study the performance of catalysts in oil shale liquefaction processes

2. Literature Survey and Theory

This chapter contains a literature survey of what is known about oil shale and kerogen as well as theoretical background for the catalyst preparation and characterization techniques used in the project work. Theoretical background for liquefaction is also described.

2.1 Oil Shale

Oil shale is the term used to describe the unconventional hydrocarbon resource of sedimentary rock containing carbonaceous material bound within the mineral matrix[5]. The rock has low porosity and contains organic matter (OM) such as soluble bitumen and insoluble kerogen. The kerogen will convert to liquid and gaseous hydrocarbons at a temperature of 50-100 ºC, given geological time. This conversion is also related to a geothermal gradient, which is the temperature variance with regards to depth in subterranean formations. The geothermal gradient, while varied, is generally around 25 ºC/km[5].

2.1.1 Oil shale reserves

An estimated 2.8-3.3 trillion barrels of oil is recoverable from oil shale worldwide[6]. Compared to the amount of crude oil reserves at 1.2 trillion barrels, this is at least three times more. The deposits are found on all continents, with over 600 known deposits, and the largest oil shale reserves are found in USA, with an estimated 72 % of the world's reserves. Within the United States, the most concentrated deposits are found in the Green River Formation[7], which covers three states (Colorado, Utah and Wyoming).

An estimated 1 trillion barrels of oil can, based on current technology and economics, be recovered from oil shale resources[7]. The average yield is assumed greater than 25 gallons of oil per ton of oil shale. **Figure 1** displays the amount of recoverable oil from oil shale in the United States compared to oil reserves in other countries.

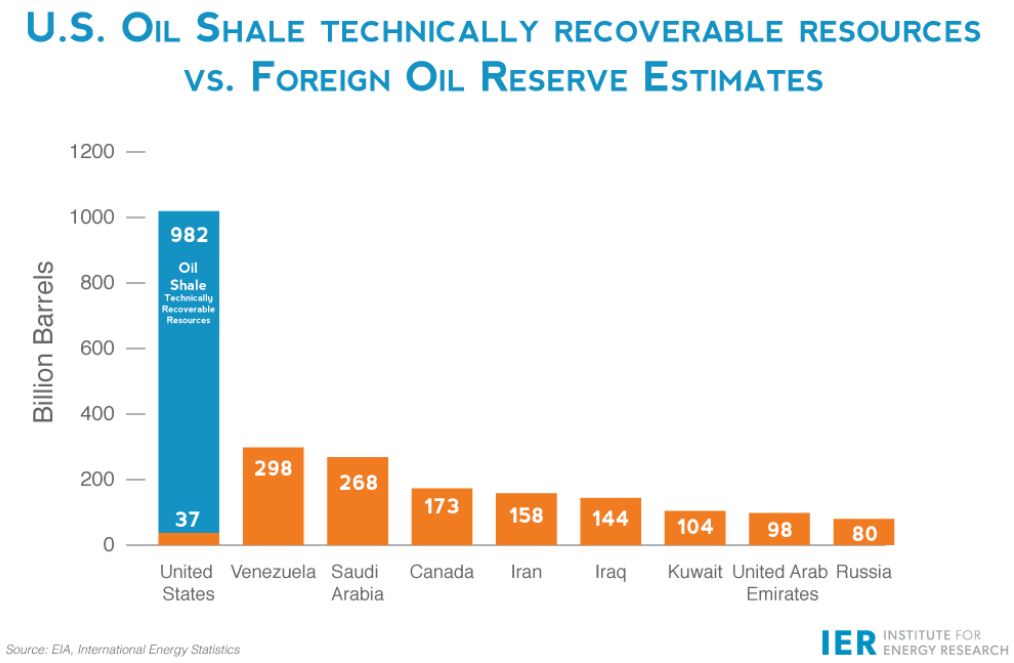

Figure 1 Comparison of technically recoverable oil shale resources in the United States and oil reserves in other countries[7].

2.1.2 Production of fuel from oil shale

Fuel can be produced from oil shale; however, production requires high temperature and has several environmental issues. Two main routes exist to produce crude oil from oil shale: in situ and ex situ.

An existing ex situ production process developed by Enefit Outotec Technology in Estonia is the Enefit280[8]. The process consists of oil shale mining, crushing the oil shale to increase surface area, drying the crushed sample, and finally heating to decompose the sample. In the Enefit280 process, several additional processes are applied to utilize all organic matter, for example by power production. **Figure 2** displays the process flow scheme for the complete Enefit280 process. Ex situ production is economically viable, as evidenced by Enefit producing 1700 thousand barrels of oil in 2014 compared to 1300 thousand in 2013.

Some drawbacks of ex situ production include need for land reclamation, water pollution and overburden rock disposal.

The alternative to ex situ retorting is in situ pyrolysis. This process involves drilling wells to heat the oil shale subsurface. As kerogen is decomposed and bitumen is liquefied, it can be pumped up to the surface by traditional oil recovery processes.

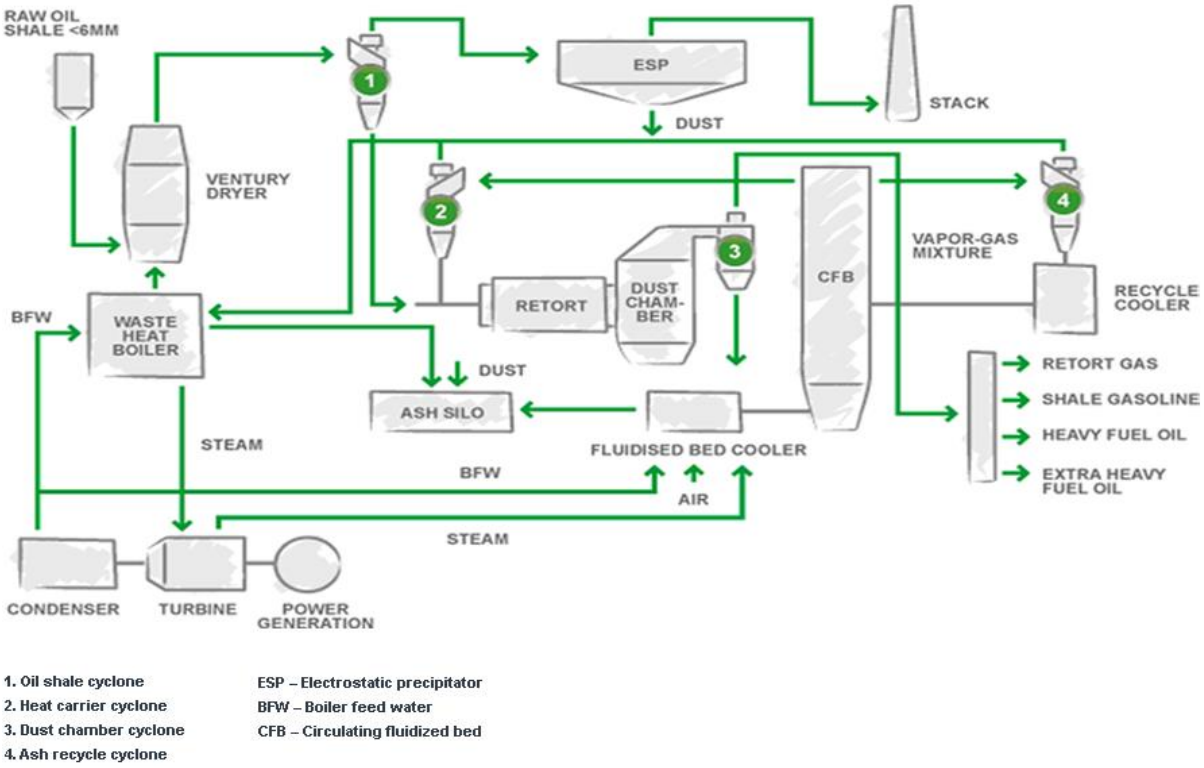

Figure 2 Process flow diagram of the Enefit280 oil shale retorting process[8].

Shell has developed an in situ conversion process (ICP) in which the shale rock is heated to approximately 350 ºC to achieve high liquid product yield while minimizing secondary reactions[5]. A freeze wall circulates ammonia to prevent groundwater from seeping into the extraction zone, while also keeping hydrocarbons and other products from contaminating the surrounding area. The main advantage of in situ production compared to ex situ retorting is the reduction of waste generated by mining. Disadvantages include the remaining uncollected liquid products that may leach into groundwater and the substantially longer production time (two to three years).

Modifications can be made to the in situ processes to improve performance. This can be done by mining, drilling and fracturing near the target deposit before heating, to create 20-25 % void space. Creating void space will increase surface area as well as improve the flow of gases and liquids through the rock formation.

Regardless of production method, use of oil shale has negative environmental impact. Significant amounts of sulfur and nitrogen in the oil shale can produce hydrogen sulfide, sulfur dioxide and ammonia[9]. Heavy metals can also remain in waste, which could leach into surface or groundwater. Water pollution is also of concern, due to the need for water in production. According to Enefit, their Enefit280 process only uses 1.06 barrels of water per barrel of oil

produced; however, processed water must be treated in water treatment plants which introduces an additional production cost.

2.2 Kerogen

Kerogen is the organic matter that is locked in the oil shale. It is a likely precursor to crude oil, and generates petroleum and natural gas when heated. Kerogen is also insoluble in organic solvents, and can thus not be extracted without thermal upgrading.

In order to better understand which products can be obtained by thermally upgrading kerogen, it is important to analyze how kerogen originates and matures. While arguments can be made that thermally upgrading kerogen at high temperatures may also change the chemistry of the reactions[5], laboratory experiments are unable to simulate kerogen maturation over geological time by other means.

2.2.1 Kerogen evolution and classification

Kerogen has been found to originate from two main producers: algae and terrestrial plants[10]. Petroleum source rock can therefore be classified as either aquatic (algae and bacteria) or terrestrial (lignin-related components). Kerogen matures over geological time, and its maturity is defined based on four stages; early diagenesis, diagenesis, catagenesis and metagenesis[10].

The first stage, early diagenesis, is the sedimentation step, and its occurrence is limited to a small depth range of a few meters. Nitrogen rich organic debris settles on surficial sediments followed by biodegradation processes or reaction of organic matter with their metabolic products. Nitrogen is lost by generation of amino acids and ammonium ions. If the environment is sufficiently oxic, partial oxidation may also occur, reducing total organic carbon (TOC) and increasing oxygen content.

The second stage, diagenesis, occurs over a larger depth range (>1000 m). A large amount of oxygen is lost during this stage, in form of mainly CO_2 and H_2O. The amount of humic and fulvic acids also decreases, and the end of diagenesis is defined as the point in time when the content of these acids is negligible. Kerogen transformation is driven by cracking reactions, which depend on temperature and time.

The third stage, catagenesis, occurs over a depth range of >2000 m. Loss of hydrogen and carbon identifies this as a stage of petroleum formation. With the consideration of hydrocarbon formation by $(CH_2)_n$ a larger amount of hydrogen is lost, resulting in a more aromatic kerogen. Oxygen content continues to decrease. This is partly due to further loss by CO or CO_2; however,

the heavier oils such as asphaltenes and resins produced earlier during catagenesis also contain hetero elements such as oxygen. The end of catagenesis is generally at a H/C ratio of 0.5, at which point all kerogen types are plotted in the same area of the Van Krevelen diagram.

In the final stage, metagenesis, aromatic CH_3 groups are eliminated as CH_4. Also occurring is a release of hetero elements such as CO_2, N_2 and H_2S. Methane is the only hydrocarbon generated, with a similar amount regardless of kerogen type: 50 mg/g C. This indicates that all kerogen types have a similar aliphatic to aromatic carbon ratio at this stage.

A Van Krevelen diagram is a plot of the atomic H/C ratio versus the atomic O/C ratio. The diagram is derived from elemental analysis, and kerogen has been classified as different types based on this diagram. **Table 1** sums up the general characteristics of these four types.

Table 1 Summary of the general characteristics of kerogen types[5].

Kerogen type	H/C ratio	O/C ratio	Origin	Composition	Product
I	>1.25	<0.15	Aquatic (Alginite)	Aliphatic, few cyclic/aromatic structures	Liquid HC
II	<1.25	0.03-0.18	Aquatic (Lipinite) Terrestrial (Exinite, Cutinite, Resinite, Lipinite)	Few cyclic/aromatic structures	Gas and oil
III	<1.0	0.03-0.3	Terrestrial (lacking in lipids, formed from cellulose)	Low hydrogen content, extensive ring and aromatic systems	Gas and coal
IV	<0.5	-	-	Decomposed OM (poly-cyclic aromatic HC)	No HC

A Van Krevelen diagram for the maturation of kerogen is displayed in **Figure 3**.

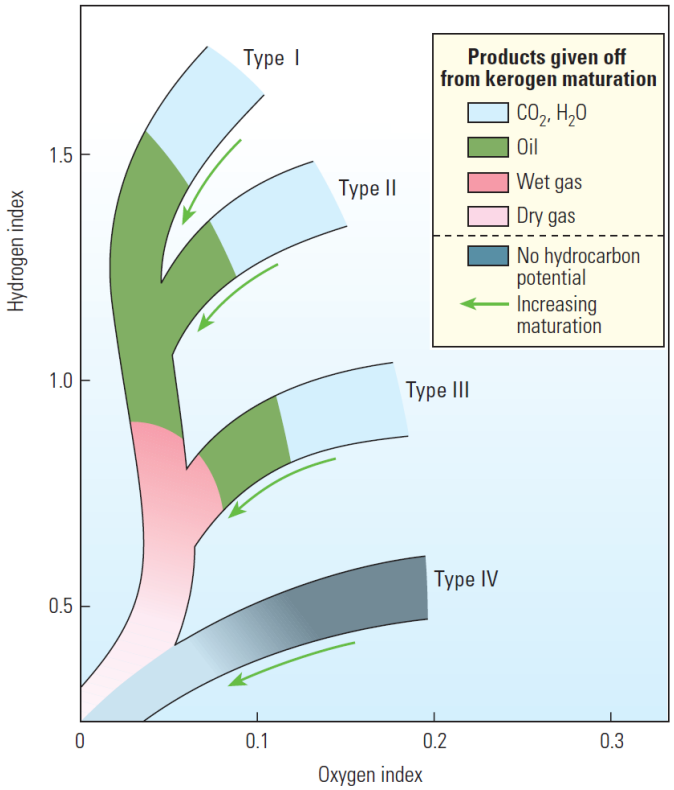

Figure 3 Van Krevelen diagram showing maturation paths for the four types of kerogen[11].

2.2.2 Green River Formation kerogen

Oil shale sample from the Green River Formation is used in the project work described in this report. Kerogen from this oil shale is a very complex macro organic compound containing both aliphatic and aromatic groups. An example model of kerogen molecules identified in this oil shale is presented in **Figure 4**.

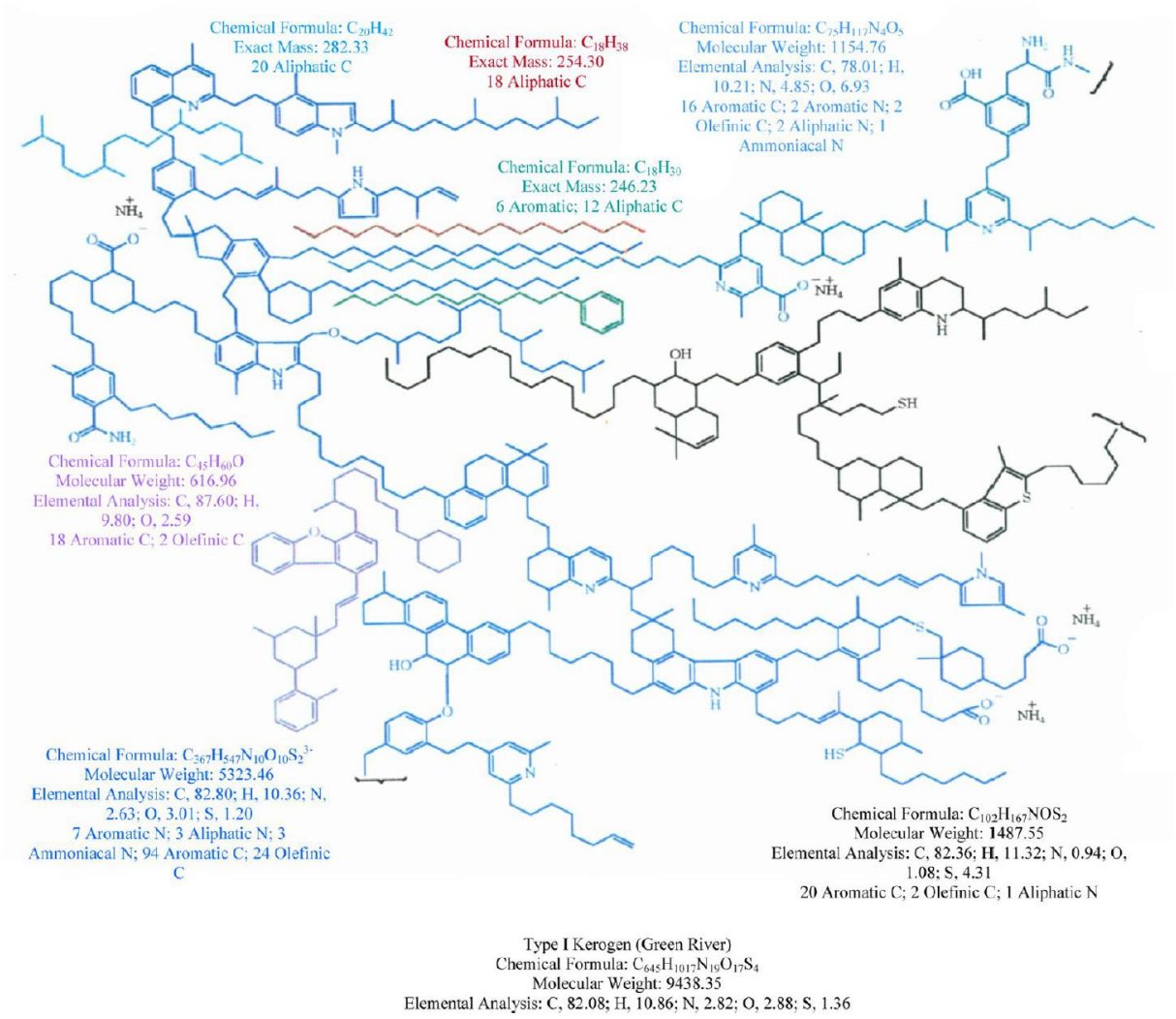

Figure 4 2D Siskin model of Green River oil shale[12].

2.2.3 Previous analysis of oil shale sample

Analysis of the oil shale sample used in this project work has been performed previously[13]. Performed analyses include TOC and Rock-Eval pyrolysis, elemental analysis and ICP, XRD and FTIR, N_2-physisorption as well as TGA/DSC. Results of the Rock-Eval pyrolysis are summarized in **Table 2**.

Table 2 Rock-Eval pyrolysis results of oil shale HC# (hydrocarbon)[13].

S1 (mg/g)	S2 (mg/g)	S3 (mg/g)	HI (mgHC#/g TOC)	OI (mg/g TOC)	T_{max} (°C)	TOC (%)
5.43	152.84	2.06	621	8	433	24.6

A TOC value of 24.6 % indicates good potential for petroleum generation. The S1 peak represents 0.54 wt% of bitumen and S2 indicates 15.3 wt% of kerogen at the maximum

temperature of 433 ºC. Evaluation of hydrogen index (HI), oxygen index (OI) and maximum temperature (T_{max}) leads to the classification of this oil shale as a type I kerogen sample.

Results from ICP and elemental analysis are summarized in **Table 3**.

Table 3 Elemental composition by weight percentage in raw oil shale[13].

Method	Mass percentage (wt %)					
ICP	Al	Ca	Mg	Fe	K	Na
	2.0	9.7	4.1	1.0	0.88	0.76
Elemental analysis*	C	H	O	N	S	
	20.8	2.7	2.4	0.7	0.5	

*Only the evolved gases were analyzed.

Of note from the elemental analysis is the low content of nitrogen and sulfur contained in the oil shale sample.

Surface area of the oil shale was determined by N_2-physisorption, and a low value of 3.4 m^2/g was obtained, with pore diameter concentrated around 2-10 nm.

2.2.4 Catalytic upgrading of kerogen

Analysis has found that using metal chlorides as catalysts on kerogen is thermally stable for kerogen decomposition[13]. Chloride was excluded from having any catalytic effect, and metal oxides and acids were tested, but found to have no promotive effect as catalysts.

2.3 Preparation of catalyst

Catalysts for the experiments performed in this project have been prepared by incipient wetness impregnation. The process of incipient wetness impregnation, or capillary impregnation, consists of two main steps. The first step involves absorbing a liquid containing the catalytically active components onto a solid support, and the second step is drying the catalyst to remove solvent.

A simple impregnation process[14] involves contacting a dried support of a specific pore volume with the same volume of solution containing the precursor of the active phase. Capillary forces will pull the solution into the pores, and assuming proper wetting no solution will remain outside of the pore space. **Figure 5** shows the main flow patterns found during incipient wetness impregnation.

Due to the air occupying the support pores prior to the impregnation process, pores with small radii have capillary pressures higher than the pressure of the entrapped air. This compressed air will generally dissolve or escape through larger pores; however, sometimes the support does not have sufficient mechanical strength to withstand the forces, and the catalyst grains may burst. If this is an issue, impregnation may be performed under vacuum, or with the addition of a surfactant. Another alternative is wet impregnation, which consists of fully submerging the support, leading to a diffusion-based impregnation. This is however significantly slower and less efficient with regard to precursor consumption and deposition. The process of incipient wetness impregnation is exothermic, due to the replacement of a solid/gas interface by a solid/liquid interface[15].

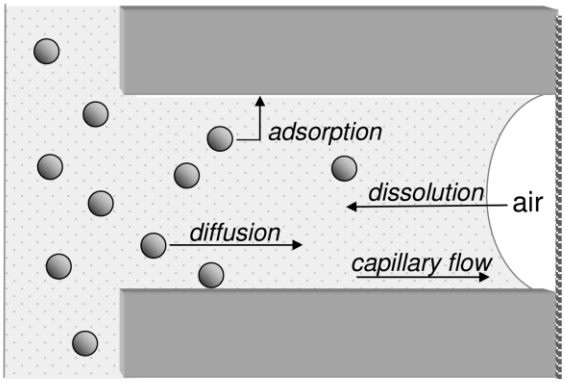

Figure 5 Graphical representation of incipient wetness impregnation[14].

After impregnation, the system is dried. This is done by heating in an oven up to the boiling point of the solvent. The process can be static or under gas flow. Temperature and heating rate during the drying process will lead to different precursor distribution within the support pores.

2.4 Characterization

The catalyst characterization performed in this project work includes evolved gas analysis (EGA) as well as flash pyrolysis. Products from both methods are analyzed by on-line gas chromatography (GC) and mass spectrometry (MS).

2.4.1 Evolved gas analysis (EGA)

Evolved gas analysis can be used to determine the amount of volatile product as well as the nature of the product formed during thermal degradation of the sample[16]. The method consists of dropping a sample into a furnace at low temperatures, followed by a programmed temperature increase up to a set temperature, such as 600-800 ^{o}C. Compounds in the sample

will evolve as the temperature increases, and detecting the gas as it exits the furnace results in a plot comparing detector response versus furnace temperature.

EGA can be used in combination with a gas chromatograph and mass spectrometer to obtain ion chromatograms. These can in turn be used to identify the thermal zone where compounds of interest evolve. The GC chromatogram can also be used to identify a suitable temperature for pyrolysis analysis.

2.4.2 Pyrolysis

Thermochemical decomposition of organic matter in the absence of oxidizing agents is known as pyrolysis. Usual temperature for pyrolysis is 300-650 ºC[17]. The sample is rapidly heated to the pyrolysis temperature, and held at that temperature for a time. The products received are gases, solid char and ash, and liquid product. Overall product composition depends on factors including heating rate and final temperature. Pyrolysis is classified based on the heating rate, which is the time required to heat the sample to the required temperature, where faster pyrolysis produces less char and ash, and more gases. Flash pyrolysis is used in this project, which requires the products from the pyrolyzer to have a short residence time of 30-1500 ms[17].

Using on-line gas chromatography as well as mass spectrometry, the products from pyrolysis can be analyzed. In the GC column products are separated by retention, and the exiting products are identified both in abundance and ion fragmentation by MS.

2.4.4 Scanning electron microscopy (SEM)

Scanning electron microscopy creates high resolution images of a sample by using an electron beam (“gun”). Images produced by a SEM show the surface topography of the sample as well as variations in the chemical composition. This is done by the electron gun which can be either thermionic or fitted with a single-crystal tungsten tip[18] along with several detectors for different signal types. A typical SEM schematic is shown in **Figure 6**. The electron gun uses a large energy range, between 0.1 keV and 30 keV, and the significant kinetic energy carried by the electrons creates various signals when interacting with the sample. Signals produced include secondary electrons, backscattered electrons, diffracted backscattered electrons, photons (X-rays), visible light and heat. Secondary electrons and backscattered electrons are usually detected to create images of the sample, where secondary electrons show the morphology and topography, while backscattered electrons show contrasts in composition.

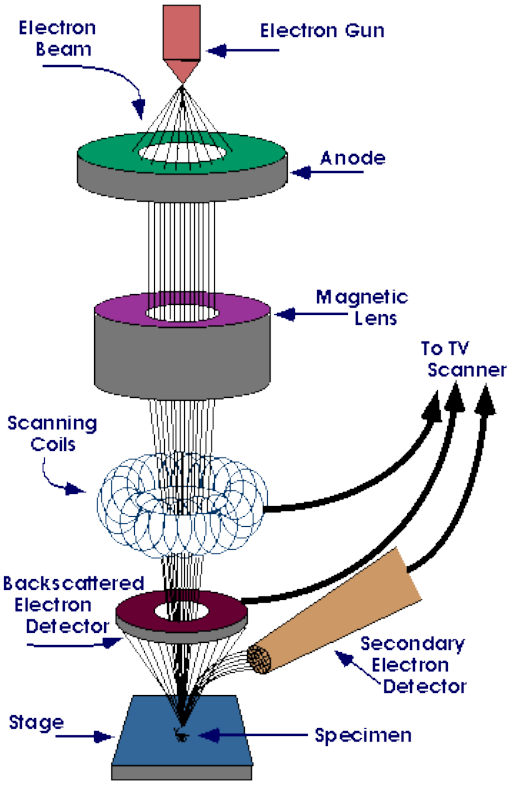

Figure 6 Schematic showing the components of a scanning electron microscope (SEM)[19].

It is also possible to couple SEM with energy-dispersive X-ray spectroscopy (EDS) to produce qualitative and semi-quantitative compound analysis. X-rays are produced as inner-shell electrons and are displaced to the outer shells by the electron beam. As outer-shell electrons fall back into the inner shell, an X-ray photon is emitted. By detecting the energy of the photon, which is characteristic of the atom that released it, elemental analysis can be performed for the sample. The resulting analysis can show elemental distribution on the sample as well as a quantitative measurement for all detected elements.

2.4.5 Thermogravimetric analysis (TGA)

Thermogravimetric analysis involves weighing a sample as it undergoes programmed temperature variations. The measurements can be used to study sample characteristics such as volatile content, thermal stability, sample degradation or decomposition, activation energy and effect of catalysts[20]. Atmosphere in the instrument can be altered, primarily using inert atmosphere or air. Other atmospheres can also be used depending on the desired reaction, such as hydrogen, hydrogen sulfide and carbon dioxide[21]. A TGA instrument is generally comprised of a balance, a furnace and a recorder.

Other instruments are also often coupled with a TGA, including differential scanning calorimetry (DSC) and mass spectrometry (MS). DSC is used to analyze the required amount

of heat to increase the temperature of the sample, where the difference recorded is compared to a reference with known heat capacity[22]. Resulting analysis may be used to differentiate between endothermic or exothermic events. By using an MS, the gases from sample decomposition or oxidation can also be recorded as a function of temperature.

2.4.6 X-Ray Fluorescence

X-ray fluorescence (XRF) utilizes photons of sufficient energy to eject electrons from their atomic orbital. Based on Planck's Law ($\lambda = \frac{h\nu}{E}$), the energy of the photon (hν) needs to be larger than the energy binding the electron to the nucleus of the atom[23]. When an inner orbital electron is ejected from the atom, an electron from the higher energy orbitals will drop to the inner orbital. As this occurs a photon may be emitted from the atom which has a specific energy that is always equal to the energy difference between the two orbitals. This characteristic x-radiation can be attributed to one specific element[24]. The first element in the periodic table to be detectable by this method is sodium.

Detection of the fluorescent X-rays can be done with a variation of detectors, including proportional counters, gas detectors, scintillation detectors, Ge(Li), Si(Li), or Silicon Drift Detectors to name some. Quantification can be performed using several different methods, such as empirical and theoretical influence coefficients, classical fundamental parameters, or Monte Carlo[24]. For the purposes of this report, only the empirical influence coefficients (EIC) method is of interest, as the analysis is focused on bulk quantification. This quantification method uses simple mathematics to describe a relationship between the photon count detected and the concentration of the element in the sample.

2.5 Liquefaction

Liquefaction is a term with different possible meanings. For the purpose of this report, it is used for a process with similarities to coal or biomass liquefaction; liquefaction is the process of producing liquids with higher content of hydrogen (particularly compared to pyrolysis products). Several methods exist for liquefaction of coal, such as pyrolysis, indirect liquefaction and direct liquefaction. Pyrolysis involves high temperatures in a nonoxidizing atmosphere, producing gases, liquid and char. For indirect liquefaction oxygen and steam is employed to produce synthesis gas which can be converted to liquid products in processes such as Fischer-Tropsch, methanol synthesis and dimethylether production. Of primary interest for this report; however, is direct liquefaction.

Direct liquefaction (of coal) involves reacting the coal in a hydrogen-donor solvent at high temperatures and pressures, often using gaseous hydrogen[25]. The process can be performed either with or without catalysts, with conditions determining the resulting product.

2.5.1 Liquefaction mechanism

Describing coal liquefaction mechanisms can be difficult due to the heterogeneous structure of the sample, as is also the case for oil shale, thus mechanisms focus on the concept of an average structure. Without added catalysts liquefaction is considered a pyrolytic process, where cyclical compounds are ruptured at 400-450 °C. Functional groups are cleaved, creating free radicals which in turn can be stabilized by hydrogen atoms, dispersing low molecular mass fragments into the solvent. If hydrogen donation does not occur, larger molecular mass products can combine to eventually produce char or coke. Using a solvent-assisted process, cleavage of strong bonds can occur by radical hydrogen transfer, as depicted in **Figure 7**. The use of a solvent can produce radicals that support in H-atom transfer, leading to scission of strong bonds[25].

2.5.2 Coal liquefaction products

Liquefaction products will always contain a distribution of light gases, distillate liquids and non-distillable liquids. The liquids are generally separated based on their solubility into other organic compounds, such as pentane and benzene. Processing also has an effect on the products, such as long hydrotreatment increasing the aromaticity of asphaltenes at the cost of polar functional groups and molecular mass.

2.5.3 Liquefaction solvents

The choice of solvent is of great importance in liquefaction, governing processes such as transport of product and heat, and transferring hydrogen. It is also of interest to use a solvent that is produced during the liquefaction process, so that it can be recycled and sustained by the process itself. Liquefaction solvents with a partially hydrogenated aromatic structure are the most effective hydrogen donors[25]. As an example, decahydronaphthalene (decalin) with two fully saturated aromatic rings is less efficient than 1,2,3,4-tetrahydronaphthalene (tetralin) with one saturated and one unsaturated aromatic ring. Even more active than tetralin is 9,10-dihydrophenantherene with two unsaturated and one saturated aromatic ring. Stability of the solvent at the given process conditions is also of importance; solvents may undergo isomerization, cracking and polymerization.

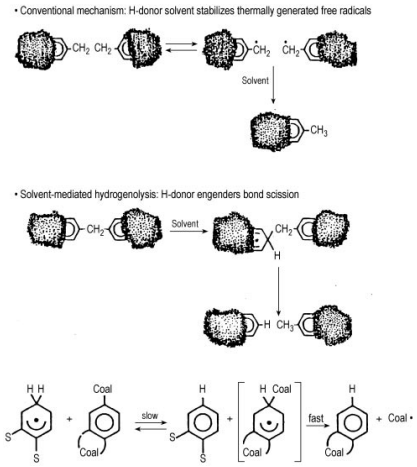

Figure 7 Comparison between a conventional coal liquefaction mechanism and a solvent-mediated hydrogenolysis mechanism[25].

2.5.4 Catalysis in liquefaction

Catalysts can be used in a liquefaction process, either dispersed in a slurry or supported in fixed or ebullated bed reactors[25]. These catalysts may promote desired liquefaction products, such as iron catalyst in tetralin activating molecular hydrogen to transfer to coal fragment radicals. Molybdenum-based catalysts may be used for the removal of heteroatoms through reaction such as hydrodesulfurization and hydrodenitrogenation. Using sulfided Ni-Mo or Co-Mo catalysts can remove oxygen, sulfur and nitrogen in aromatic rings. The choice of dispersed versus supported catalysts depends on which part of the process is being catalyzed.

Supported catalysts have the advantage of high dispersion and low metal concentrations; however, small pore sizes will not allow large molecules to be converted, making supported catalysts more suitable for liquid processing. Dispersed catalysts have the disadvantage of difficult or expensive recovery after use, making disposable catalysts more attractive for this application. By utilizing the exterior surface of the particles as active sites there is no porosity, and this type of catalysis is more efficient at promoting solid conversion. Catalysts such as molybdenum, iron, tungsten, cobalt, nickel, tin and zinc have been tested, and pyrite and iron have shown good potential[25]. Higher concentrations of cheaper iron catalysts are equally active as low concentration of expensive catalysts such as molybdenum, making them more attractive.

There are several ways to introduce disposable catalysts to a process, including physically mixing small particles into a slurry, precipitating precursors from aqueous solutions, adding catalysts in their oil-soluble forms, or by impregnating the feed solid with water-soluble compounds[25]. The use of soluble precursors has shown high activities; however, some results indicate that the soluble precursors form crystallites or agglomerates during liquefaction,

limiting the high dispersion. Using incipient wetness impregnation gives high dispersion of the catalyst precursor on the solid, and for coal (and oil shale) the mineral matrix may help maintain the high dispersion.

2.5.5 Review of similar liquefaction experiments

Liquefaction of oil shale shares several similarities with coal liquefaction, both having low organic carbon content contained in a mineral matrix. Liquefaction of oil shale using tetralin as a solvent and several catalysts in a batch autoclave has been reported[26]. The report states that tetralin as a hydrogen-donor solvent is stable for long reaction times at temperatures below 450 °C, decomposing primarily to naphthalene and 1-methyl-indan, ethyl benzene and toluene. Pajak and Socha[27] performed studies showing that high-rank coals with low oxygen content were less reactive in tetralin and not significantly affected by pressure, unlike low-rank coals with high oxygen content where increased pressure improved performance. Robinson and Cummins[28] showed that conversion is quite low below 300 °C (less than 30 %), and at 350 °C, longer reaction times increased solid conversion significantly, from 75.8 % to 94.5 % between 24 and 144 hours.

Johannes et al.[26] performed experiments on an Estonian carbonaceous kukersite oil shale, using Co, Mo and Ni supported catalysts as well as powdered pyrite crystals (FeS_2). Using a ratio of tetralin to OM of 1:1 and catalyst to OM of 0.1:1, their results are summarized as; tetralin as a solvent increases maximum yield of total extract as well as reducing the OM remaining in solid residue. While the best catalyst was concluded to be the commercial catalyst DN 3100 Th without activation, pyrite showed promising results as well.

Vasilakos and Augsten[29] performed liquefaction experiments on α-cellulose, comparing both tetralin and isopropanol as hydrogen-donor solvents. Effect of Raney nickel, palladium and potassium hydroxide as catalyst, as well as hydrogen pressure, was also analyzed. A ratio of solvent-to-OM of 1:0.1 volume-to-weight was used. Isopropanol is limited to a reaction temperature of 330 °C due to the thermal breakdown at higher temperatures; however, the solvent is supercritical at this temperature (T_c = 235 °C), creating its own pressure, thus the reaction can be run without initial pressurization of the reactor.

While tetralin could use a reaction temperature of 400 °C, resulting in a solid conversion of 98.8 %[29], isopropanol at 330 °C only had a solid conversion of 84.7 %. This is however significantly better than tetralin at 320 °C, with a solid conversion of 72.5 %. Use of palladium catalyst in tetralin improved solid conversion at 360 °C to 100 %, and 320 °C to 97.3 %.

Similarly, addition of Raney nickel to isopropanol improved solid conversion at 330 °C to 92.8 %. Using potassium hydroxide as a catalyst for isopropanol appeared to lower solid conversion, to 78.9 % at 330 °C.

Addition of an initial hydrogen pressure was also tested, where tetralin with palladium catalyst at 320 °C received different initial hydrogen pressures, from 0-500 psig. While solid conversion was lowered by 0.7 %, at 500 psig the oil yield was improved from 53.5 % to 62.8 %. Addition of hydrogen to isopropanol with potassium hydroxide improved solid conversion at 300 °C, from 60.7 % with 0 psig hydrogen pressure, to 84.4 % with 400 psig hydrogen pressure. Oil yield was also significantly improved, from 51.5 % to 77.3 %, respectively.

Ross and Blessing performed detailed analysis on the use of alcohols as hydrogen-donor solvents in coal conversion. Their analysis included isopropyl alcohol[30] and methanol[31], also introducing potassium hydroxide as catalyst. They found that isopropyl alcohol can act as a hydrogen donor, being promoted by the presence of a base, such as potassium isopropoxide or potassium hydroxide. As a result of hydrogen donation, acetone is formed from the alcohol in quantities that relate to the amount of hydrogen transferred.

3. Material and Methods

This chapter describes the experimental methods used. Pretreated sample was used, and the pretreatment is described. Detailed information of catalyst preparation and characterization is also presented.

3.1 Pretreatment

Oil shale sample from the Green River Formation is used in this project work. The sample was supplied by Statoil. Using a laboratory disk milling machine from Fritsch, the sample is crushed and milled to fine particle sizes and sieved to less than 53 μm. The milled sample was subsequently subjected to Soxhlet extraction. This extraction removes the bitumen from the sample by use of dichloromethane (DCM, CH_2Cl_2). DCM is used at a ratio of 150 mL to extract 6.5 grams of oil shale, and the extraction is performed at 60 ^oC for 18 hours.

After extraction, insoluble carbonates and dolomite are removed. Removal is done by use of 6 M hydrochloric acid (HCl) mixed with an equal volume of water (75 mL). A sample of approximately 8 grams is used, and the reaction continues for 24 hours. Product is subsequently washed repeatedly by hot distilled water until a pH of 7 is obtained, followed by drying in a vacuum oven at 100 ^oC. The resulting product is denoted in the following report as decarbonated kerogen; oil shale free from bitumen, calcite and dolomite.

3.2 TGA of original and decarbonated oil shale

TGA was performed using a Netzsch STA 449 C Jupiter. To identify the amount of organic matter in the oil shale, TGA was performed on original oil shale as well as decarbonated kerogen. Synthetic air atmosphere (20 % O_2 and 80 % N_2) was used with 75 mL/min flow rate and protective argon gas flow of 25 mL/min. A sample weight of ~15 mg was used. Organic matter is identified as the amount of weight loss attributable to loss of organic carbon, and as such a Netzsch QMS 403C Aëolos MS is connected to the gas outlet and set to identify H_2O and CO_2 (m/z 18 and 44). A starting temperature of 35 °C was used, with a 10 °C/min heating rate up to a maximum temperature of 800 °C.

3.3 Preparation of catalyst

Catalyst was prepared with the goal of optimizing active material, using different transition metal chloride salts as the precursors. These catalysts were cobalt, chromium, copper, iron, manganese, nickel, vanadium and zinc. The precursor is directly impregnated onto

decarbonated kerogen using incipient wetness impregnation. Sample pore volume was determined by wetting a known mass of kerogen to be roughly 1 mL water per gram kerogen.

The dissolved precursor was mixed with the decarbonated kerogen and the resulting solution was then stirred continuously for more than 10 minutes to ensure complete wetting as well as homogeneous precursor distribution, before being left overnight to dry at room temperature. The dried sample was subsequently left in a vacuum oven at 80 °C overnight to ensure complete dryness while avoiding potential oxidation of the kerogen by oxygen. Method for calculating the theoretical catalyst loading can be seen in Appendix **A) Calculation of catalyst loading**.

3.4 Catalyst characterization and optimization

The prepared catalysts were screened by an EGA/PY-3030D pyrolyzer, with on-line GC/MS analysis by an Agilent 7820A GC and an Agilent 5977E MSD. Ion fragmentation pattern is analyzed using the NIST library. A schematic of the pyrolyzer is displayed in **Figure 8**.

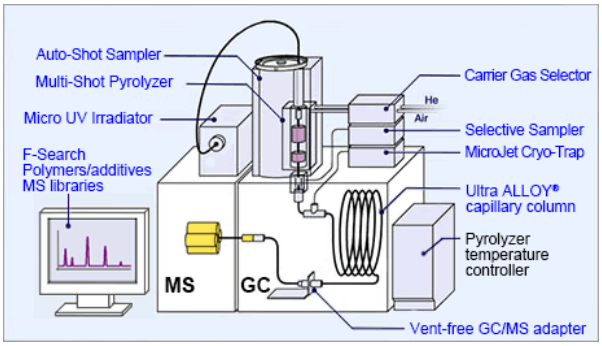

Figure 8 Schematic of the EGA/PY-3030D Multi-Shot Pyrolyzer used to perform pyrolysis and EGA analysis[16].

3.4.1 Evolved gas analysis

The evolved gas analysis was performed using a starting temperature of 100 ºC, a final temperature of 700 ºC and a heating rate of 10 ºC/min. For the primary comparison run shown in **4.2 Catalytic thermal upgrading of kerogen**, a heating rate of 25 °C/min was used instead. Sample used was weighed to ca. 0.5 mg. The GC inlet temperature was 300 ºC and oven temperature was constant at 300 ºC. The column used in the GC oven was the Frontier Lab Ultra Alloy EGA Tube DTM-2.5N, and a helium flow of 1 mL/min was supplied. The MS scan range was 20-550 (m/z) at a scan speed of 2.8 (scans/s).

3.4.2 Pyrolysis

Pyrolysis was performed using a pyrolyzer temperature determined by EGA. For pyrolysis performed to analyze catalyst performance on impregnated kerogen samples, a temperature of 550 ^{o}C was used. The GC inlet temperature was 300 ^{o}C, and oven temperature settings were: 40 ^{o}C for 2 minutes, followed by a 10 ^{o}C/min ramping rate up to a maximum temperature of 340 ^{o}C, with 20 minutes hold time. The column used in the GC oven was the Frontier Lab Ultra Alloy Capillary Column 5-30M-1.0F, and a helium flow of 1 mL/min was supplied. The MS scan range was 29-600 (m/z) at a scan speed of 4.87 (scans/s).

3.4.3 Scanning electron microscopy

Scanning electron microscopy (SEM-EDS) was performed on a Hitachi TM3000. Imaging was performed with variable beam conditions, using 5 kV to analyze surface details, 15 kV to achieve the best resolution and "Analysis" to perform elemental analysis. Two different levels of magnification were utilized, using 80x and 300x. Decarbonated kerogen sample impregnated with Zn^{2+} and Co^{2+} catalyst was analyzed to determine dispersion as well as particle size.

3.5 Liquefaction

Due to the high olefin-to-paraffin ratio achieved in regular pyrolysis experiments, upgrading of the products is necessary. Liquefaction may improve the quality of the product received by simply changing reaction conditions. The catalysts chosen for liquefaction experiments were Zn^{2+} based on good results during pyrolysis experiments, Co^{2+} due to decent performance in the temperature range used based on EGA, as well as good performance in other liquefaction experiments, and KOH for isopropanol experiments based on the results from Ross and Blessing[30].

Liquefaction was performed using a simple Swagelok reactor, with a total volume of approximately 1.7 mL, seen in **Figure 9**. Decarbonated kerogen, with or without impregnated catalyst (10 wt% Zn^{2+} or Co^{2+}), was loaded into the reactor using 200 mg of decarbonated kerogen (containing approximately 50 % organic matter). Using a solvent-to-OM ratio of 1:0.1, 1 mL of solvent (2-propanol, tetralin or decalin) was added to the kerogen before closing the reactor. For the isopropanol experiments, a solution of isopropanol with KOH of 85 % purity was used, containing 60 % of the added weight of kerogen. This value was selected due to it being the highest soluble amount of KOH in the amount of isopropanol used in the experiments, with the assumption that higher concentration (between ratios of 0.1 and 1 KOH-to-kerogen

ratio) yields better results[30]. A final experiment was also performed similarly without any catalyst or solvent to compare the performance.

Figure 9 Swagelok reactors used for liquefaction experiments.

All experiments were heated in an oven at three different temperatures. For isopropanol, these temperatures were 270, 300 and 330 °C. For tetralin and decalin, temperatures were 300, 350 and 400 °C. The oven used a heating rate of 3 °C/min and remained at max temperature for 60 minutes, before being cooled down over the course of 2 hours and left at room temperature overnight.

Before extracting the product, the reactors were weighed, evacuated and weighed again to measure gas production. Subsequently, extraction was performed using DCM to extract all liquids and solids from the reactor. The extracted sample was centrifuged at 11000 RPM for 30 minutes before decanting the liquid. Extraction and centrifuge was performed a second time to ensure near-complete extraction from the solid residue. Extracted liquid and solid was left to dry at room temperature overnight, and stored for further analysis.

3.6 Further analysis of liquefaction product

Further analysis of the products obtained from the liquefaction experiments was performed for both the solid residue and the liquid product.

Solid residue was analyzed with SEM-EDS, using 5 kV to analyze surface details, 15 kV to achieve the best resolution and “Analysis” to perform elemental analysis. The analysis was performed for solid residue from Zn^{2+} catalyzed experiments with tetralin as well as isopropanol.

Further analysis was performed on the solid residue by means of TGA. Analysis was performed with identical conditions as described in **3.2 TGA of original and decarbonated oil shale**. The purpose of the analysis was to get an accurate measurement for solid conversion by detecting remaining organic matter after reaction.

X-ray fluorescence was performed on the liquid product to analyze the amount of catalyst (Zn^{2+}, Co^{2+} and Cl^{2-}) that is transferred to the liquid phase during reaction and extraction. XRF was performed using a Rigaku Supermini200 with helium atmosphere. The liquid product was dissolved in toluene and isopropanol and transferred to liquid holders for the XRF machine. XRF is unable to detect hydrocarbons, and as such calcium nitrate was added in a known amount to compare to the weight of the catalyst.

For analysis of product from the liquefaction experiments, pyrolysis was performed, similar to what was described in **3.4.2 Pyrolysis**. A temperature of 440 ^{o}C was used for the propanol experiments, while 460 ^{o}C was used for tetralin and decalin. The temperature was selected to obtain the largest quantity of product to analyze, while simultaneously limiting pyrolysis cracking reactions. GC temperature programming, flow and MS settings remained unchanged from 3.4.2.

4. Results and Discussion

This chapter summarizes and discusses the results obtained during the experiments performed throughout the project work. Organic matter content in a Green River Formation oil shale was determined. Performance of several metal chloride catalysts was analyzed by EGA and the effect of Zn^{2+} catalyst on pyrolysis of kerogen has been investigated and catalyst loading has been optimized. Pyrolysis-GC/MS has been used to analyze product composition, with particular weight on paraffin-to-olefin ratio. SEM-EDS was used to characterize decarbonated kerogen with catalyst. Liquefaction reactions were performed to analyze the effect of different solvents and catalysts on the liquid product. TGA was used to analyze the solid conversion, while XRF and pyrolysis-GC/MS was used to analyze the liquid product.

4.1 Organic material content of the oil shale sample

TGA was performed to analyze the amount of organic material available in the oil shale sample used for all subsequent experiments. The profile received by TGA of this original oil shale is shown in **Figure 10**.

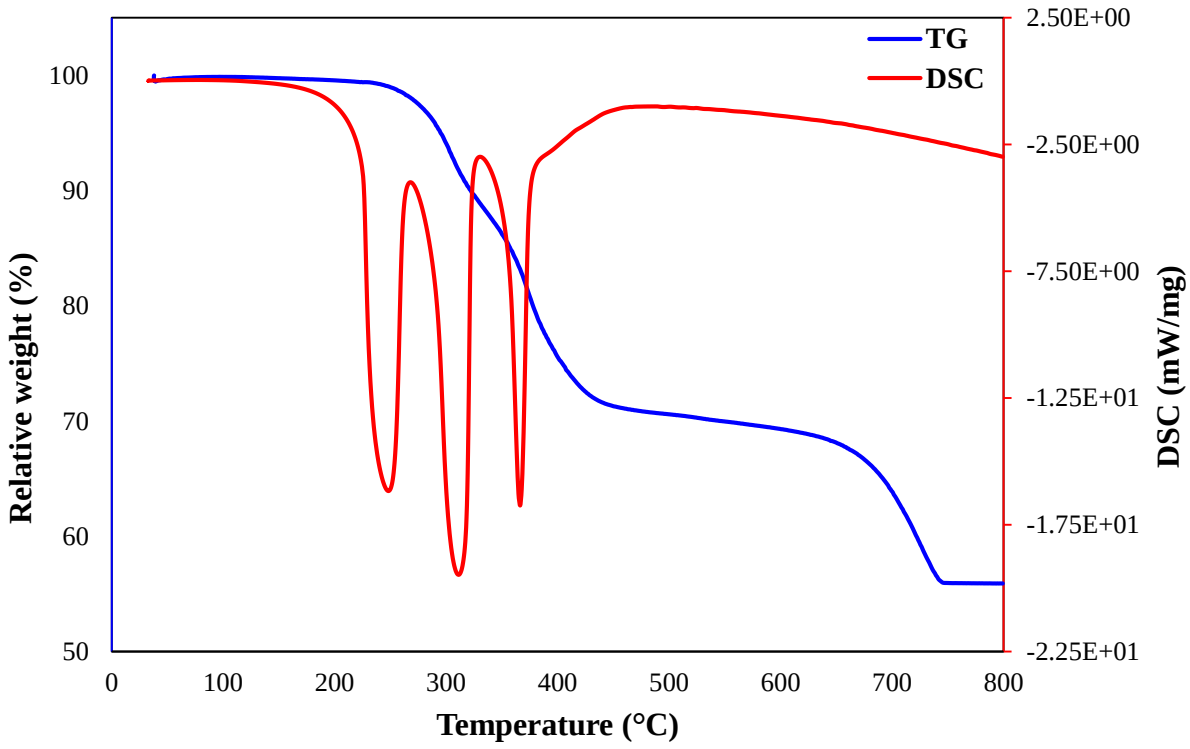

Figure 10 TGA-DSC profile of untreated original oil shale.

Two major weight losses can be observed from the TGA profile. The primary weight loss between 200-500 °C is caused by combustion, supported by the exothermic DSC-profile as well as the MS detecting both H_2O and CO_2 in this temperature range, shown in **Figure 11**. The

secondary weight loss is decomposition, largely due to dolomite and calcite in the oil shale, supported by the lack of change in the DSC profile as well as the MS detecting only CO_2 in this temperature range.

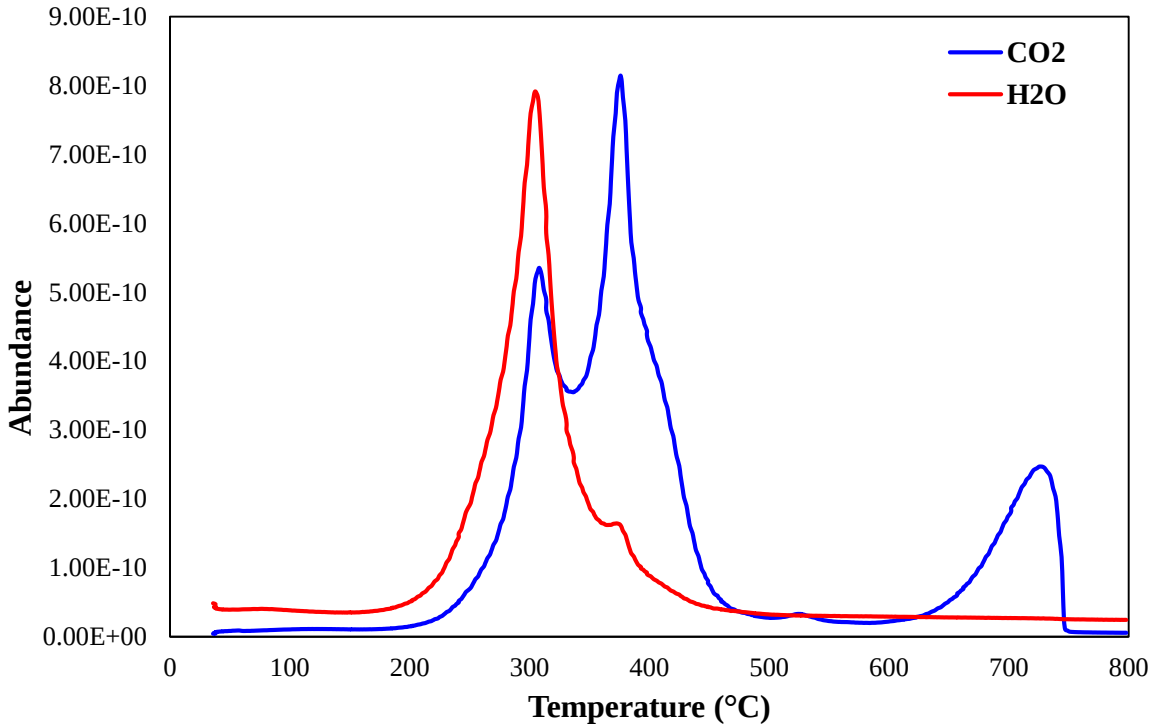

Figure 11 MS profile for H_2O and CO_2 during TGA analysis of untreated original oil shale.

TGA was also performed on the sample treated by Soxhlet extraction and decarbonation (decarbonated kerogen), shown in **Figure 12**. There is no longer any decomposition after 500 °C, indicating that all carbonates have been completely removed from the sample. The overall weight loss is also noticeably larger, indicating less inorganic content (due to the loss of carbonates) as well as more organic content available for thermal decomposition, likely due to improved pore volume. In the MS plot for TGA of decarbonated kerogen in **Figure 13**, it can be seen that no CO_2 production occurs after 500 °C, again demonstrating the complete removal of all carbonates.

The bitumen extracted by Soxhlet extraction was weighed, and the amount of bitumen in the original oil shale was found to be 3.58 wt%.

As decarbonated kerogen is being used for all experiments, the total available organic content of the sample is found from the weight loss in the TGA curve, being 45.29 % in the temperature range 200-500 °C.

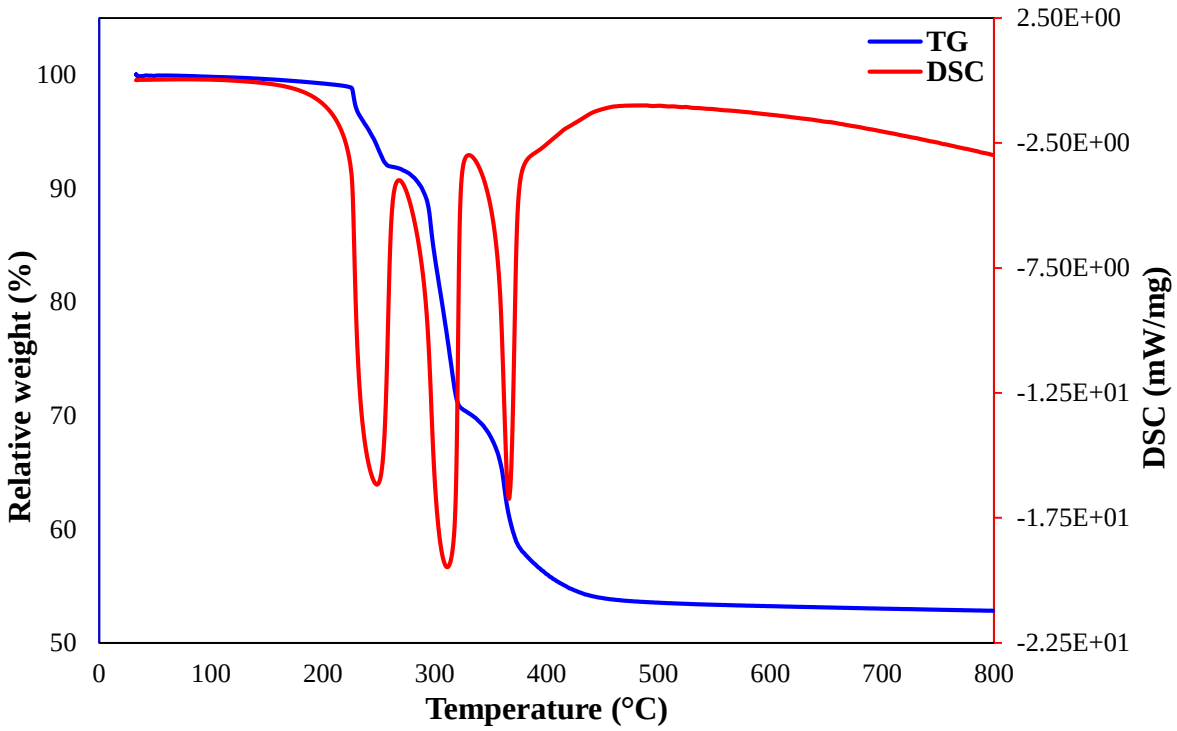

Figure 12 TGA-DSC profile of oil shale sample after Soxhlet extraction and decarbonation (decarbonated kerogen).

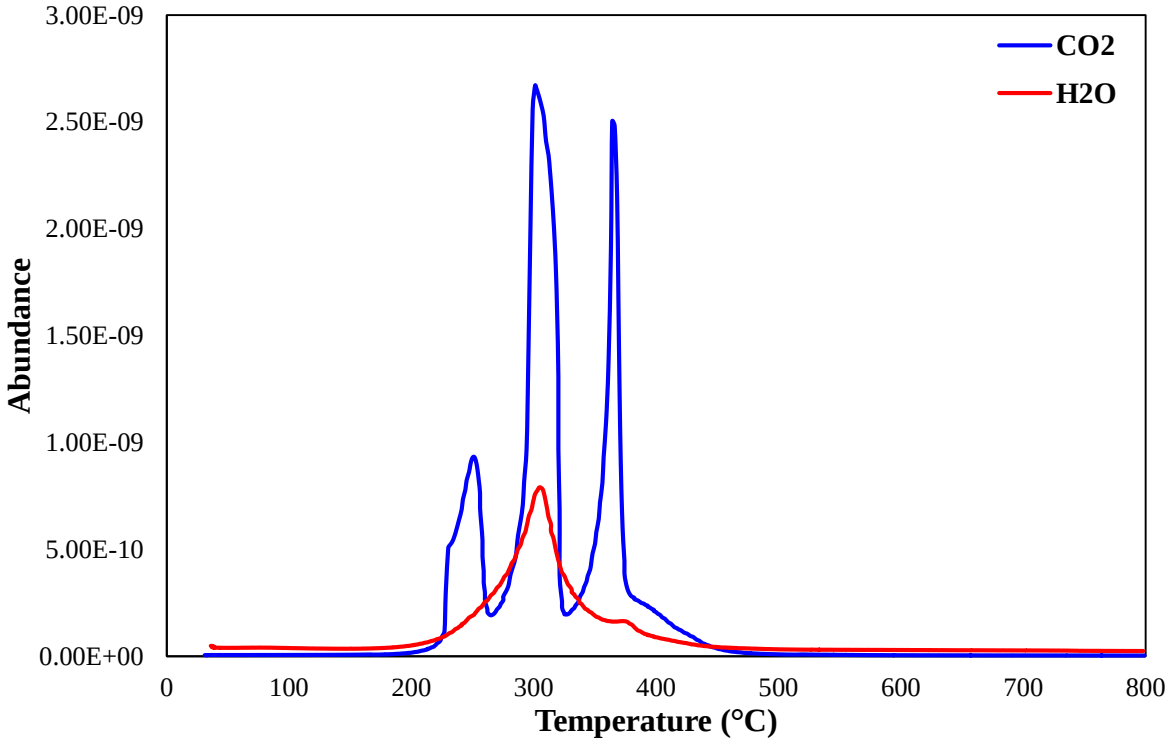

Figure 13 MS profile for H_2O and CO_2 during TGA analysis of decarbonated kerogen.

4.2 Catalytic thermal upgrading of kerogen

Catalyst screening was performed, and catalyst performance is judged based on shifting the temperature at maximum conversion (T_{max}) in the EGA profile towards lower temperatures. All catalyst samples compared were run in sequence on the same day, and variance in T_{max} based on several runs with the same sample was found to be approximately 2 ^{o}C. This rather large error is attributed to the heterogeneity of the kerogen sample, particularly due to the small sample size (0.1-0.5 mg), as well as a smaller instrumental error. All EGA profiles have been normalized with regard to abundance.

4.2.1 Catalyst performance

In **Figure 14** the EGA profiles of all catalysts are presented. All catalysts tested had a theoretical loading of 10 wt% based on the total weight of decarbonated kerogen. Zinc has the greatest performance, with a large temperature shift of 30 °C (from 470 to 440 °C). Other catalysts also perform well, such as iron, nickel, cobalt and copper; however, zinc shows significant temperature reduction for pyrolysis at all temperatures, starting at a lower temperature than others (~100 °C lower). Based on these results, zinc is selected as the catalyst for further analysis.

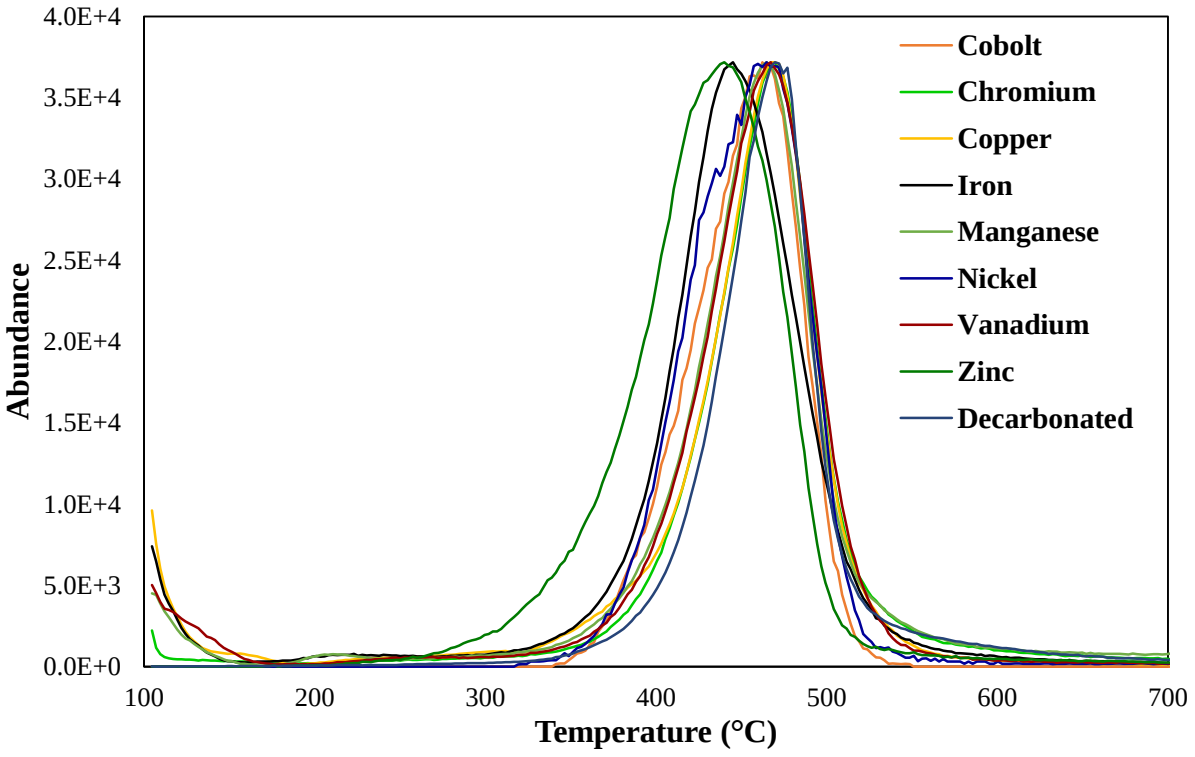

Figure 14 EGA profiles of several catalysts tested (decarbonated kerogen impregnated with metal chloride salts).

4.2.2 Effect of catalyst preparation

The effect of catalyst preparation on catalytic performance has been analyzed using zinc chloride precursor, comparing two samples of the same catalyst loading (5 wt%) to decarbonated kerogen without catalyst. The samples were prepared similarly; however, a different amount of water was added, resulting in either wetness impregnation (WI) or incipient wetness impregnation (IWI). Results are shown in **Figure 15**. The method of preparation has a significant effect: the observed T_{max} for decarbonated, 5 wt% (WI) and 5 wt% (IWI) are 437 ^{o}C, 431 ^{o}C and 423 ^{o}C, respectively. This corresponds to an error of more than 50 % if the method of preparation is incorrect. To optimize catalyst performance, preparation should be done by incipient wetness impregnation using an appropriate amount of water; however, errors are highly possible due to the small pore volume coupled with the heterogeneity of the kerogen. These errors may have a profound effect on the results of catalyst testing.

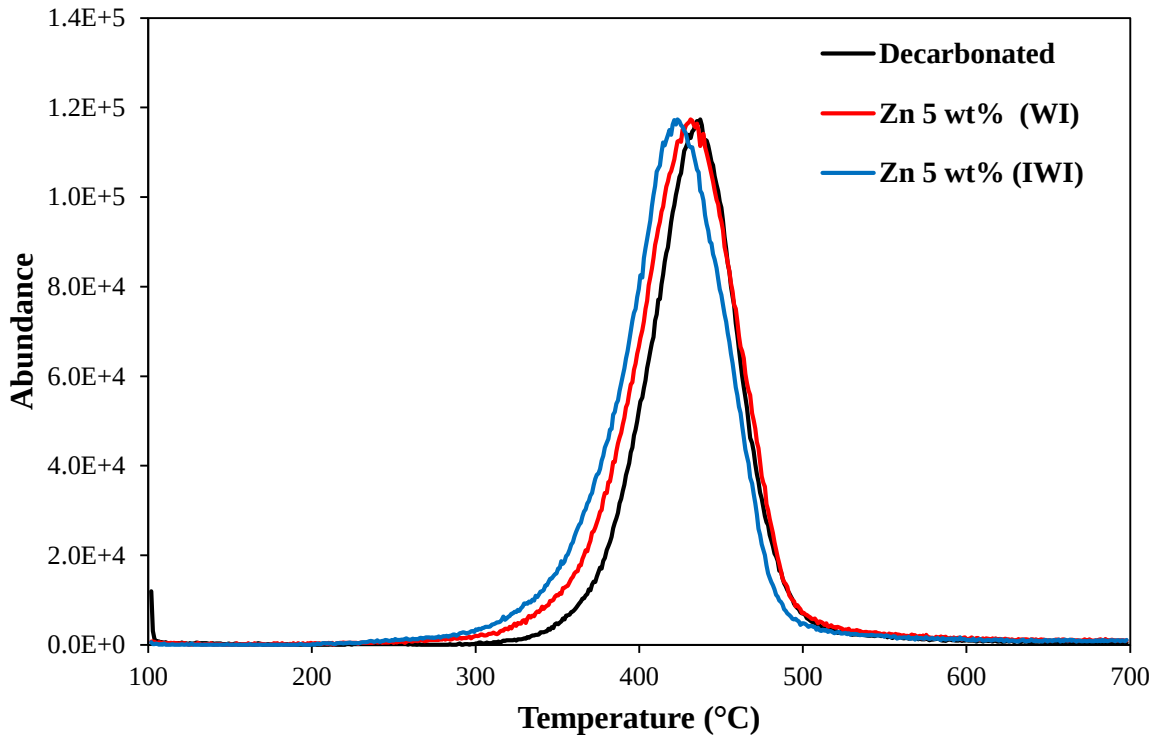

Figure 15 Effect of catalyst loading on temperature shift during EGA analysis, comparing wetness impregnation (WI) to incipient wetness impregnation (IWI). 5 wt% Zn^{2+}, 10 ^{o}C/min heating rate, helium atmosphere.

4.2.3 Effect of EGA heating rate

During EGA analysis temperature increases linearly from one point to another. A comparison was made between two different heating rates (10 ^{o}C/min and 25 ^{o}C/min) to see what effects can be observed. Results are displayed in **Figure 16**. The more obvious effect of increasing the

heating rate is a shift in T_{max} to higher temperatures; however, other effects can also be observed. The values of T_{max} for all samples are summarized in **Table 4**. T_{max} is shifted to a higher temperature (from 400 ^{o}C to 440 ^{o}C for the 10 wt% Zn^{2+} catalyzed kerogen) with increased heating rate. The observed catalytic effect is also decreased at higher heating rate (from 37 ^{o}C reduction in T_{max} to 30 ^{o}C), as is expected with the experiment being performed in a smaller window of time. Also to be noted is that the observed starting point of the reaction for both samples remains the same, at around 220 ^{o}C for catalyzed sample and around 320 ^{o}C without catalyst. Optimization of catalyst loading is based on T_{max} shift compared no catalyst, and heating rate is therefore not expected to have any effect on the observed optimized catalyst loading; however, higher heating rates may conceal smaller shifts in T_{max}. A heating rate of 10 °C/min is therefore used throughout all remaining experiments.

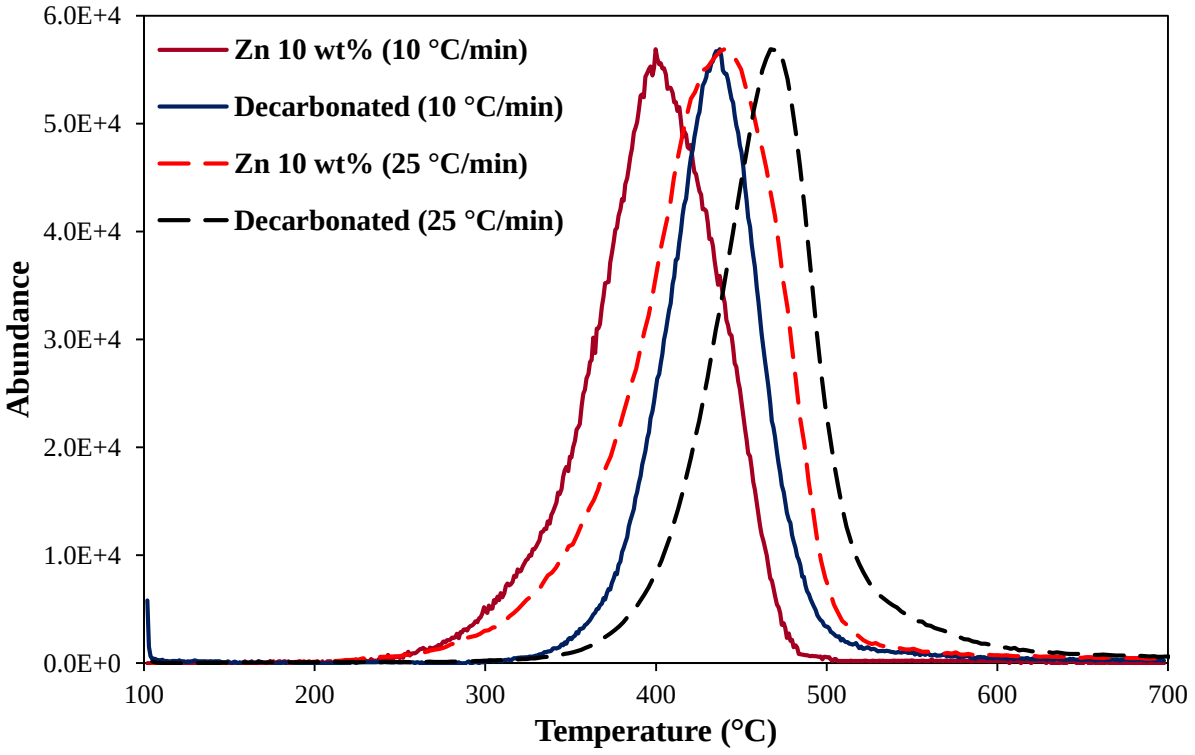

Figure 16 Effect of heating rate during EGA analysis, comparing 10 ^{o}C/min (solid line) to 25 ^{o}C/min (dashed line), helium atmosphere.

Table 4 Effect of heating rate on T_{max}, comparing 10 °C/min to 25 °C/min.

Heating rate	Sample	T_{max} (°C)
10 °C/min	Zn 10 wt%	400
	Decarbonated	437
25 °C/min	Zn 10 wt%	440
	Decarbonated	470

4.2.4 Optimization of catalyst loading

In order to optimize catalyst loading, several samples were prepared using $ZnCl_2$ precursor to analyze by EGA. The samples tested were (in weight percentage of zinc loaded on decarbonated kerogen): 1 %, 2 %, 5 %, 8 %, 10 % and 12 %. Decarbonated kerogen without catalyst was also tested to compare to the samples. The results of the experiment are displayed in **Figure 17**.

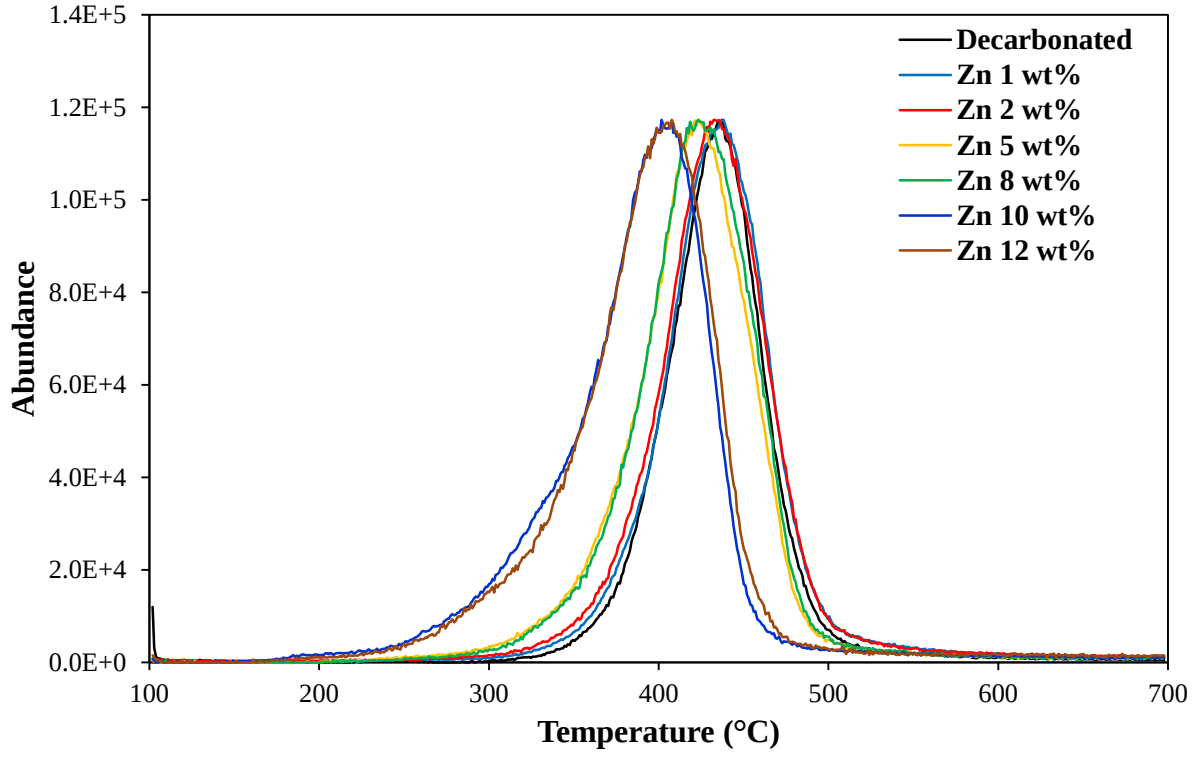

Figure 17 EGA analysis of all prepared Zn^{2+} catalyzed samples compared to decarbonated kerogen without catalyst in order to find optimized catalyst loading, 10 °C/min heating rate, helium atmosphere.

From the results, 10 wt% loading of Zn^{2+} appears to be the optimal catalyst loading. At 12 wt% loading, there is no further shift in T_{max} compared to 10 wt%, which could be due to catalyst

covering the kerogen surface, hindering the thermal reaction. No shift is observed when loading is increased from 5 wt% to 8 wt%. This is however likely due to the preparation, where the 8 wt% sample received more water relative to pore volume. Expected performance for 8 wt% is somewhere between 5 and 10 wt%.

Based on the results, 10 wt% loading of Zn^{2+} catalyst is selected as the optimal catalyst loading. At this loading, and with a heating rate of 10 ^{o}C/min, T_{max} is found to be 402 ^{o}C, compared to 437 ^{o}C for decarbonated kerogen without catalyst.

For pyrolysis, a temperature of 550 °C is selected based on EGA results, in order to maximize the amount of product obtained. This temperature is the point at which pyrolysis reactions cease for most samples.

4.3 SEM-EDS of impregnated samples

SEM was performed for decarbonated kerogen with both Zn^{2+} and Co^{2+} catalyst impregnated. The purpose was to analyze both particle size as well as catalyst loading and dispersion. Two different levels of magnification were used, 80x and 300x. Low magnification is used to reveal heterogeneity of the sample, while high magnification is used to determine particle size and identify the location of catalyst on the particles.

From the SEM image in **Figure 18**, Zn^{2+} catalyzed decarbonated kerogen at 80x magnification can be seen. Brighter spots indicate different elements, and will for most areas identify higher concentration of catalyst. As seen for Zn^{2+}, there is an even spread of catalyst, and it appears to be well-dispersed. Results are supported by EDS, which are reported in **Table 5**. Similar zinc wt% for both 80x and 300x magnification indicate that the catalyst is equally concentrated in most areas on the sample.

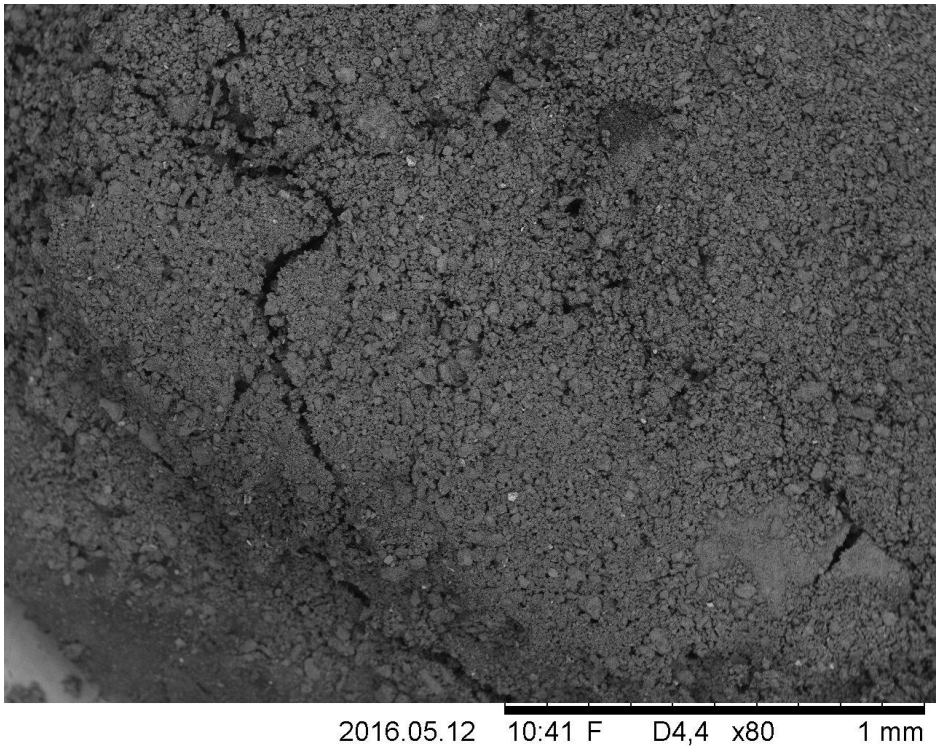

Figure 18 SEM image of Zn^{2+} catalyzed decarbonated kerogen at 80x magnification.

In **Figure 19** some catalyst is observed deposited on the outside of the particles; however, combined with the EDS results, this amount is small compared to the overall catalyst content, indicating that most of the catalyst has been deposited into the pores of the decarbonated kerogen. Particle size can also be observed to be less than 53 µm, with most particles being finely crushed to ~10 µm.

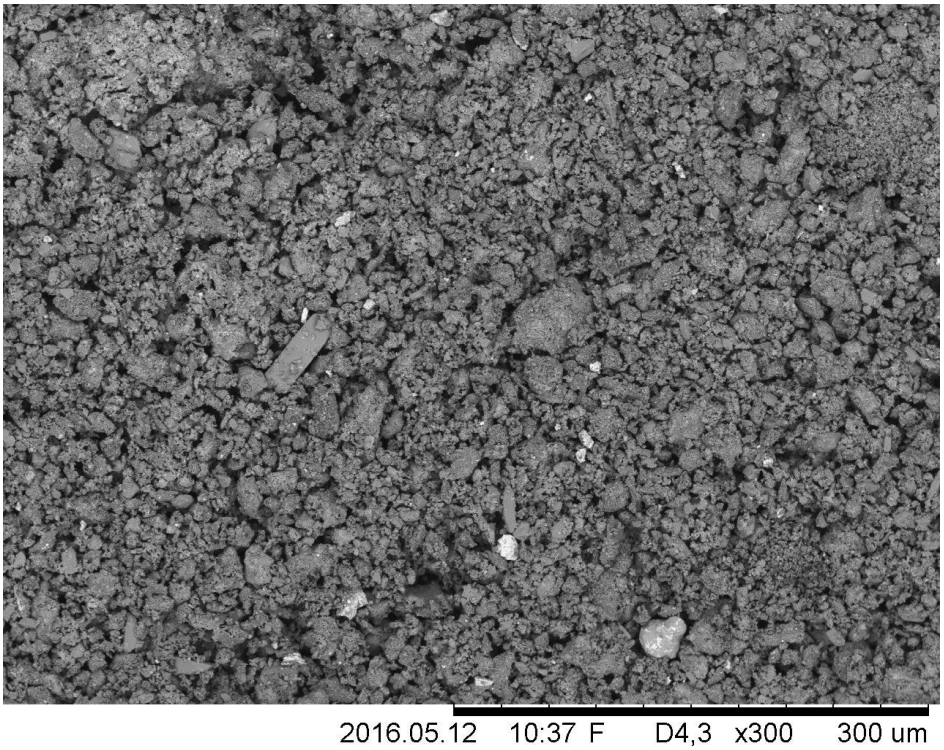

Figure 19 SEM image of Zn^{2+} catalyzed decarbonated kerogen at 300x magnification.

Table 5 Results from EDS at different magnifications for decarbonated kerogen impregnated with zinc catalyst.

80x magnification		300x magnification	
Element	Content (wt%)	Element	Content (wt%)
Carbon	40.77	Carbon	40.59
Oxygen	22.94	Oxygen	22.97
Chlorine	13.73	Chlorine	13.08
Silicon	10.23	Zinc	10.88
Zinc	10.14	Silicon	10.54
Aluminium	2.19	Aluminium	1.94

From **Table 6**, the loading of Co^{2+} catalyst appears lower than the theoretical loading of 10 wt%, being only 6.57 wt% on the large-scale 80x magnification. Using 300x magnification yields different results, with a significantly higher 11.56 wt% cobalt.

Table 6 Results from EDS at different magnifications for decarbonated kerogen impregnated with cobalt catalyst.

80x magnification		300x magnification	
Element	Content (wt%)	Element	Content (wt%)
Carbon	42.42	Carbon	38.85
Oxygen	25.11	Oxygen	22.78
Silicon	11.16	Chlorine	13.25
Chlorine	10.29	Cobalt	11.56
Cobalt	6.57	Silicon	9.07
Aluminium	2.54	Iron	2.31
Iron	1.92	Aluminium	2.19

In **Figure 20** the catalyst is clearly deposited in large quantities on the outside of the particles. This could be caused by several factors, such as the addition of more water than pore volume or poor stirring. Due to the significant deposition outside of pores, it is likely that catalyst remained in solution before drying and thus dried on the wall of the container used to prepare it in, reducing catalyst loading compared to the theoretical value.

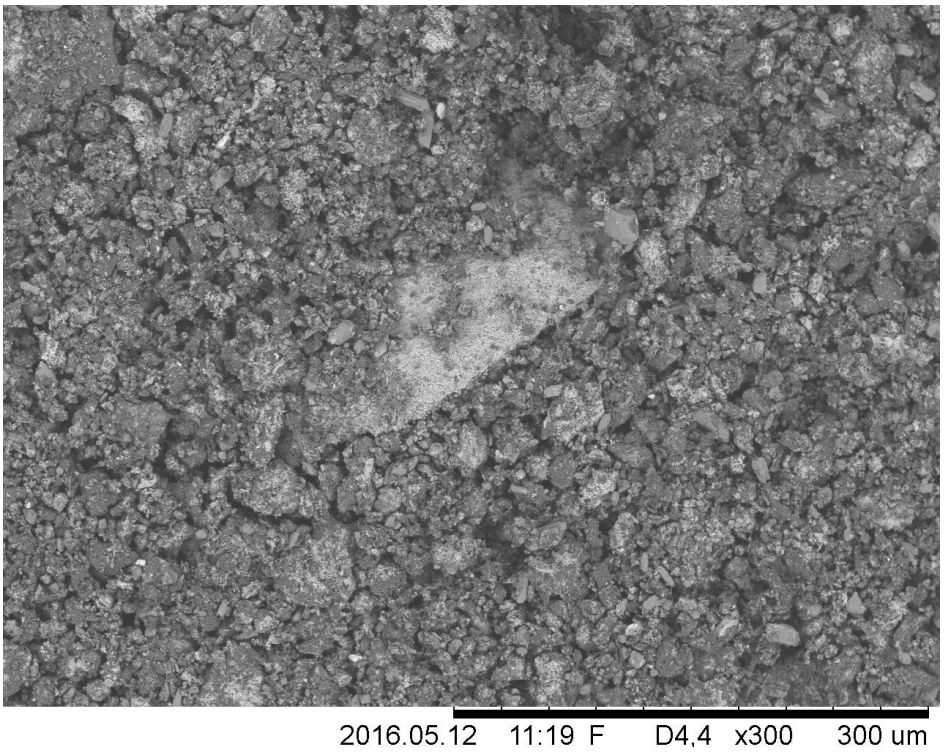

Figure 20 SEM image of Co^{2+} catalyzed decarbonated kerogen at 300x magnification.

4.4 Pyrolysis analysis of 10 wt% Zn^{2+} catalyst

Pyrolysis-GC/MS (Py-GC/MS) was performed to qualitatively and quantitatively investigate the product distribution obtained by pyrolysis of 10 wt% Zn^{2+} catalyzed decarbonated kerogen at 550 ^{o}C. Results are compared to a similar analysis performed for original oil shale and decarbonated kerogen without any added catalyst.

4.4.1 Qualitative analysis of pyrogram (Py-GC/MS)

The resulting pyrogram from Py-GC/MS analysis of 10 wt% Zn^{2+} catalyzed kerogen is presented in **Figure 21**. Peaks are identified by MS ion fragmentation pattern using the NIST library, and labelled based on their carbon number as well as saturation (C' represents olefins while C represents paraffins).

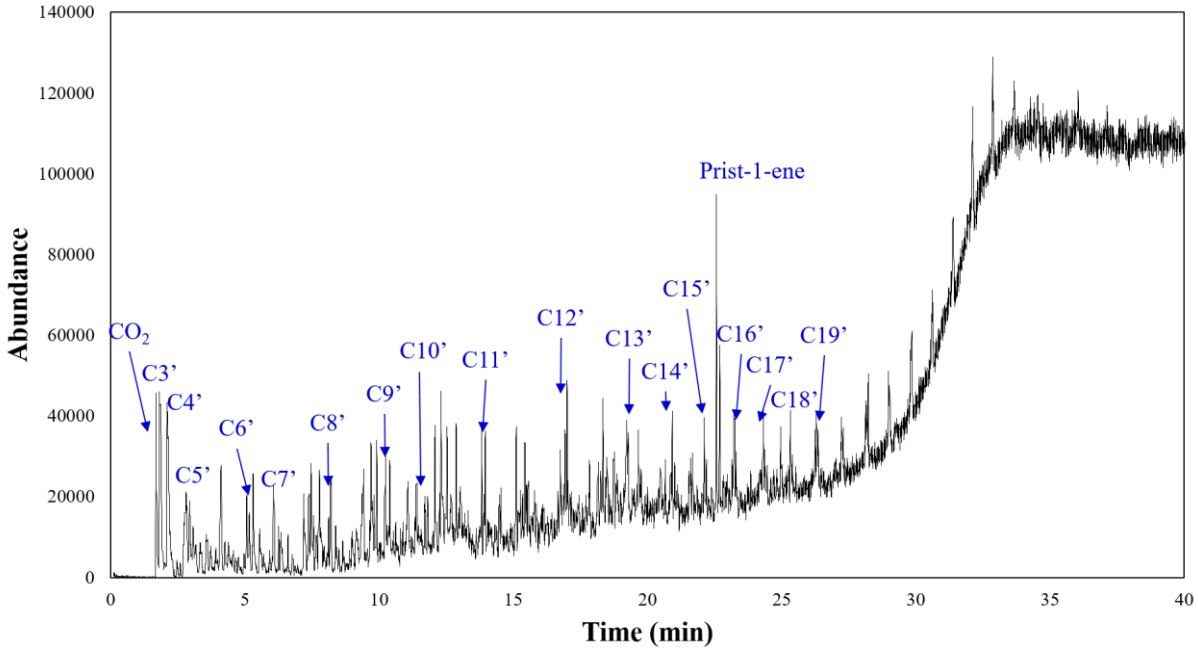

Figure 21 Pyrogram resulting from Pyrolysis-GC/MS at 550 ^{o}C for 10 wt% Zn^{2+} catalyzed kerogen. Peaks are labelled based on MS ion fragmentation pattern by use of the NIST library. C' represents olefins and C represents paraffins.

More detailed peak identification is presented as magnified pyrograms in **Figure 22 - Figure 25**. The major products obtained are linear hydrocarbons, while aromatic fragments such as toluene, xylene, trimethylbenzene (TMB) and naphthalenes are also observed. Prist-1-ene is also a characteristic compound found in pyrolyzates from organic matter formed from algae sources. Past C_{22}, the ratio of noise and the identification of silicates (likely from the GC column) makes compound identification difficult; however, the peak areas are sufficiently small to neglect contribution to the product composition.

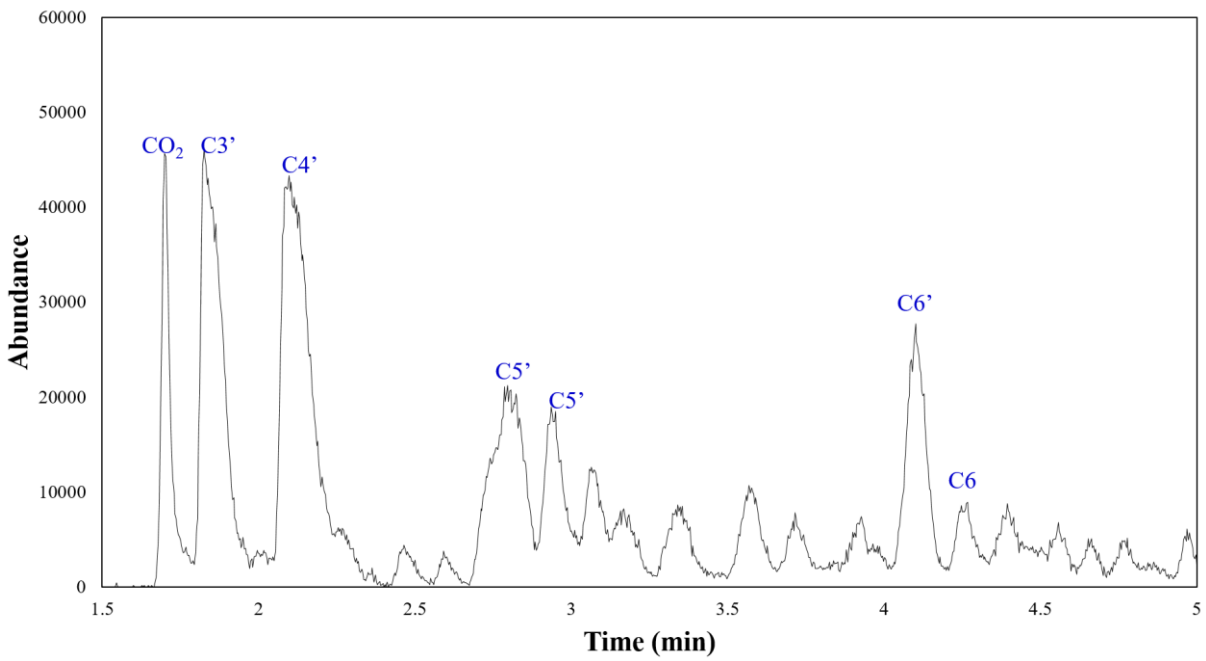

Figure 22 Magnified pyrogram (1.5-5 minutes retention time) for 10 wt% Zn^{2+} catalyzed kerogen.

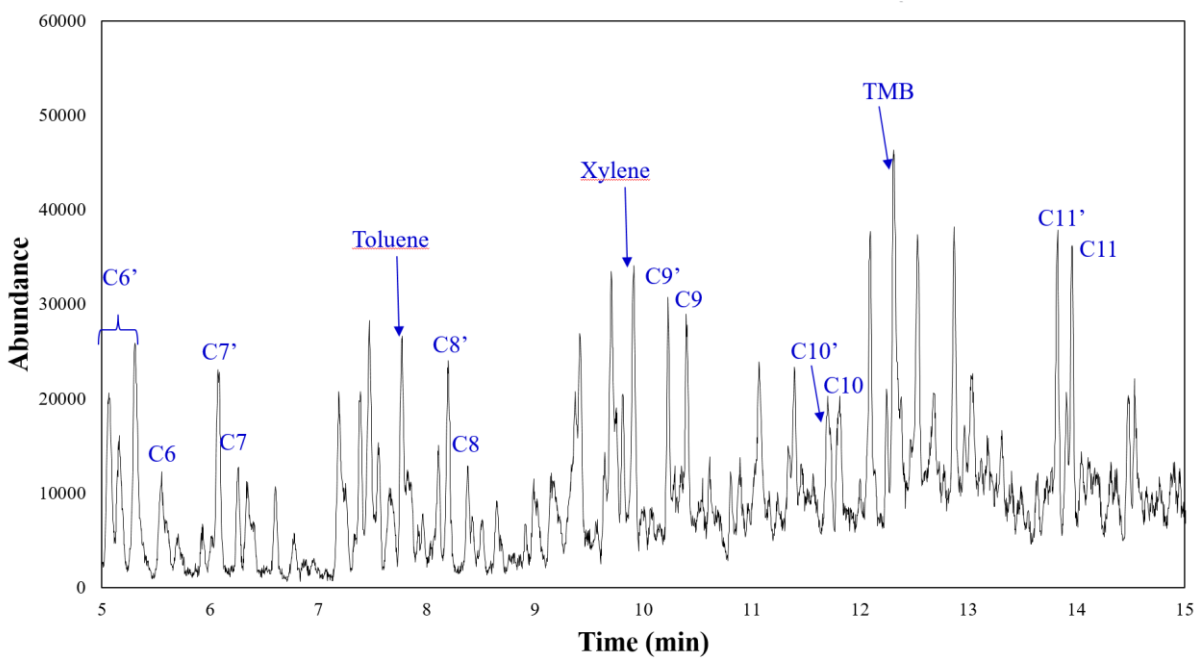

Figure 23 Magnified pyrogram (5-15 minutes retention time) for 10 wt% Zn^{2+} catalyzed kerogen.

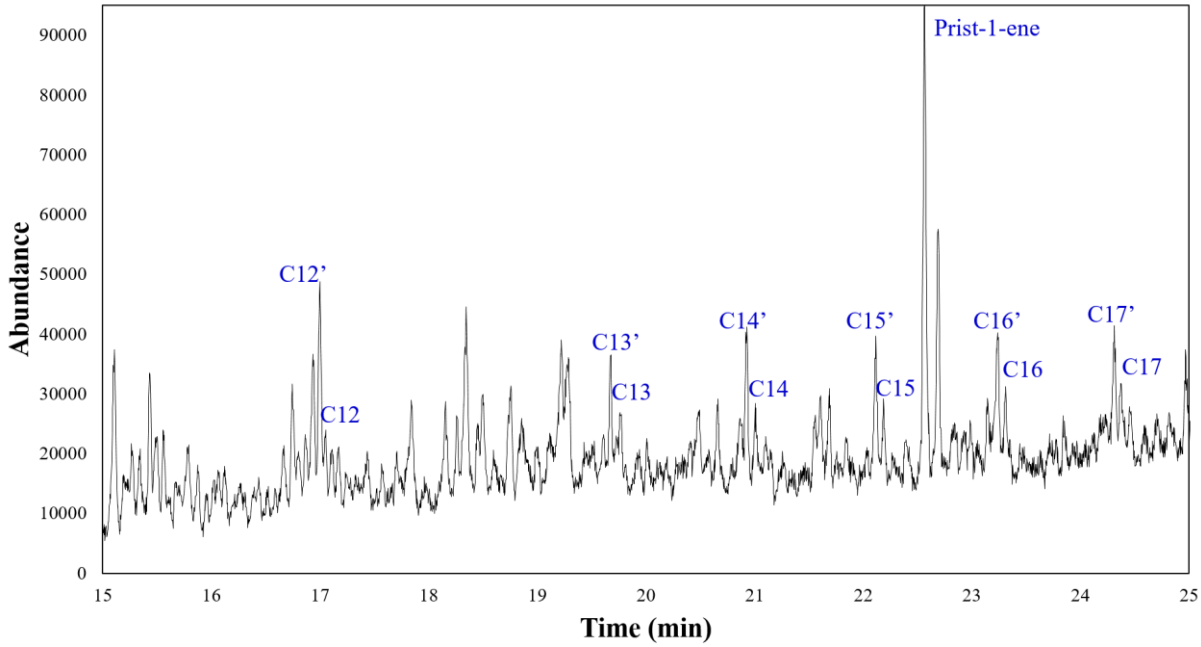

Figure 24 Magnified pyrogram (15-25 minutes retention time) for 10 wt% Zn^{2+} catalyzed kerogen.

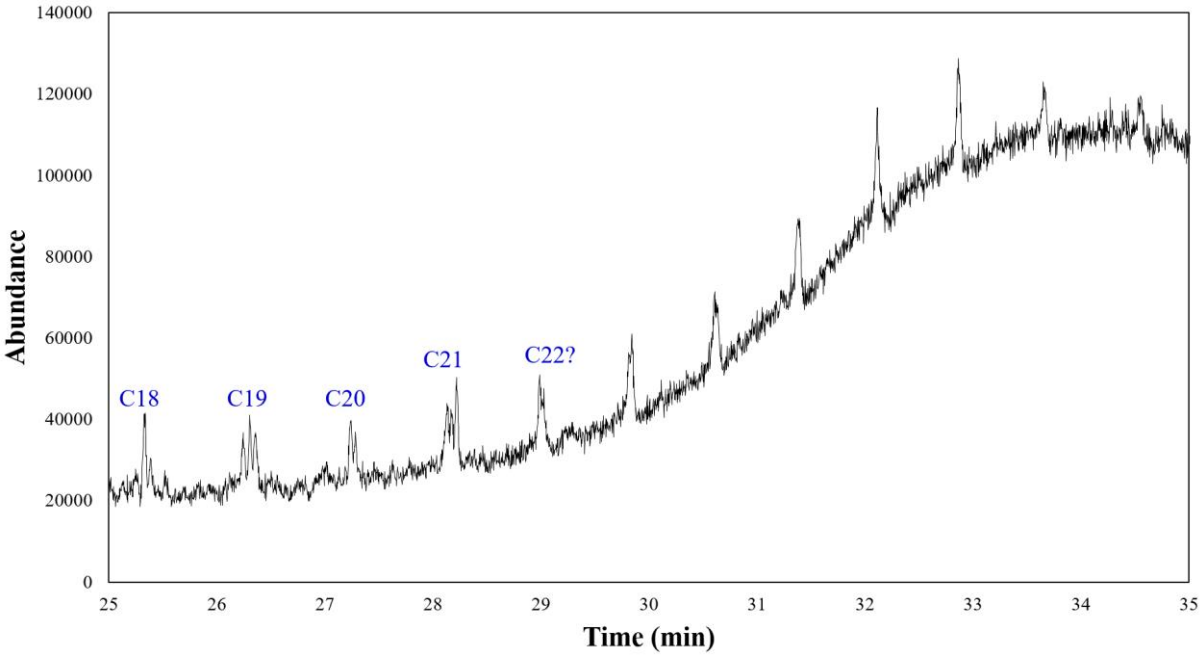

Figure 25 Magnified pyrogram (25-35 minutes retention time) for 10 wt% Zn^{2+} catalyzed kerogen.

4.4.2 Quantitative analysis of pyrogram (Py-GC/MS)

A semi-quantitative analysis is performed by integrating the pyrogram to receive peak areas. The analysis is referred to as semi-quantitative due to the compound analysis only accounting for one existing compound in each peak. Several of the identified peaks are likely to comprise a mixture of compounds (including varied olefins or paraffins of similar carbon number); however, this would severely complicate the analysis. The unidentified compounds are in low

quantity, and the analysis should give a sufficiently accurate representation of the product composition. Any peak area below 0.4 % of the total is excluded from the analysis. **Figure 26** summarizes the overall distribution based on carbon number in the pyrolysis products. The largest fraction is C_{12} hydrocarbons. In comparison to the results from decarbonated kerogen without catalyst in **Figure 29**, products have shifted to shorter hydrocarbon chains. The longest observed hydrocarbon chain was C_{33} for decarbonated kerogen without catalyst, while the longest observed hydrocarbon chain is C_{22} for 10 wt% Zn^{2+} catalyzed kerogen. An increase in C_{10}-C_{16} hydrocarbons indicates that the catalyst promotes cracking of longer hydrocarbon chains to C_{10}-C_{16}.

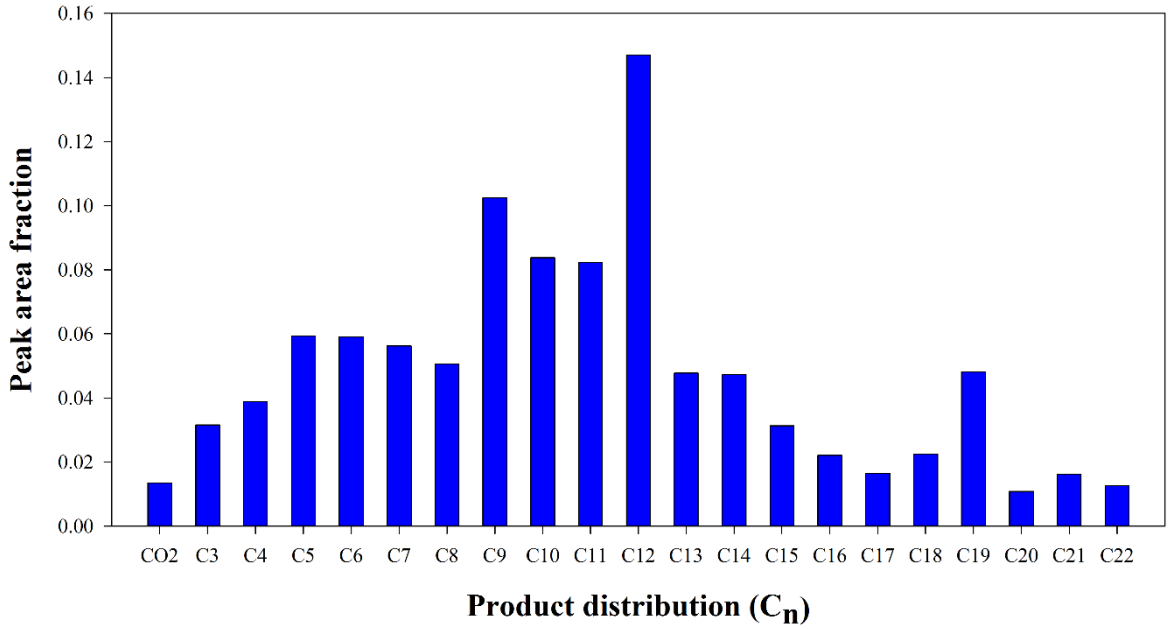

Figure 26 Pyrolysis product distribution for 10 wt% Zn^{2+} catalyzed kerogen, based on carbon number.

Further analyses of the product distribution of paraffins, aromatics and olefins are shown in **Figure 27** and **Figure 28**. Paraffins and olefins display similar trends, with the most abundant fraction being C_{12}. Aromatics are concentrated in the C_7 (toluene) – C_{14} range, with the most abundant fractions being C_{12} (dimethyl naphthalenes) and C_9 (TMB). The overall distribution indicates 65.7 % olefins in the product mixture. A similar distribution is observed for pyrolysis of decarbonated kerogen and original oil shale, in **Figure 30**. Decarbonated kerogen appears to improve paraffin-to-olefin ratio compared to original oil shale, increasing paraffin fraction from 13.6 % to 33.8 %, while reducing olefin fraction from 66.9 % to 55.8 %. High olefin content is expected due to a H/C ratio of 1.9[13] leading to a shortage of hydrogen during bond cleavage. Increased olefin content when zinc catalyst is introduced is expected due to cracking reactions

being catalyzed. Further upgrading of the product is needed and can be done by hydrogenation. Another possibility is to introduce hydrogen donating species such as tetralin[32].

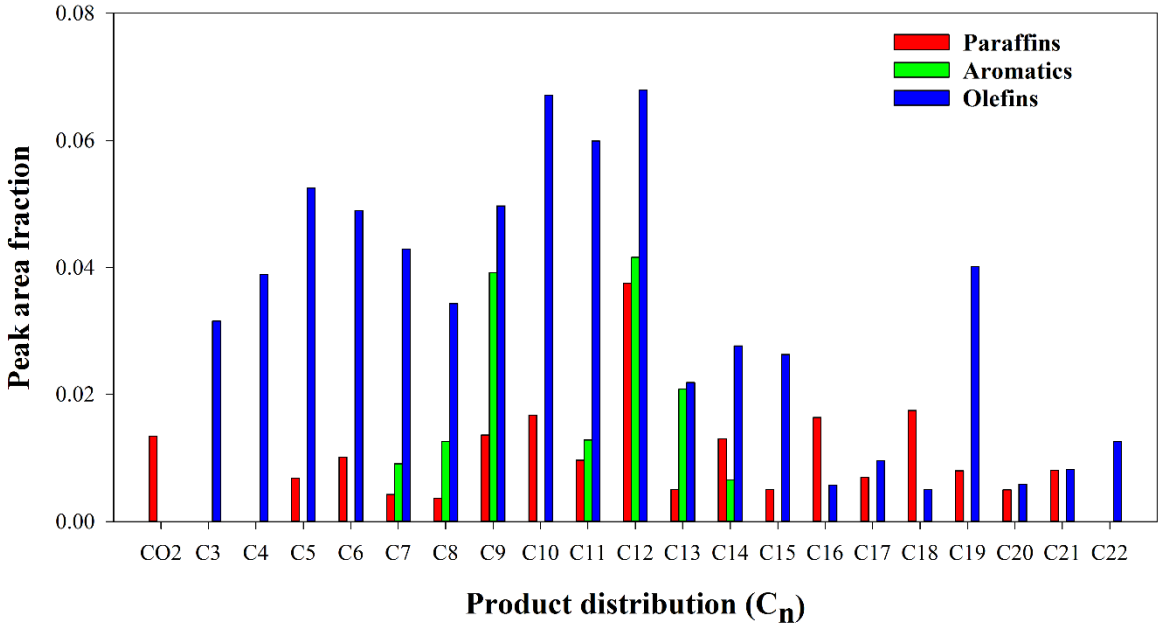

Figure 27 Pyrolysis product distribution for 10 wt% Zn^{2+} catalyzed kerogen for paraffins, aromatics and olefins, based on carbon number.

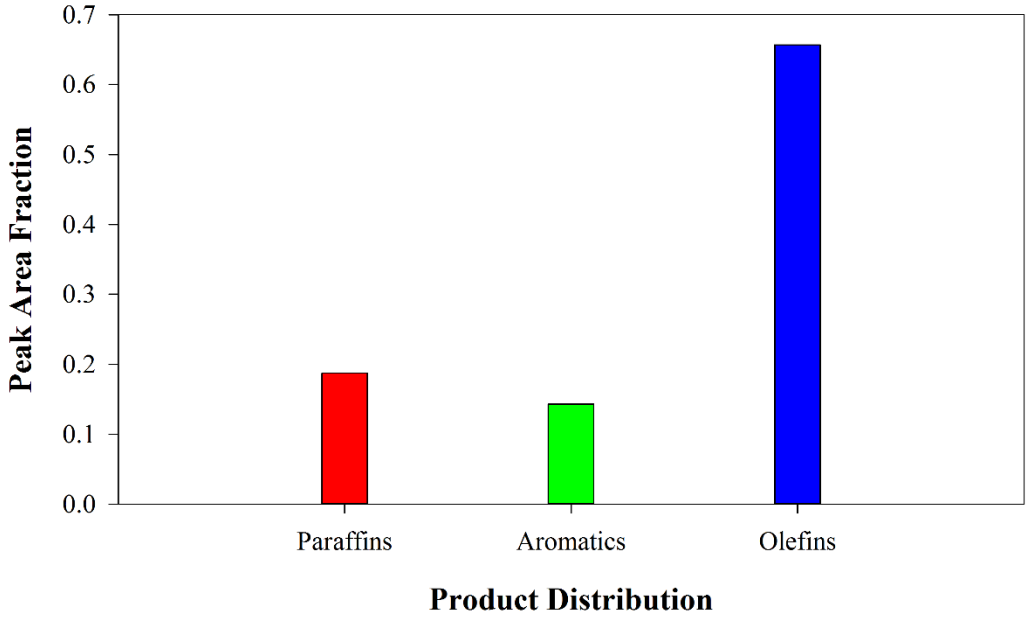

Figure 28 Pyrolysis product distribution for 10 wt% Zn^{2+} catalyzed kerogen.

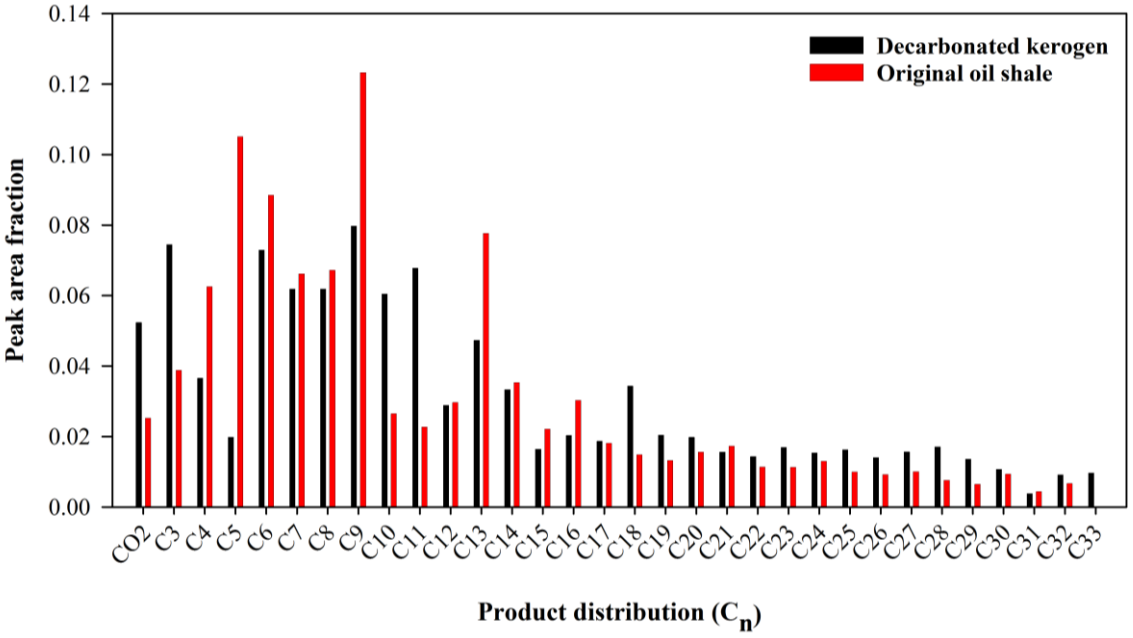

Figure 29 Pyrolysis product distribution for decarbonated kerogen and original oil shale, based on carbon number.

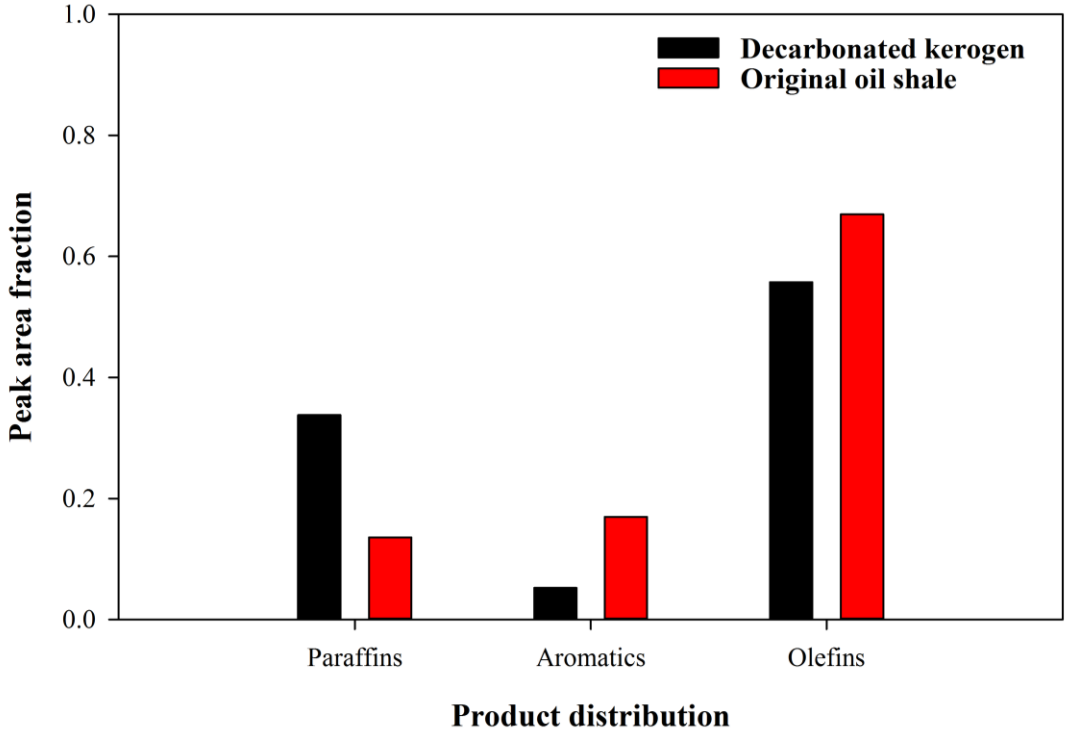

Figure 30 Pyrolysis product distribution for decarbonated kerogen and original oil shale.

4.5 Liquefaction

Due to the large amount of olefins present, upgrading of the product is attempted by introducing hydrogen-donor liquids. This is done by performing liquefaction as opposed to pyrolysis, using isopropanol, tetralin or decalin as hydrogen-donor solvents. To separate performance difference due to increased reaction time, a blank experiment was also performed, using no solvent or catalyst under similar conditions. Several methods were used to analyze the performance, including TGA, XRF, SEM-EDS and Py-GC/MS. Both catalyzed and un-catalyzed liquefaction was explored, using Zn^{2+}, Co^{2+} and KOH (for isopropanol only) as the catalysts.

4.5.1 SEM-EDS of solid residue

SEM-EDS was performed on the solid residue after reaction at the maximum reaction temperature for both isopropanol (330 °C) and tetralin (400 °C) with zinc catalyst. The purpose was to identify catalyst dispersion and other details about the reaction. In **Figure 31** a SEM image of the solid residue after reaction with Zn^{2+} catalyzed decarbonated kerogen in isopropanol is shown at 80x magnification. What can be seen is a concentration of brighter spots, unlike what was seen on the sample before reaction in **4.3 SEM-EDS of impregnated sample**. At higher magnification in **Figure 32** it can be seen that the catalyst particles are creating agglomerates, as described in **2.5.4 Catalysis in liquefaction**. This may contribute in reducing the catalytic dispersion, lowering activity of the catalyst.

In **Table 7** the EDS results of solid residue after reaction at 330 °C in isopropanol solvent for decarbonated kerogen with zinc catalyst are presented. Zinc concentration after reaction with isopropanol is lower than initial loading. This is expected as the catalyst is soluble in the solvent, and will be dispersed in the liquid phase during reaction, and some catalyst will then be extracted along with the liquid product. It is also worth noting that EDS detects carbon content, which is lower after reaction. This results in a higher than expected value for catalyst content related to the amount of conversion achieved.

Table 7 Results from EDS of solid residue after reaction at 330 °C in isopropanol solvent for decarbonated kerogen with zinc catalyst.

80x		300x	
Element	Content (wt%)	Element	Content (wt%)
Oxygen	38.57	Oxygen	39.99
Silicon	31.45	Silicon	30.2
Carbon	17.36	Carbon	16.53
Aluminium	6.07	Zinc	6.16
Zinc	5.11	Aluminium	5.96
Chlorine	1.45	Chlorine	1.17

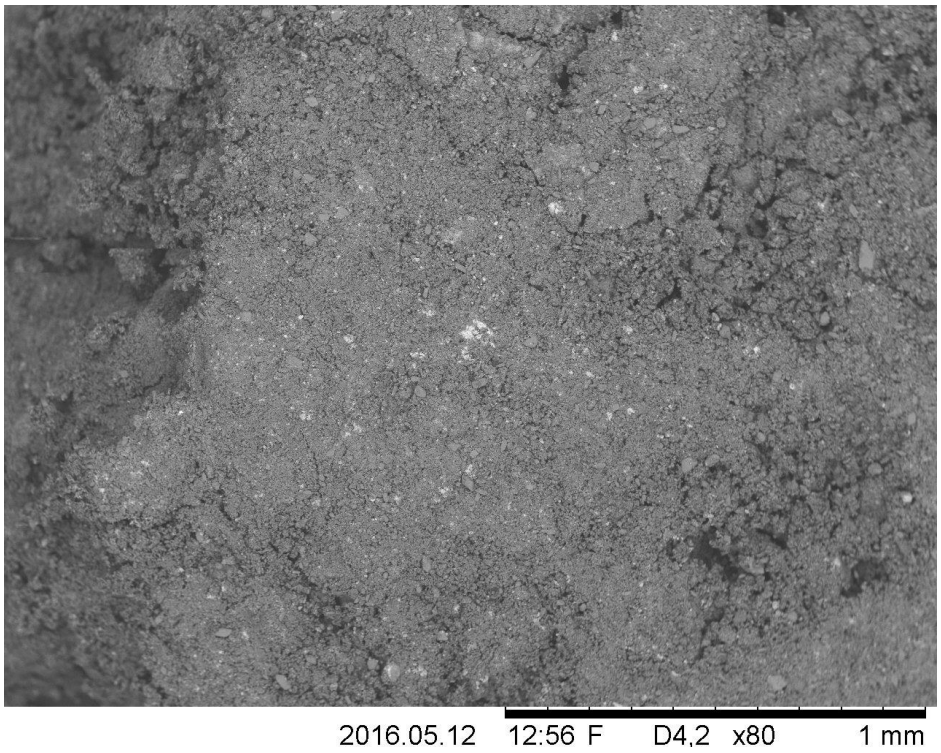

Figure 31 SEM image of solid residue with zinc catalyst after reaction at 330 °C in isopropanol at 80x magnification.

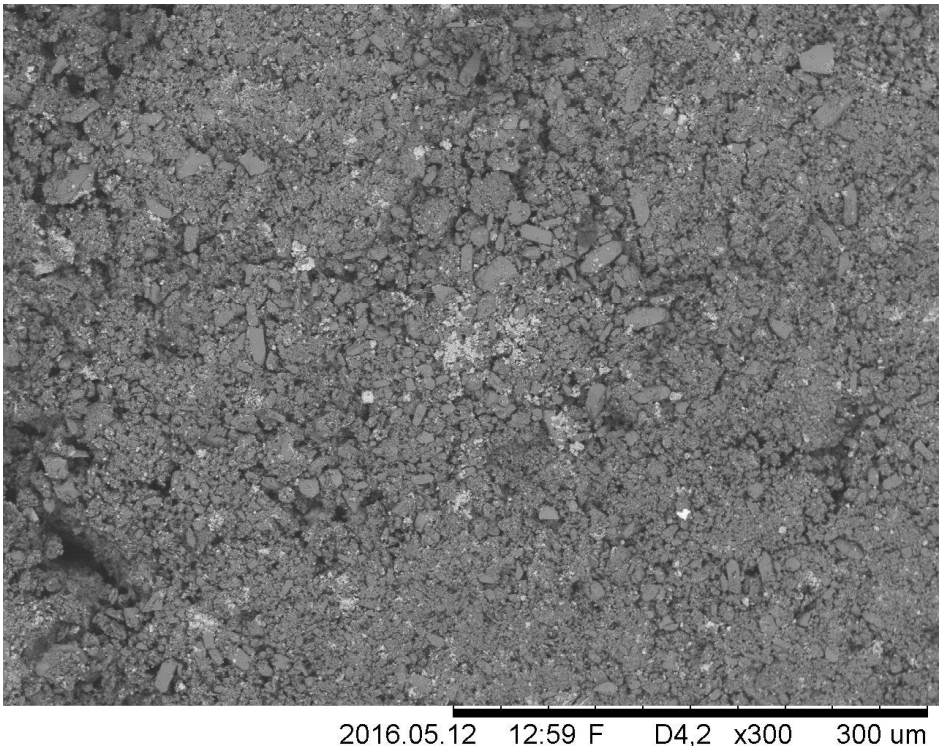

Figure 32 SEM image of solid residue with zinc catalyst after reaction at 330 °C in isopropanol at 300x magnification.

In **Figure 33** a SEM image of the solid residue after reaction with Zn^{2+} catalyzed decarbonated kerogen in tetralin is shown at 300x magnification. While it appears brighter than the unreacted sample, no agglomeration can be seen. The catalyst precursor is not soluble in tetralin, so dispersion into the liquid phase is not expected to a similar degree as for isopropanol. This is supported by the EDS results in **Table 8** where catalyst concentration increased compared to initial loading, again due to the lower carbon content. While loading appears higher, some catalyst is still lost from the solid in the process, likely due to the catalyst being deposited inside pores where reactions occur. Organic matter is converted and the catalyst deposited is removed from the site and dispersed in the liquid product. The high catalyst loading suggests that the oil shale mineral matrix acts as a catalyst support, maintaining high catalyst dispersion.

Table 8 Results from EDS of solid residue after reaction at 400 °C in tetralin solvent for decarbonated kerogen with zinc catalyst.

80x		300x	
Element	Content (wt%)	Element	Content (wt%)
Oxygen	28.6	Oxygen	29.05
Silicon	20.91	Silicon	19.55
Chlorine	16.4	Chlorine	18.48
Zinc	15.9	Zinc	13.96
Carbon	8.72	Iron	7.62
Iron	5.22	Carbon	7.33
Aluminium	4.25	Aluminium	4.01

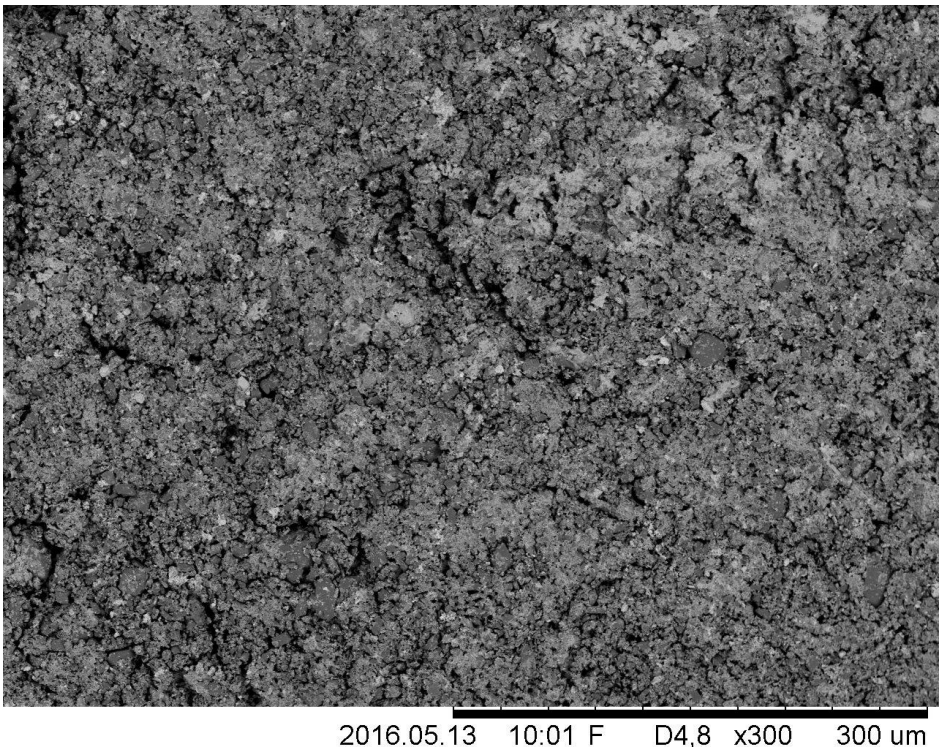

Figure 33 SEM image of solid residue with zinc catalyst after reaction at 400 °C in tetralin at 300x magnification.

4.5.2 TGA of solid residue

TGA was used to analyze the solid conversion achieved in the different reactions. By performing TGA on the solid residue, remaining organic matter can be detected and measured using air atmosphere. Comparing this remaining organic matter to the total amount of available organic matter before reaction, solid conversion is calculated. TGA is a very accurate method of measurement, which is the primary reason to perform this analysis. Liquid yield and gas yield could not be recorded due to the inaccuracies during the experiments (gas leakage, spills,

inability to separate liquid product from tetralin solvent and liquid product evaporation), particularly due to the small sample sizes used.

Figure 34 shows the results from TGA performed on the solid residue without any catalyst after reaction in tetralin at the three different temperatures used. As expected, higher temperature results in improved solid conversion, leaving less organic matter in the residue.

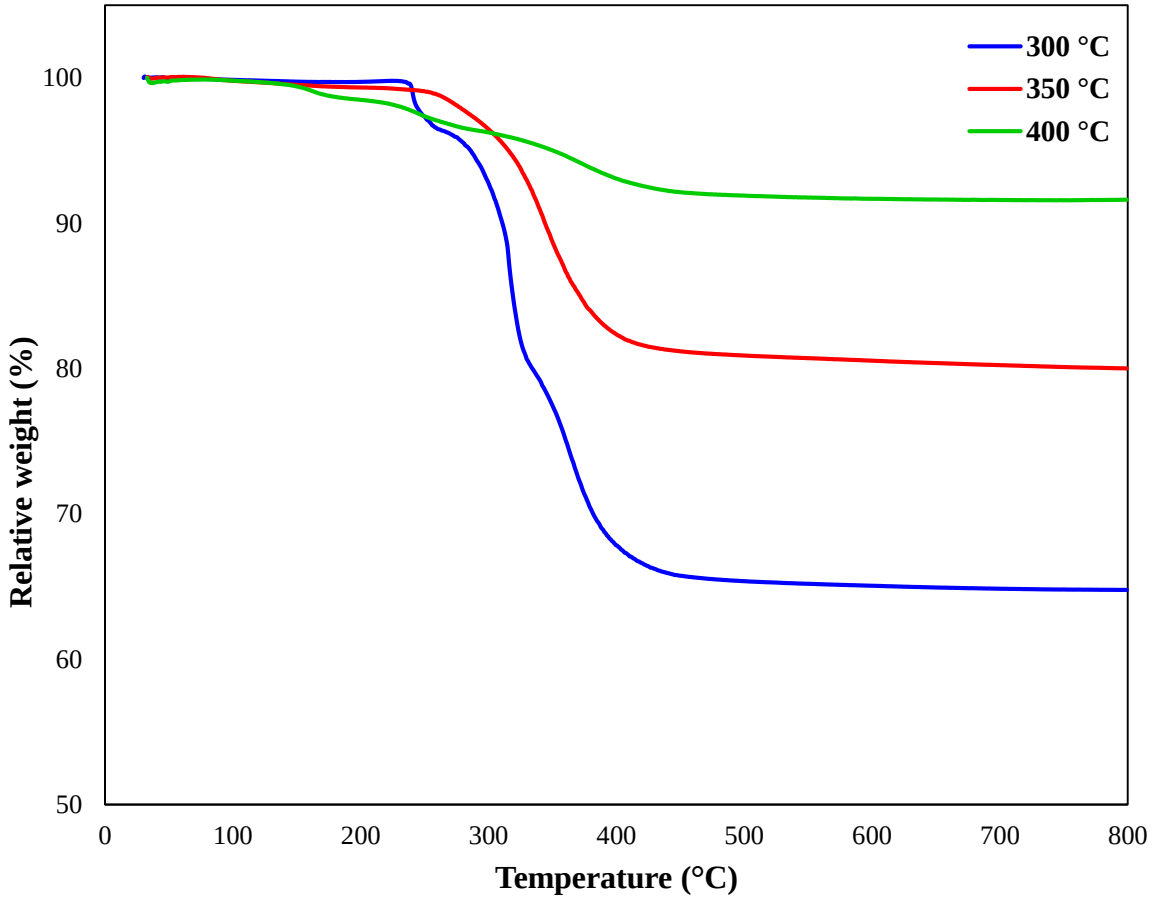

Figure 34 TGA profiles of solid residue without catalyst after reaction in tetralin at three different temperatures.

Further analysis is performed using the DSC and MS data gathered. For the solid residue after reaction at 400 °C in tetralin, a smaller drop can be observed in the 150-200 °C range which is not observed in the other two TGA curves. The DSC curve in **Figure 35** increases in this temperature range, indicating an endothermic reaction. This is expected to be caused by either tetralin remaining after extraction or water produced during the reaction, which is supported by the MS results displayed in **Figure 36**, indicating H_2O and no CO_2 in this temperature range. Remaining OM in the residue is therefore taken as the weight loss after this point, when CO_2 production is initiated (180 °C).

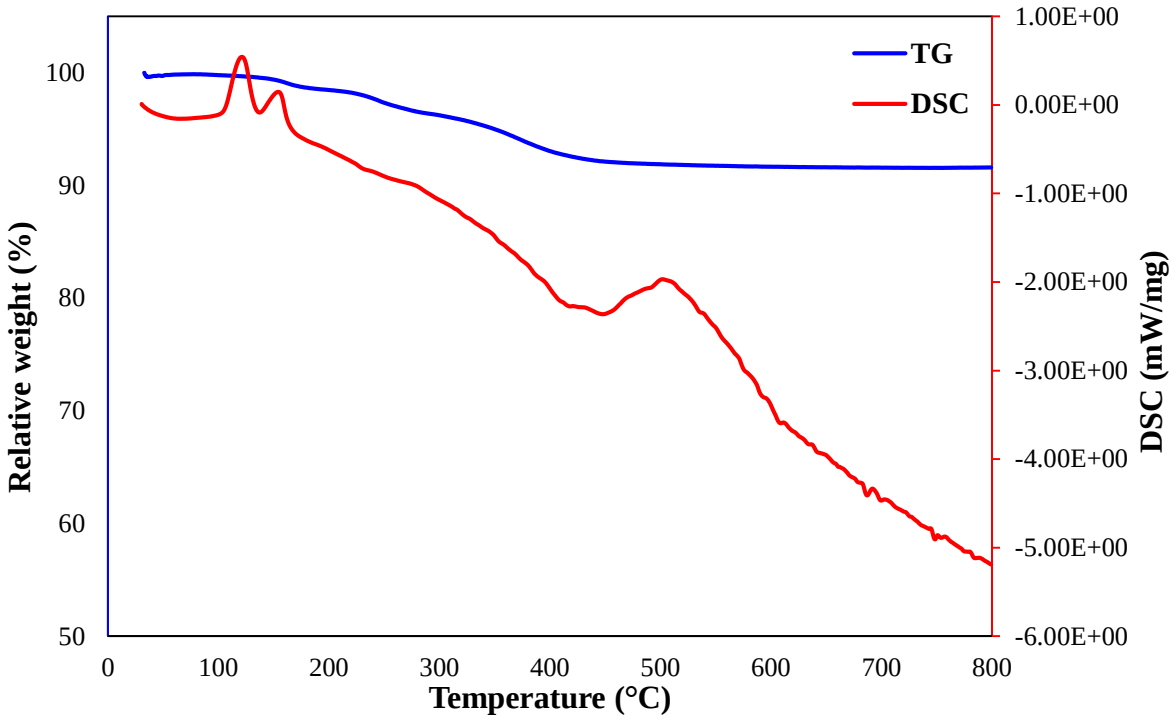

Figure 35 TGA and DSC profiles of solid residue without catalyst after reaction in tetralin at 400 °C.

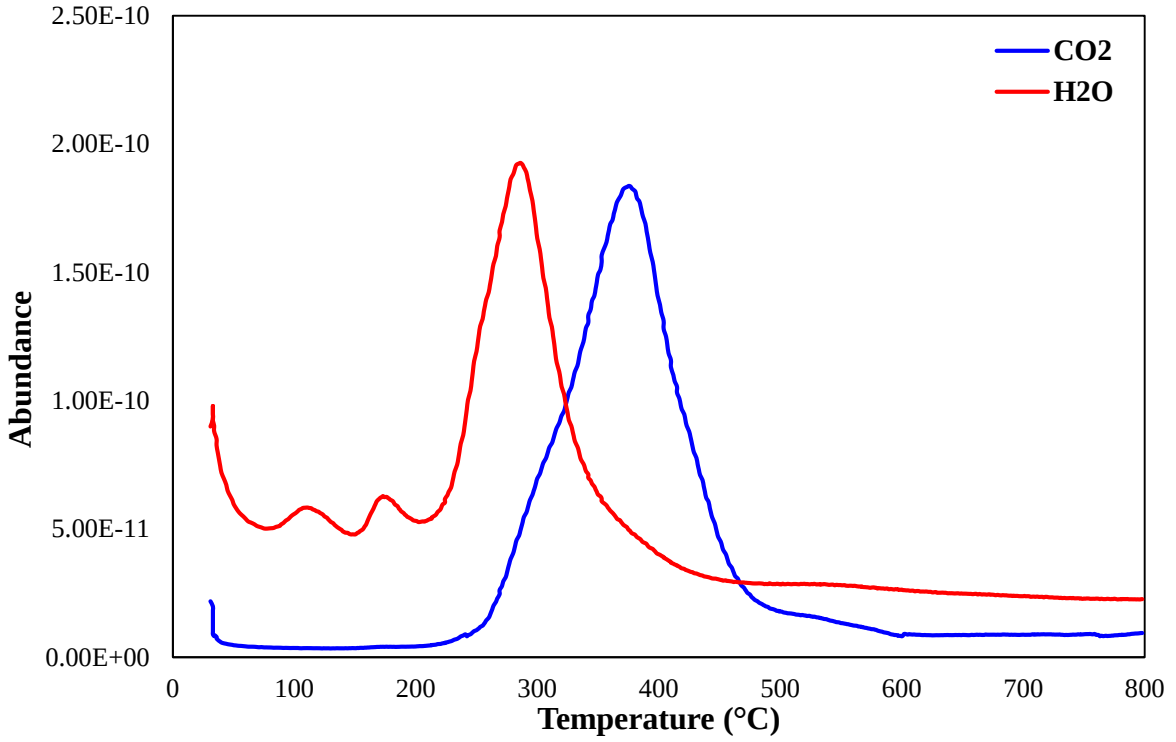

Figure 36 MS profiles for H_2O and CO_2 detected during TGA of solid residue without catalyst after reaction in tetralin at 400 °C.

Similar analyses were performed for all three solvents (tetralin, decalin, isopropanol) as well as the experiment without any solvent, at all three temperatures, and the results are summarized in **Figure 37**, showing the solid conversion achieved for the different reaction conditions. The graphs for TGA-DSC and MS used in this analysis can be seen in appendix **B) TGA-DSC and MS for solid conversion comparison of solvents**. All solvents are better than no solvent (isopropanol is better than no solvent at similar temperatures; however, can not achieve better conversion by increased temperatures). Tetralin is the best solvent, achieving the highest conversion at all temperatures, while solid conversion in isopropanol appears to not improve with an increase in temperature. A possible explanation for this is that pressure was not maintained in the reactor, supported by the numbers during weighing in **Table 9**. The performance of decalin is similar to that of tetralin; however, lower solid conversion is achieved under all conditions tested. This is in accordance to what is expected due to tetralin being a superior hydrogen-donor solvent as explained in **2.5.3 Liquefaction solvents**.

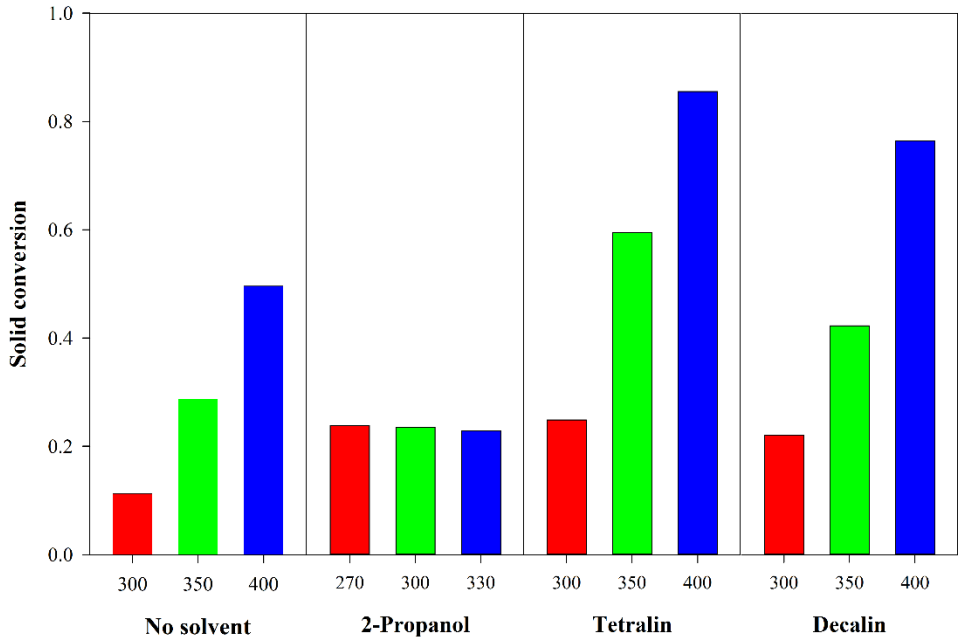

Figure 37 Solid conversion based on TGA analysis for the three different reaction temperatures and solvents.

Adding catalyst to isopropanol appears to improve conversion significantly for all cases except the lowest temperature (270 °C). The best effect is seen for 330 °C, in **Figure 38**. Zinc catalyst shows the largest improvement compared to no catalyst, improving solid conversion from 22.91 % to 76.11 %. Potassium hydroxide also shows an improvement similar to that of Co^{2+}.

Due to the existence of catalyst on the solid residue, a correction has to be made before solid conversion is calculated. Based on the results from SEM-EDS in combination with the results

from TGA, roughly 60 % of the catalyst loaded remains on the solid residue after reaction in tetralin, while only 20 % of the catalyst loaded remains on the solid residue after reaction with isopropanol. Due to SEM-EDS being performed for solid residue after reaction at maximum temperature, these values are assumed to be the maximum loss of catalyst. Loss of catalyst is not expected to vary much for isopropanol as it is related to the solubility; however, it is expected to vary for tetralin, as it is related to the solid conversion.

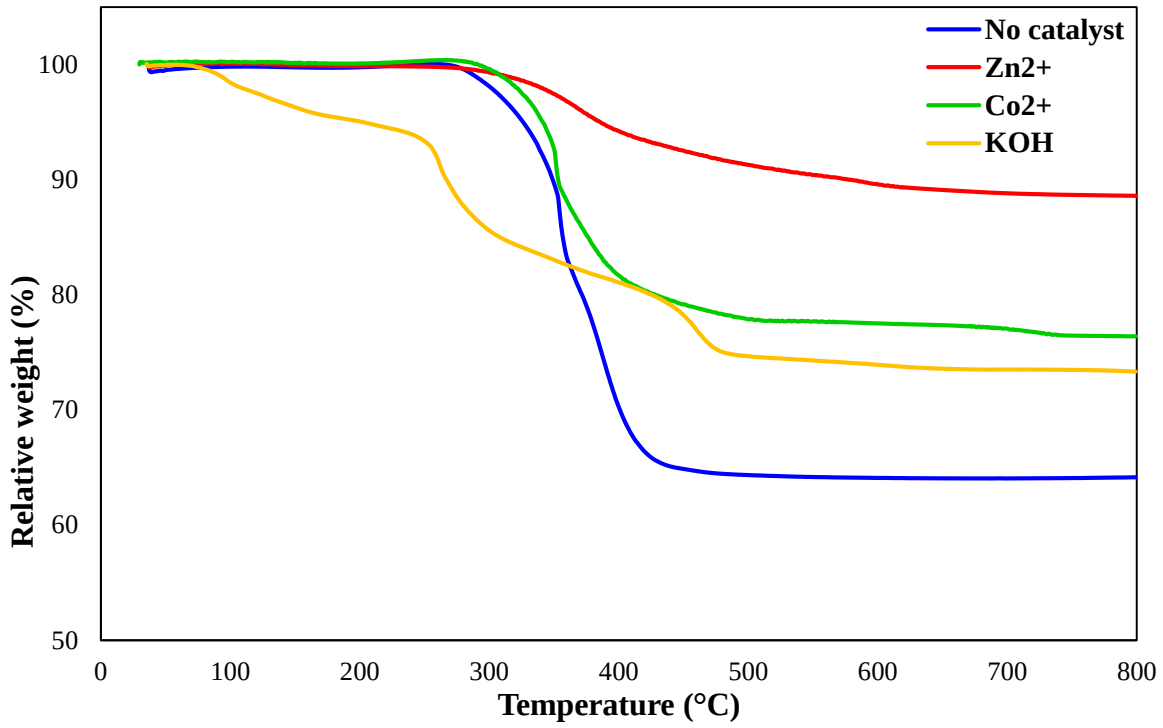

Figure 38 TGA profiles of solid residue with different catalysts (Zn^{2+}, Co^{2+}, KOH and no catalyst) after reaction in isopropanol at 330 °C.

Figure 39 summarizes the solid conversion achieved in all the reactions performed using isopropanol as a solvent, for all the different catalysts and temperatures analyzed. The graphs for TGA-DSC and MS used in this analysis as well as the similar analyses for tetralin and decalin can be seen in appendix **C) TGA-DSC and MS for solid conversion comparison of catalysts**. At 270 °C, adding catalyst appears to have little effect on conversion, likely due to the low overall conversion at this temperature. At 300 °C, cobalt and potassium hydroxide improves solid conversion significantly, from 23.52 % to 44.17 % and 35.45 %, respectively. At the highest temperature of 330 °C, all catalysts improve solid conversion by a large amount, and zinc yields the best results. The results are varied, and no specific trend can be observed. This is likely due to a loss of pressure during reaction.

Pressure is important for the liquefaction in isopropanol; however, with the simple setup it was not possible to monitor or maintain pressure during reaction. Therefore, reactors were weighed before reaction, after reaction and after evacuating the reactor to record any gas loss, indicating limited pressure capacity of the reactors. **Table 9** summarizes the gas loss recorded, and it is clear that the reactors are unable to maintain the required pressure for the reaction.

Of particular interest is the large gas loss when KOH is used as a catalyst. This loss is similar for all temperatures, and slightly higher in quantity than the amount of isopropanol added. A higher solid conversion may be possible for all isopropanol experiments given a completely sealed reactor, as may be indicated by the reaction with zinc catalyst at 330 °C, where gas loss is lower than usual and solid conversion is significantly higher.

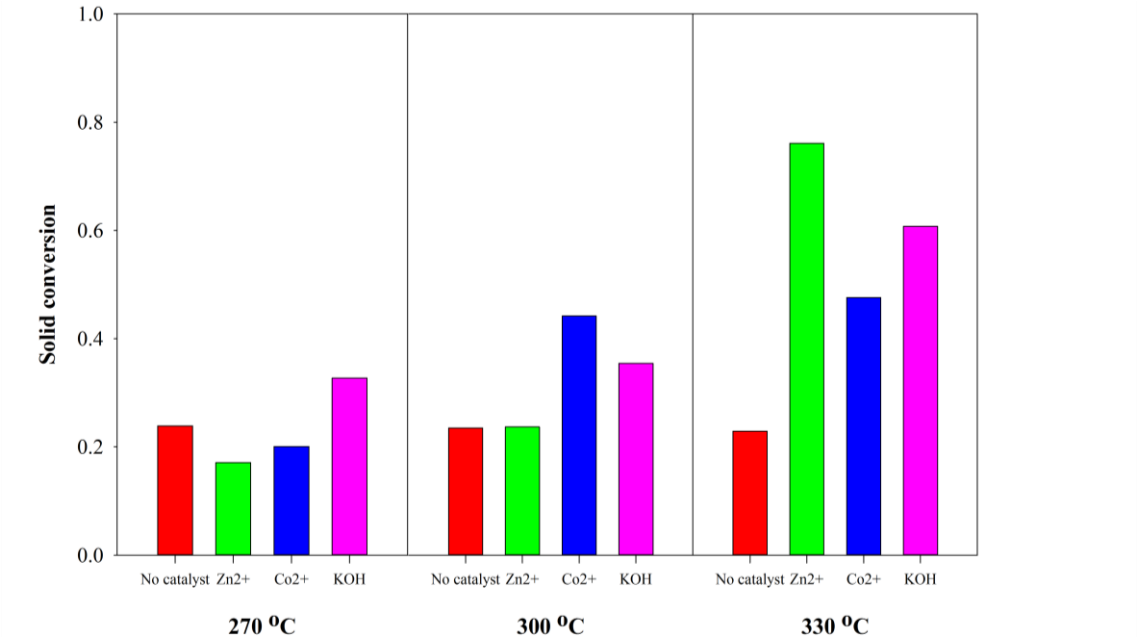

Figure 39 Solid conversion based on TGA analysis for isopropanol reaction at three reaction temperatures with different catalysts.

Table 9 Gas loss recorded during reaction by weighing the reactor before reaction, after reaction and after evacuating the reactor.

		Gas loss during reaction (g)	Gas remaining after reaction (g)
270 °C	No catalyst	0.008	0.5359
	Zinc	0.0473	0.4247
	Cobalt	0.6633	0.0632
	KOH	0.8237	0.0029
300 °C	No catalyst	0.3817	0.0534
	Zinc	0.4802	0.0901
	Cobalt	0.7178	0.0038
	KOH	0.8138	0.0003
330 °C	No catalyst	0.095	0.2725
	Zinc	0.0259	0.1679
	Cobalt	0.2796	0.1012
	KOH	0.8491	0.0007

Tetralin showed the most promising results as a liquefaction solvent, and **Figure 40** displays the TGA profiles of the solid residue after reaction in tetralin with different catalysts. A larger drop can be seen in the temperature range of ~50-180 °C in catalyzed runs, indicating either more tetralin remaining in these samples or an increased water production. The former is less likely, due to the existence of this weight loss only in catalyzed runs, thus an increased water production is observed for catalyzed runs. Solid conversion also appears lower for catalyzed runs than without any catalyst added. **Figure 41** supports this, showing the solid conversion for all runs in tetralin at the three temperatures tested, with and without catalysts. Conversion at 300 °C using zinc as a catalyst is virtually nonexistent, and TGA results show no solid conversion for this experiment.

Poor performance for the catalysts could be explained by catalyst covering reaction sites, hindering conversion to a greater degree than it is promoting. Comparing the results from tetralin to the results from isopropanol, impregnating the catalyst yields poor performance compared to introducing a soluble form of the catalyst. It is also possible that impregnation could yield better results if less catalyst was impregnated, as 10 wt% is larger than most processes use (2.5 wt% pyrite is mentioned by Kaneko et al.[25] as a high concentration). Another alternative is to use oil soluble precursors such as naphthenic acid salts.

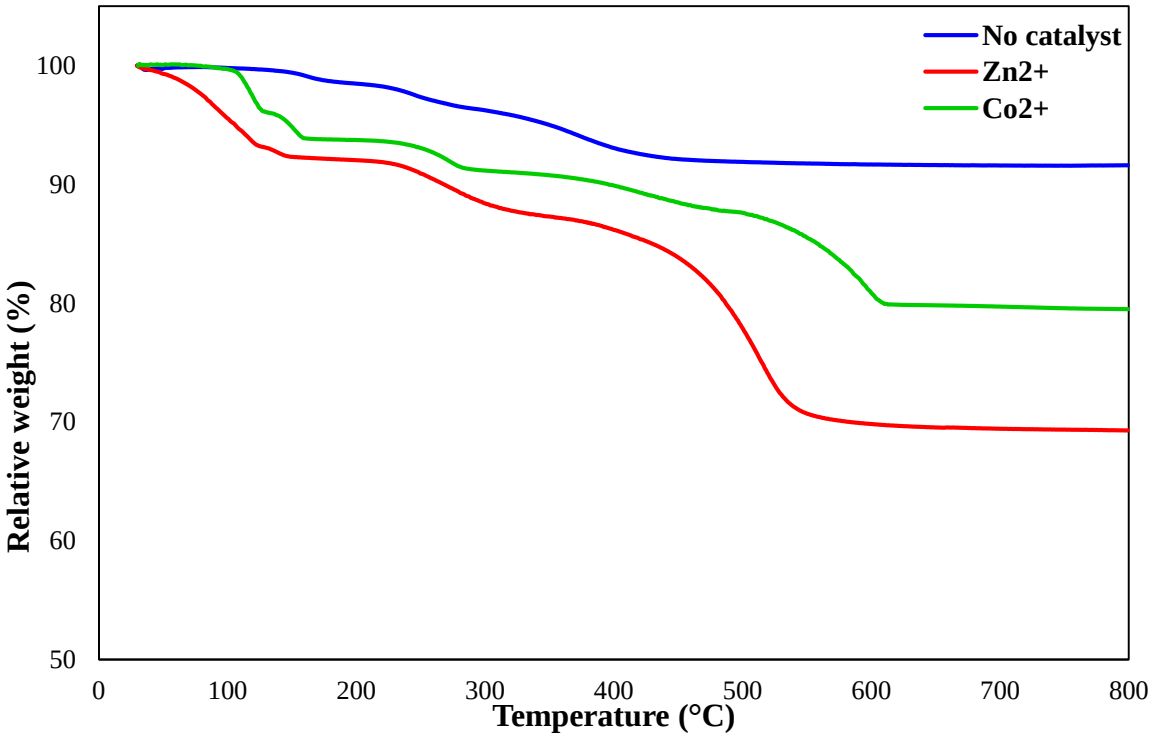

Figure 40 TGA profiles of solid residue with different catalysts (Zn^{2+}, Co^{2+} and no catalyst) after reaction in tetralin at 400 °C.

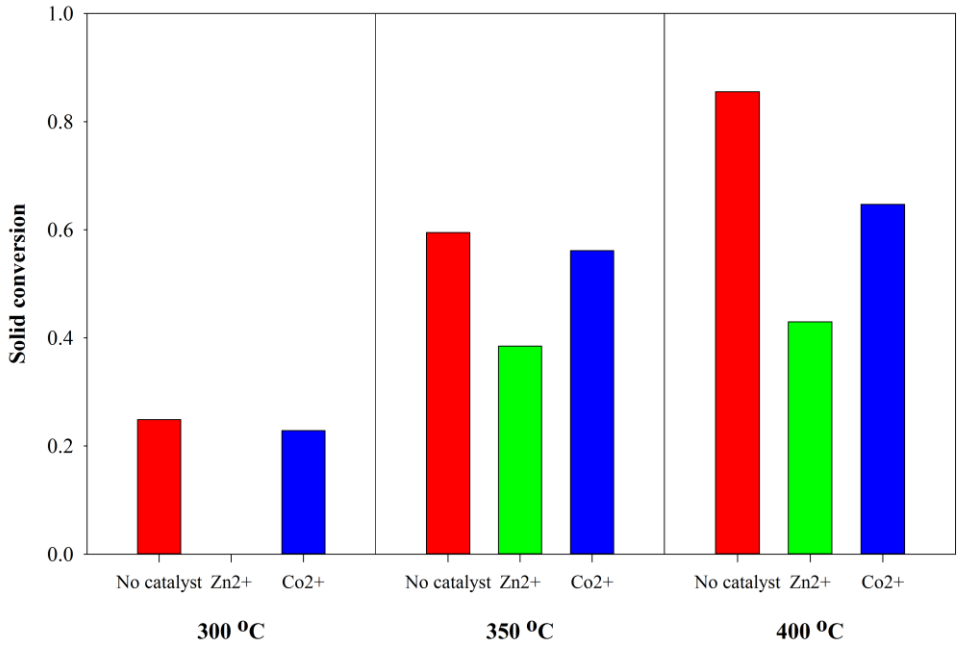

Figure 41 Solid conversion based on TGA analysis for tetralin reaction at three reaction temperatures with different catalysts.

Decalin is the third solvent tested, and has large similarities to tetralin. Without catalyst, decalin performed similarly to tetralin, while exhibiting lower solid conversions. Adding catalysts, it is

expected to see a similar trend. **Figure 42** shows the TGA profiles for the solid residue after reaction in decalin at 400 °C with and without catalysts. The profiles are similar to those from reaction in tetralin; however, there is a smaller weight loss in the 50-180 °C range, indicating less production of water. The overall solid conversion, seen in **Figure 43**, is lower than in tetralin for all conditions, and catalysts appear to exhibit lower performance than for tetralin, with the exception of 350 °C, where cobalt catalyst improves solid conversion compared to no catalyst. However, the solid conversion remains lower than that of tetralin nonetheless.

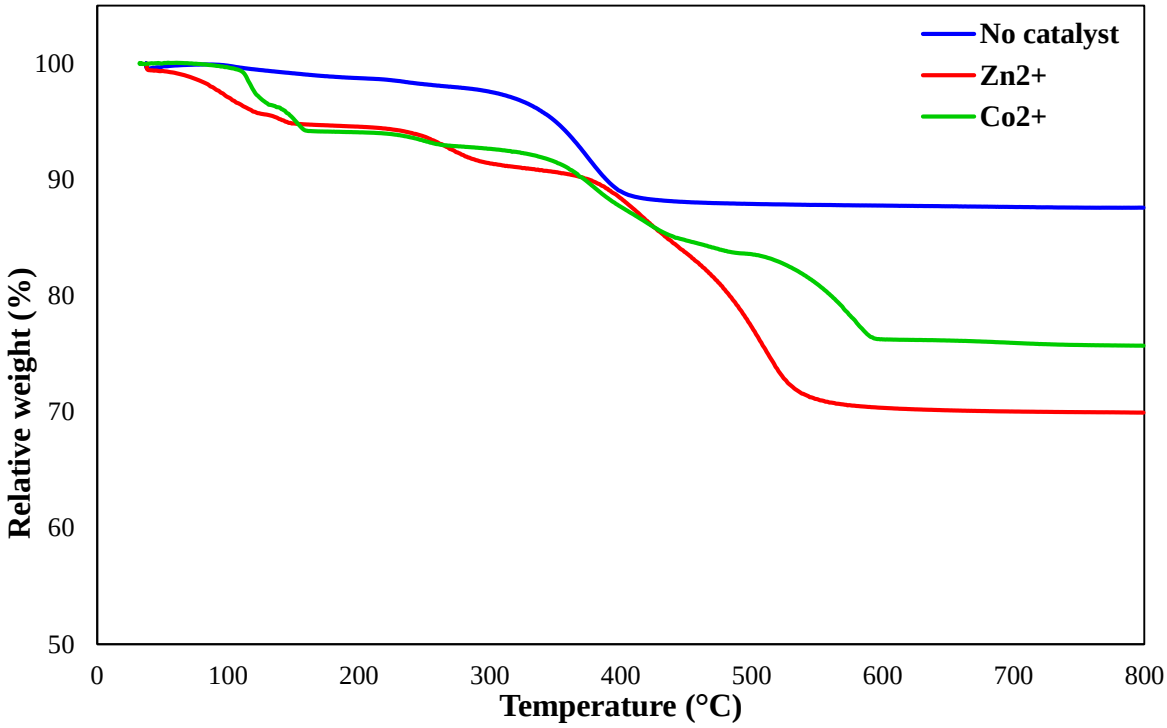

Figure 42 TGA profiles of solid residue with different catalysts (Zn^{2+}, Co^{2+} and no catalyst) after reaction in decalin at 400 °C.

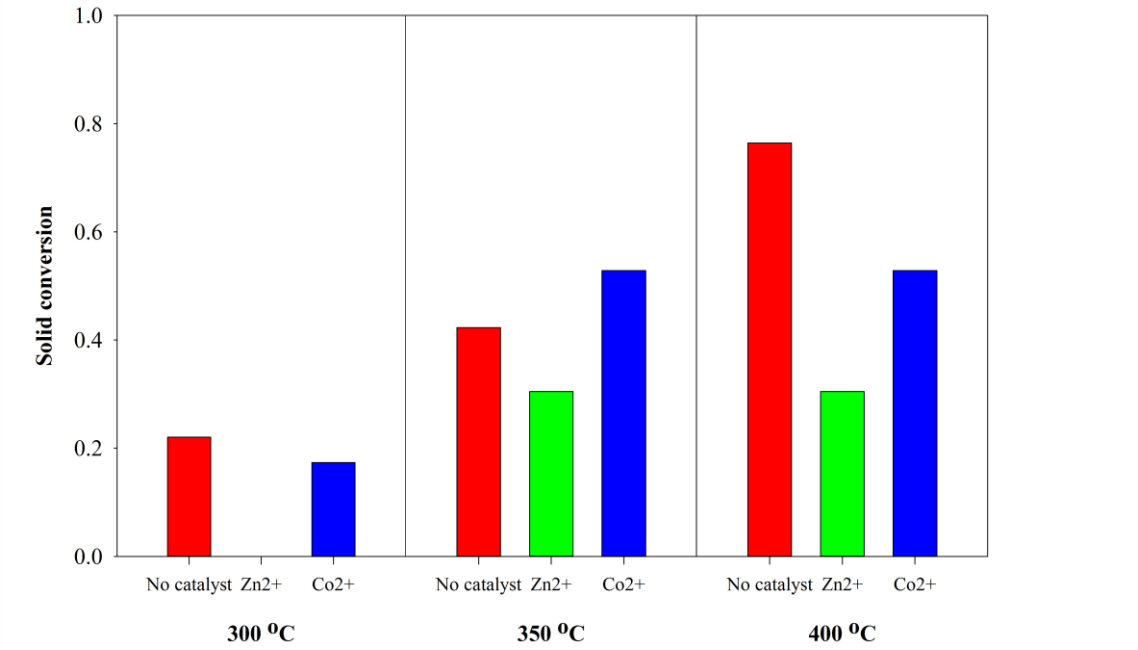

Figure 43 Solid conversion based on TGA analysis for decalin reaction at three reaction temperatures with different catalysts.

As a summary, tetralin performed best as a solvent, achieving 85.55 % solid conversion at 400 °C, without any catalyst. Decalin performed similarly to tetralin, while achieving 76.45 % solid conversion at the same conditions. While isopropanol alone did not perform appreciably, the addition of catalyst showed promise, where zinc catalyst increased solid conversion significantly, to 76.11 %. In conclusion, soluble catalyst precursors perform better than impregnated catalyst precursors.

4.5.3 XRF of liquid product

XRF was performed with the purpose of analyzing the amount of catalyst transferred to the liquid phase during reaction and extraction. Due to the XRF being unable to detect hydrocarbons (the main constituent of the liquid product), calcium nitrate was added to compare to the weight of the catalyst detected. While successful, the values obtained do not comply with results obtained in EDS. It is therefore concluded that XRF alone is insufficient to detect the amount of catalyst transferred to the liquid product.

Table 10 shows the results of the test where calcium was added to the liquid product after reaction at max temperature for both isopropanol and tetralin with Co^{2+} catalyst. The obtained percentages of 3.09 % for tetralin and 7.73 % for isopropanol do not comply with the results from EDS, where expected values are ~41 % catalyst in the liquid for tetralin and ~82 % for isopropanol.

Table 10 XRF results with calcium added to identify the amount of catalyst in the liquid product.

	Tetralin	**Isopropanol**
Calcium added (mg)	10.01	6.40
Calcium detected (wt%)	37.40	16.30
Cobalt detected (wt%)	7.12	12.10
Mass of catalyst (mg)	1.91	4.75
Percentage of loaded catalyst	3.09	7.73

XRF is insufficient to quantify the amount of catalyst in the liquid product; however, it still serves as a good qualitative analysis to detect impurities in the product received. **Table 11** shows the results from XRF on the liquid product after reaction at 330 °C in isopropanol and 400 °C in tetralin for both zinc and cobalt catalyst. Many compounds are detected, among which silicon, potassium, aluminium, iron and sulfur are not expected to be found in the liquid product. All of these elements are found on the original oil shale, and silicon in particular is found in the mineral matrix. The large quantity of some of these compounds (silicon in particular) indicates significant contamination of the liquid product by solid residue, likely during extraction. Due to this it is recommended to perform a more precise extraction, such as filtration, to separate the liquid and solid phase. It is also worth noting that chlorine is present in higher concentrations in the isopropanol product.

Table 11 Results from XRF analysis on the liquid product after reaction in tetralin at 400 °C and isopropanol at 330 °C, with zinc and cobalt catalyst.

Tetralin				**Isopropanol**			
Zn		Co		Zn		Co	
Component	Mass %	Component	Mass %	Component	Mass %	Component	Mass %
Si	34.3	Si	65	Cl	50.3	Cl	48
Cl	24.2	Al	10.1	Fe	26.9	Si	26.1
Zn	20	Cl	8.87	Zn	16.6	Fe	10.4
K	10.3	K	7.11	K	3.78	Co	6.46
S	6.55	S	4.54	Si	1.52	Al	3.75
Fe	4.61	Co	3.77	S	0.9	K	3.14
		Fe	0.69			S	1.93
						Ca	0.185

Based on the results from XRF, TGA was performed in air atmosphere on the liquid product to analyze the extent of incombustible contamination. The analysis was performed for the liquid product from reaction in isopropanol at 330 °C and tetralin at 400 °C with zinc catalyst, and can be seen in **Figure 44**. Remaining incombustibles after reaction was 12.87 % in isopropanol

and 5.80 % in tetralin. While it may seem lower for tetralin this is due to the amount of tetralin in the liquid product, which is measured as 44.87 % based on the weight loss from 50-180 °C. This results in 10.53 % incombustibles in the liquid product after reaction in tetralin. The amount of contamination is large, further advocating the need for more precise extraction.

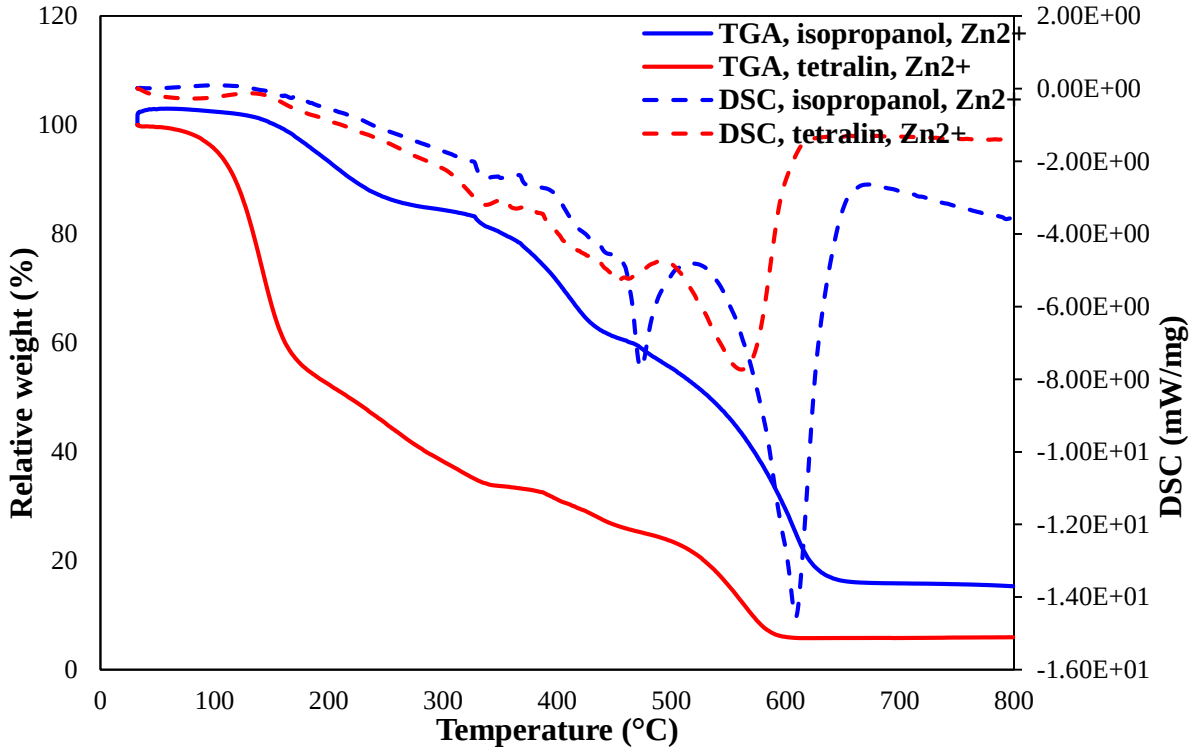

Figure 44 TGA-DSC profiles of liquid product from reaction in isopropanol at 330 °C and tetralin at 400 °C with zinc catalyst

4.5.4 Py-GC/MS of liquid product

Pyrolysis was performed on the liquid product obtained after reaction and extraction. The purpose was to use GC and MS to analyze the product distribution with a primary focus on paraffin-to-olefin ratio. Pyrolysis temperature was selected based on EGA of the liquid product, selecting a temperature for maximum product analysis while limiting pyrolysis reactions of the product. An example of this analysis can be seen in **Figure 45**. A pyrolysis temperature of 440 °C was selected for the liquid product from reaction in isopropanol, while a higher pyrolysis temperature of 460 °C was selected for the liquid product from reaction in tetralin and decalin. Similar pyrolysis temperatures were found to be optimal for all liquid products, regardless of reaction temperature and catalyst.

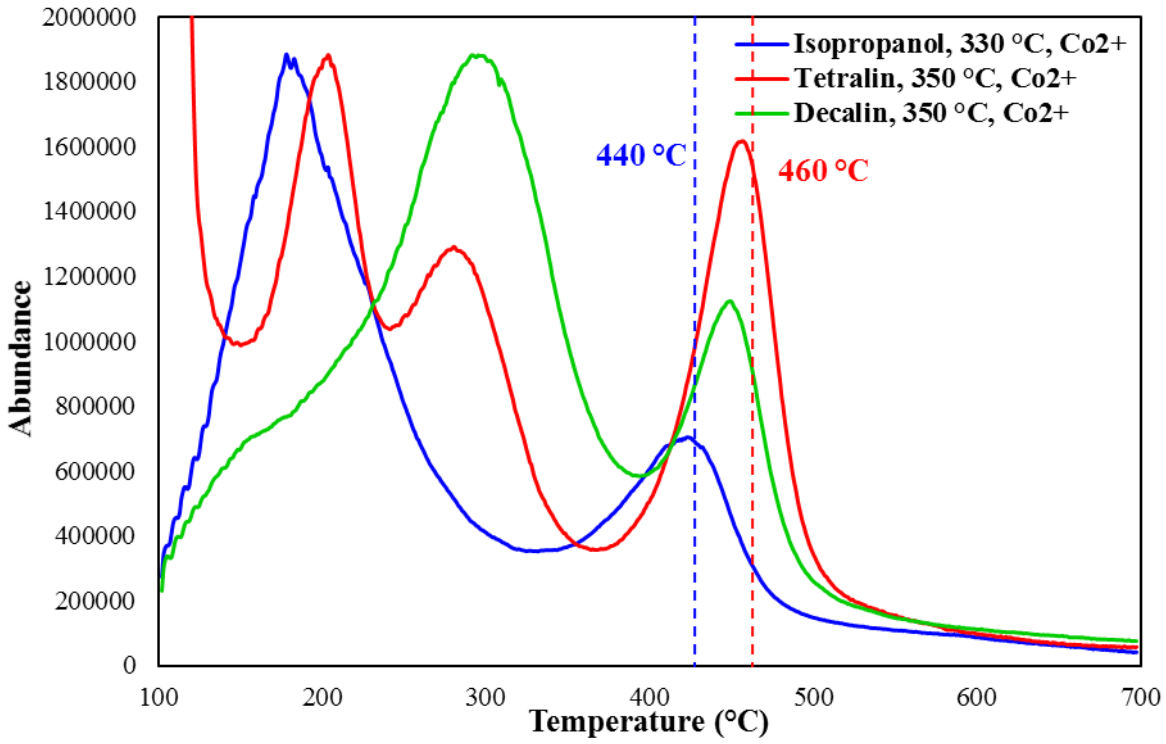

Figure 45 EGA profiles of liquid product after reaction in isopropanol (at 330 °C), tetralin and decalin (at 350 °C) for Co^{2+} catalyzed kerogen, used to find the pyrolysis temperature.

During pyrolysis analysis of tetralin and decalin, a large amount of naphtha-like products (decalin, tetralin, naphthalene) were detected. While some production of tetralin and similar compounds may occur, this is generally in small amounts (~1 % tetralin for pyrolysis of decarbonated kerogen at 550 °C), and the detected compounds here are in significant quantities. The reason for the large quantity of these compounds is the tetralin or decalin added as a solvent, which can not be separated from the liquid product. It is therefore decided to exclude all these compounds (any C_{10} or C_{20} compounds with large similarities to naphthalene, tetralin or decalin) from the quantification analysis to make the comparison between solvents more accurate. **Figure 46** shows the product distribution based on carbon number without excluding these compounds, while **Figure 47** shows the product distribution after excluding the compounds.

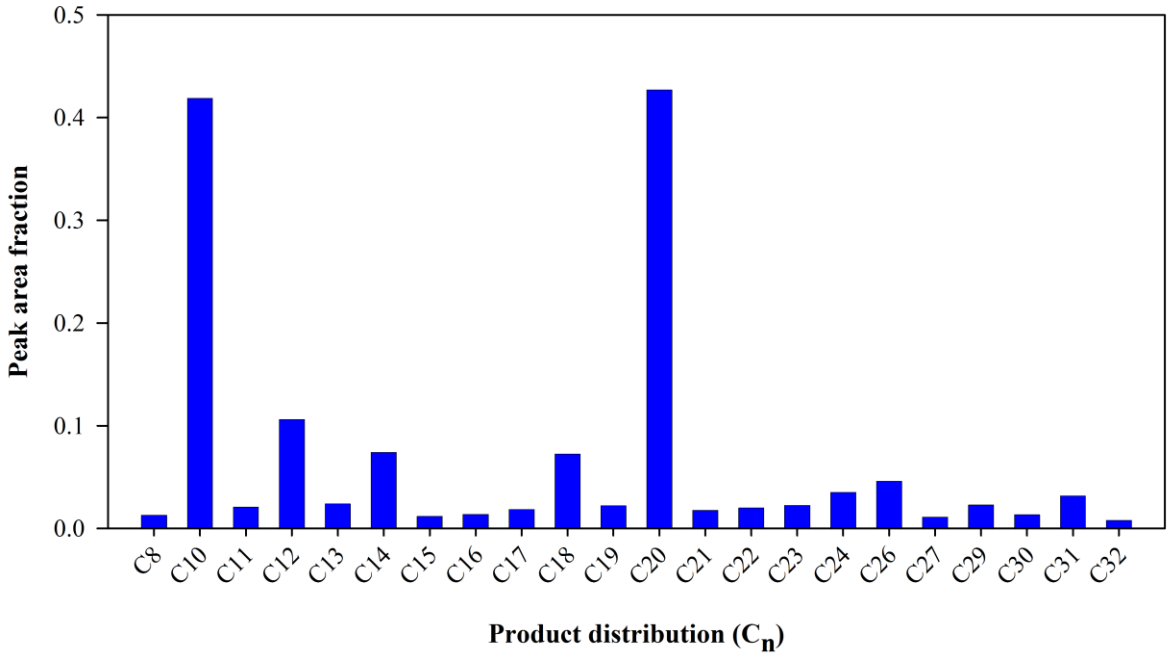

Figure 46 Liquid product distribution after reaction in tetralin at 400 °C, without added catalyst.

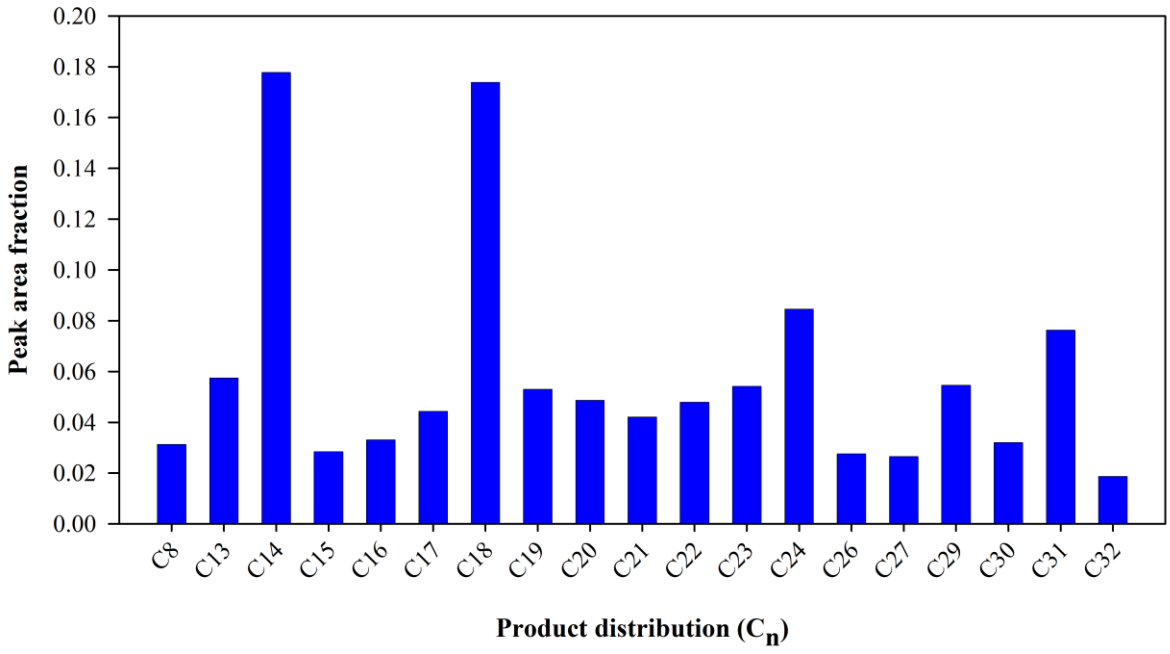

Figure 47 Liquid product distribution after reaction in tetralin at 400 °C, without added catalyst after removal of tetralin, naphthalene and coke-like compounds.

After pyrolysis, an analysis similar to that explained in **4.4 Pyrolysis analysis of 10 wt% Zn2+ catalyst** is performed for all liquid product samples. All liquid products are compared to the products from the reaction without any solvent or catalyst at a similar temperature. Results from the analysis of liquid products after reaction in isopropanol are presented in **Figure 48 - Figure 53**. It is worth noting that few low carbon number compounds (C_3-C_7) are detected during this analysis. This is a result of the drying process that was performed after extraction, which led to the loss of volatile compounds. While the lack of analysis for these compounds may skew the results to some degree, it is still expected to provide a sufficient comparison of solvent and catalyst performance.

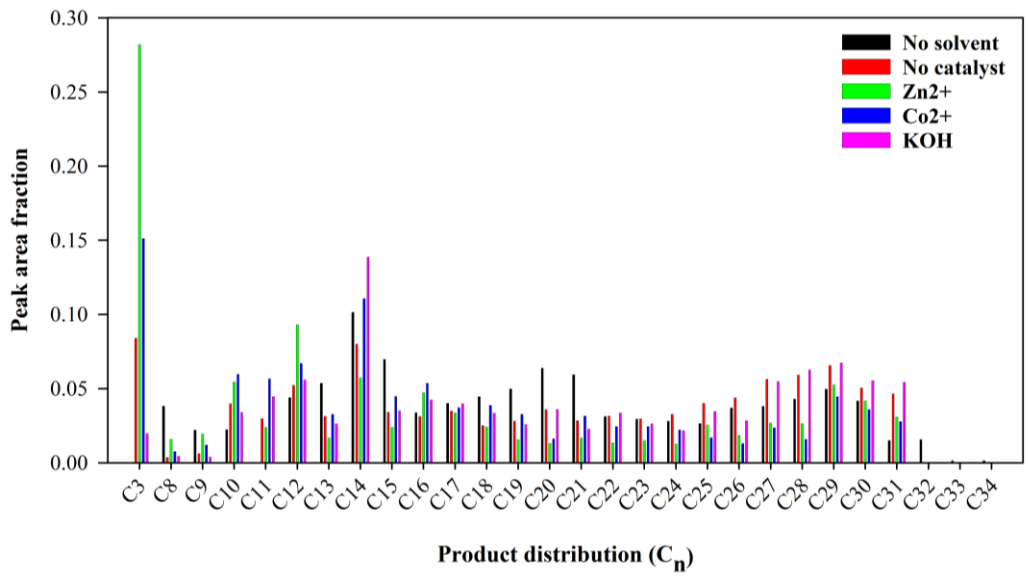

Figure 48 Liquid product distribution after reaction in isopropanol at 270 °C for the different catalysts used, compared to no solvent (at 300°C) or catalyst.

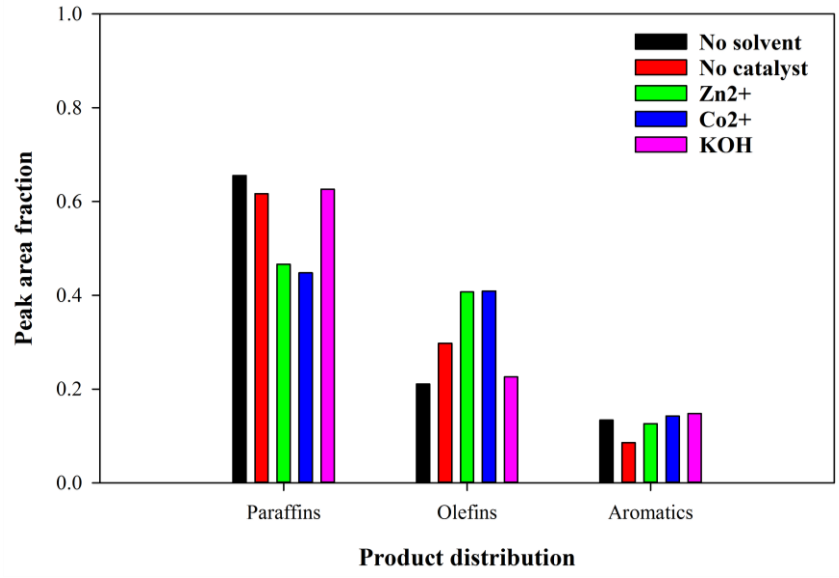

Figure 49 Paraffin, olefin and aromatics ratio of liquid product after reaction in isopropanol at 270°C for the different catalysts used, compared to no solvent (at 300 °C) or catalyst.

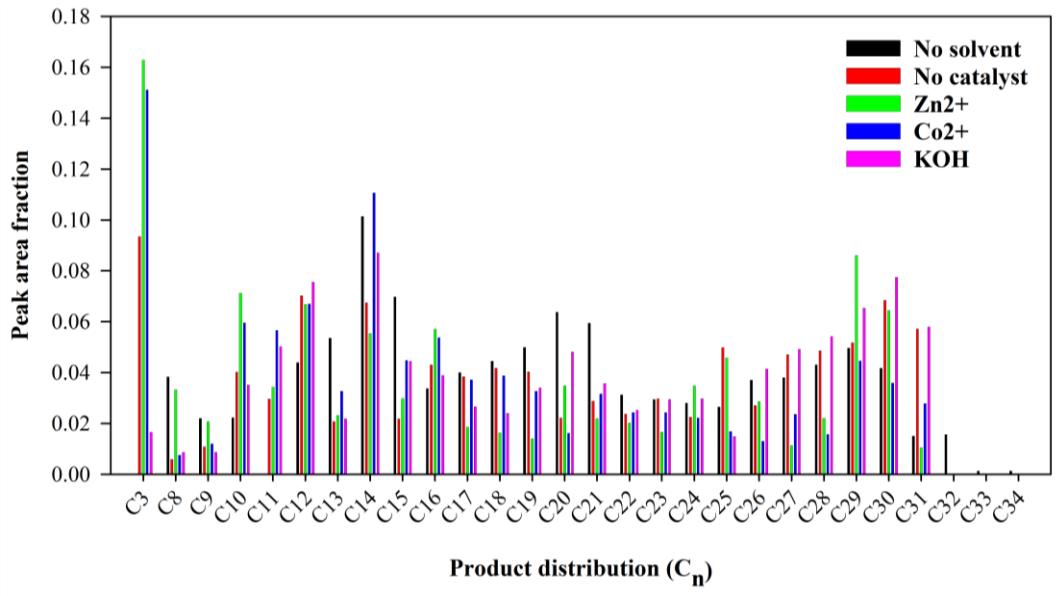

Figure 50 Liquid product distribution after reaction in isopropanol at 300 °C for the different catalysts used, compared to no solvent (at 300°C) or catalyst.

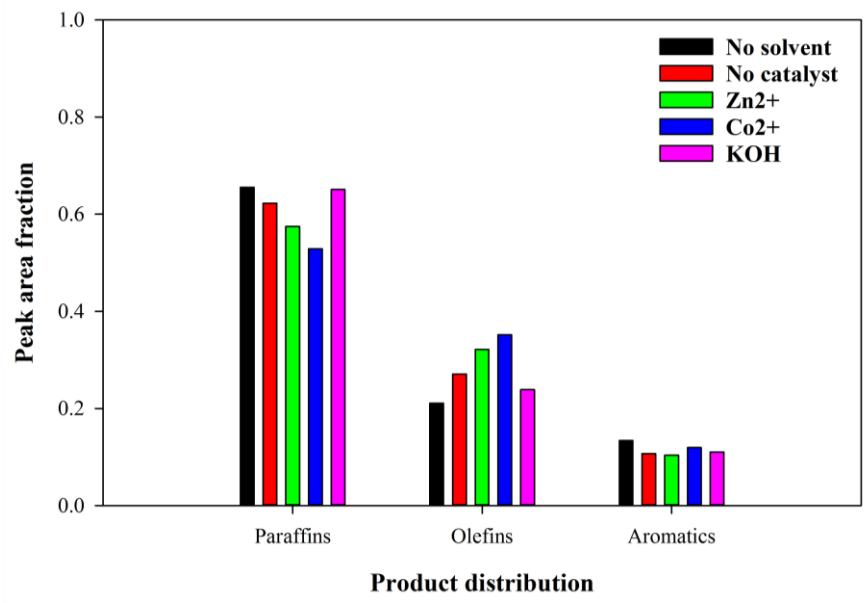

Figure 51 Paraffin, olefin and aromatics ratio of liquid product after reaction in isopropanol at 300°C for the different catalysts used, compared to no solvent (at 300 °C) or catalyst.

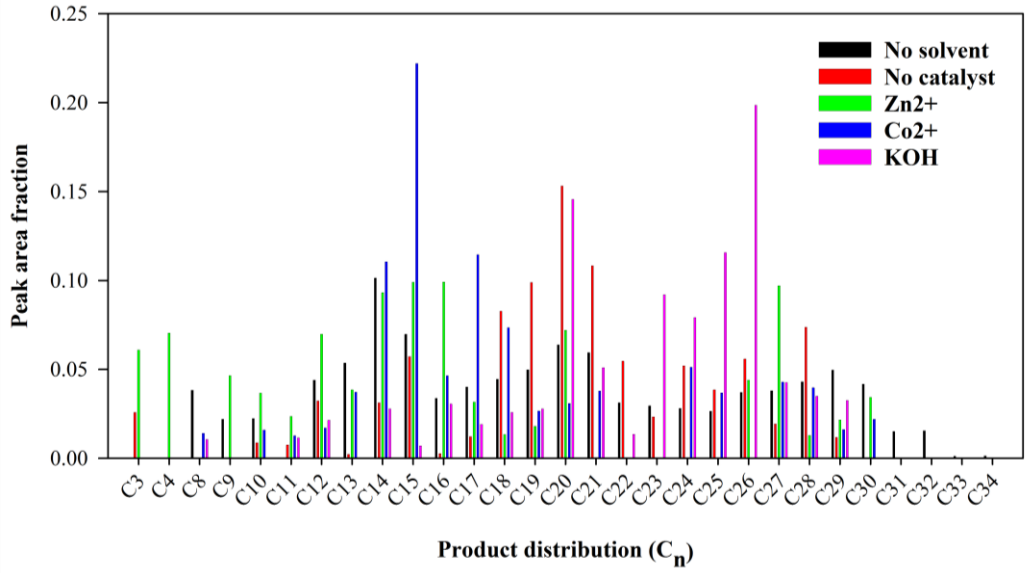

Figure 52 Liquid product distribution after reaction in isopropanol at 330 °C for the different catalysts used, compared to no solvent (at 300°C) or catalyst.

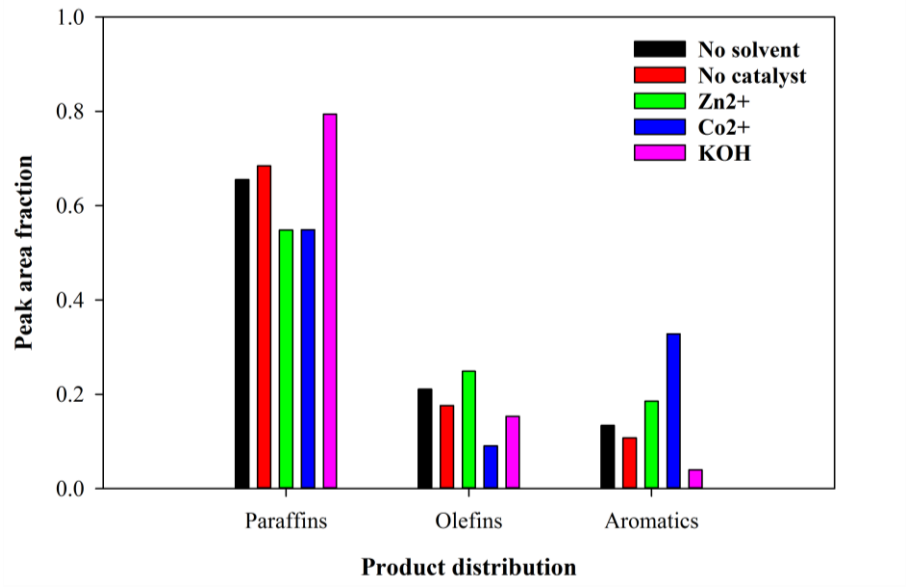

Figure 53 Paraffin, olefin and aromatics ratio of liquid product after reaction in isopropanol at 330°C for the different catalysts used, compared to no solvent (at 300 °C) or catalyst.

Effect of reaction temperature can be seen for both product distribution as well as paraffin-to-olefin-to-aromatics ratio. Comparison between **Figure 48**, **Figure 50** and **Figure 52** reveals a lower amount of C_3 with an increase in temperature, while the amount of heavier fractions (C_{15}-C_{27}) are increased. While KOH as a catalyst appears to improve heavier fraction content slightly, the metal ion catalysts seem to have a cracking effect, increasing the amount of C_3-C_{16} and reducing the amount of heavier fractions. The amount of C_3 is of importance for the isopropanol experiment. While some of the C_3 detected may be residue from the isopropanol solvent, it is expected that most of it is caused by cracking during the pyrolysis analysis. The amount of C_3 decreases with liquefaction reaction temperature, indicating less cracking reactions of the liquid product during pyrolysis.

Paraffin-to-olefin-to-aromatic ratio displayed in **Figure 49**, **Figure 51** and **Figure 53** supports this assumption, showing improved paraffin-to-olefin ratio at higher temperatures. A possible explanation to why this occurs is that the amount of liquid available is lower for the first two pyrolysis experiments (pyrolysis uses 0.1-0.5 mg of sample, introducing large sample size varieties), which in turn increases pyrolysis heating rate. While this complicates the product analysis, as pyrolysis cracking increases olefin ratio compared to the actual liquid product, it can only be concluded based on the results obtained that a higher liquefaction reaction temperature improves paraffin-to-olefin ratio in isopropanol solvent.

The effect of isopropanol as a liquefaction solvent compared to using no solvent seems to be limited for paraffin-to-olefin ratio. This could indicate poor hydrogen-donor capabilities of

isopropanol for the conditions tested. The effect of catalyst is more profound, with zinc and cobalt catalyst reducing the amount of paraffins in the product. Zinc increases the amount of olefins in the product while cobalt increases aromatic content. Potassium hydroxide (KOH) promotes the desired products, yielding more paraffinic product, with much lower aromatic and olefinic content.

Results from the analysis of liquid products after reaction in tetralin are presented in **Figure 54 - Figure 59**.

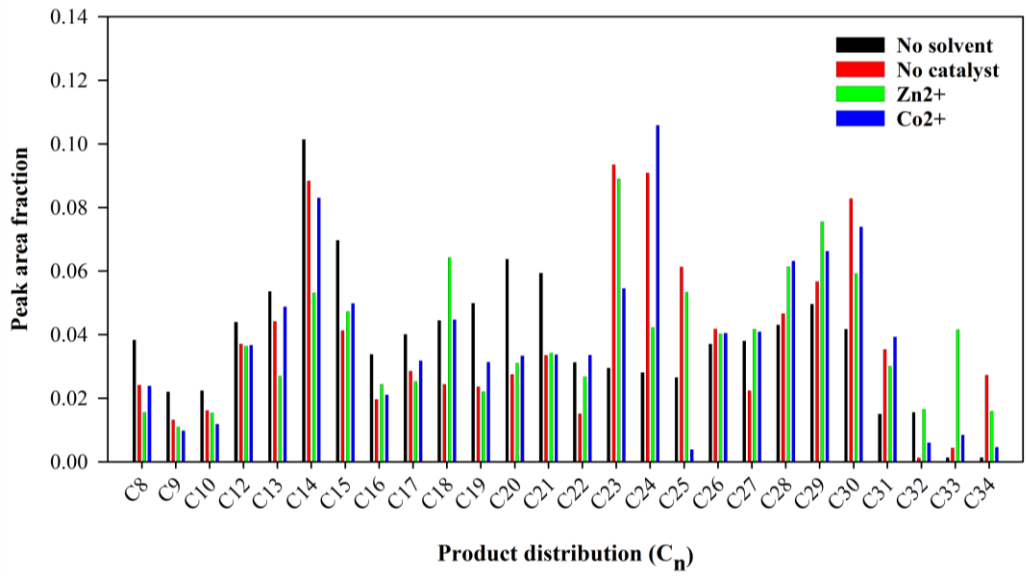

Figure 54 Liquid product distribution after reaction in tetralin at 300 °C for the different catalysts used, compared to no solvent or catalyst.

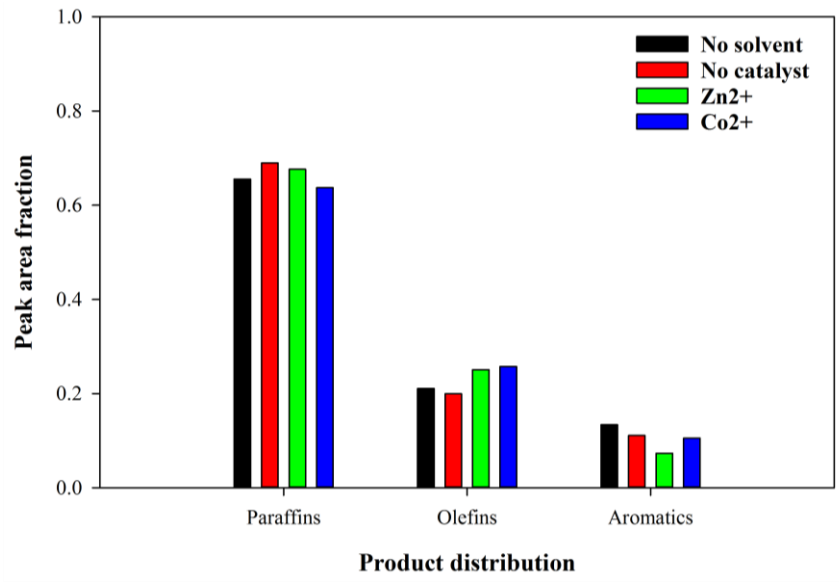

Figure 55 Paraffin, olefin and aromatics ratio of liquid product after reaction in tetralin at 300°C for the different catalysts used, compared to no solvent or catalyst.

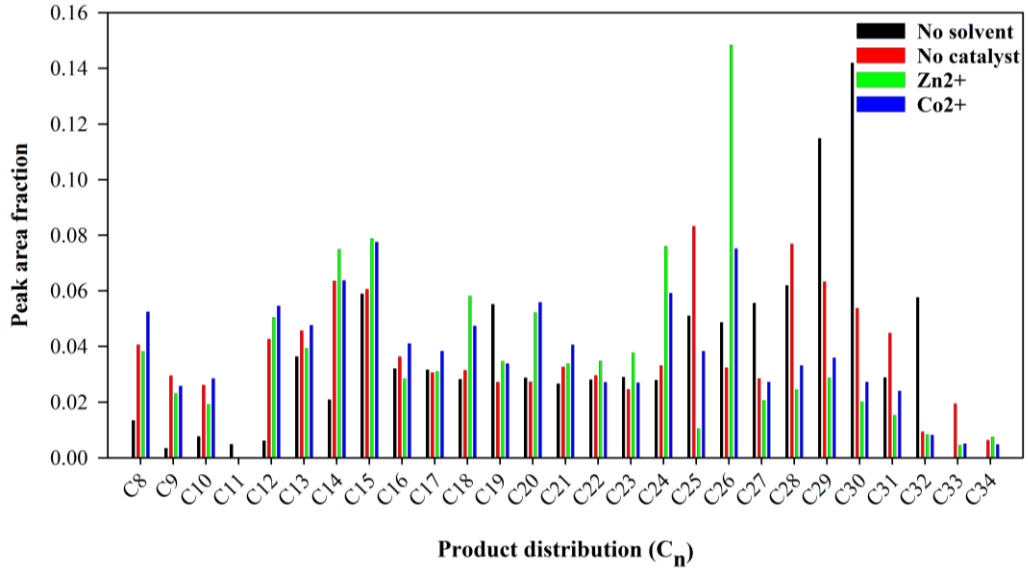

Figure 56 Liquid product distribution after reaction in tetralin at 350 °C for the different catalysts used, compared to no solvent or catalyst.

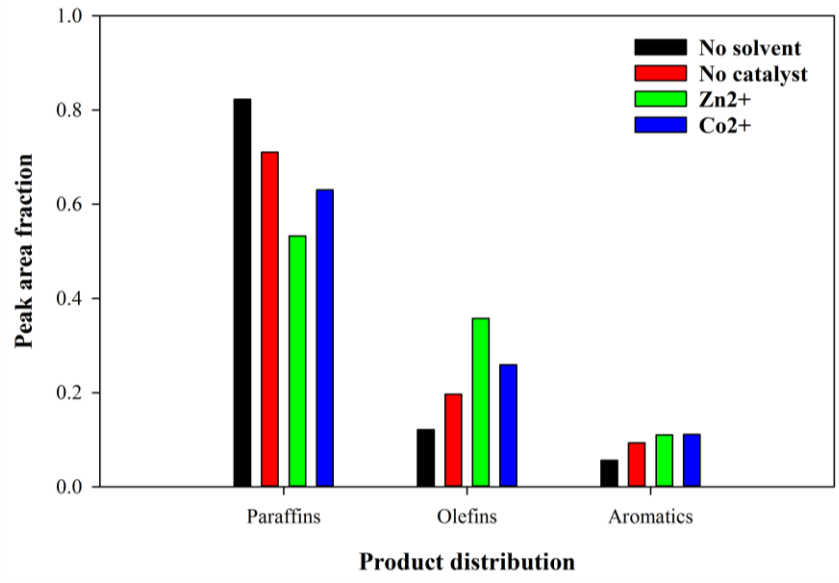

Figure 57 Paraffin, olefin and aromatics ratio of liquid product after reaction in tetralin at 350°C for the different catalysts used, compared to no solvent or catalyst.

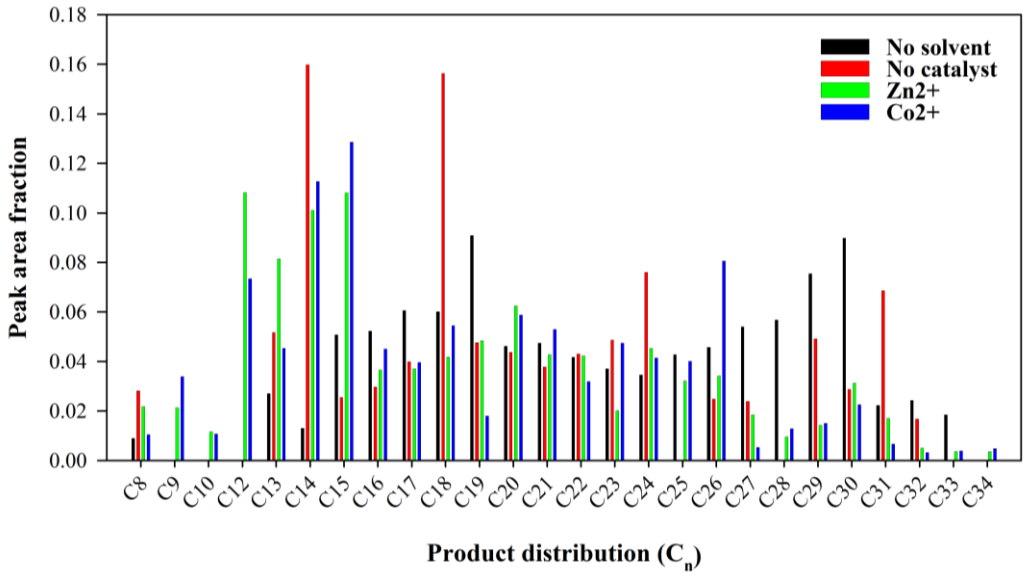

Figure 58 Liquid product distribution after reaction in tetralin at 400 °C for the different catalysts used, compared to no solvent or catalyst.

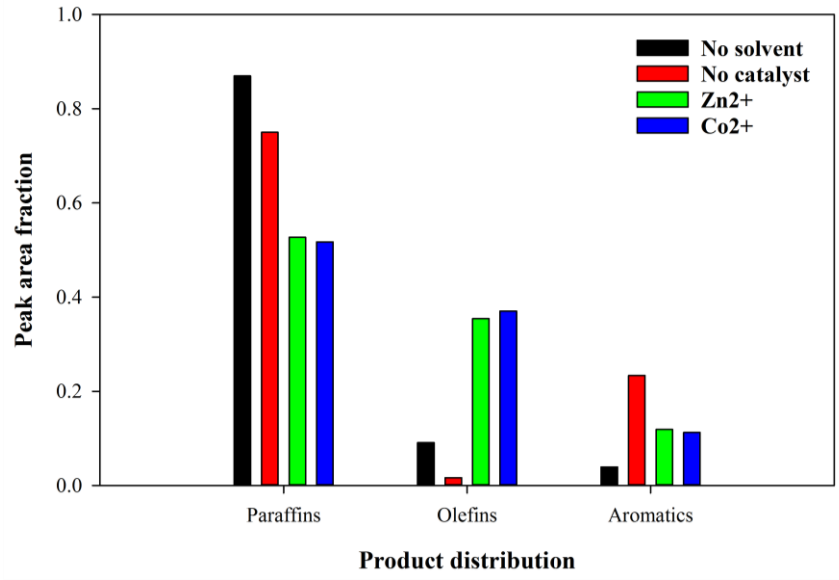

Figure 59 Paraffin, olefin and aromatics ratio of liquid product after reaction in tetralin at 400°C for the different catalysts used, compared to no solvent or catalyst.

Effect of reaction temperature on product distribution, in **Figure 54**, **Figure 56** and **Figure 58**, is more subtle for tetralin than for isopropanol; however, C_{12}-C_{18} content increases with higher temperatures, while C_{23}-C_{32} content is decreased. The metal ion catalysts again display a cracking effect, reducing the amount of larger fractions while increasing the amount of smaller fractions. C_3 is not detected in this analysis. This is mainly due to the high solvent content making the amount of C_3 insignificant and excluded from the analysis. Cracking by pyrolysis is still occurring, and while small, a C_3 peak can still be observed from the pyrogram.

Paraffin-to-olefin-to-aromatic ratios displayed in **Figure 55**, **Figure 57** and **Figure 59** show an increase in paraffinic content with increasing temperature for both the experiment without solvent as well as the experiment with tetralin. This increase in paraffinic content, despite a reduction in the amount of long hydrocarbon chains for the reaction with solvent, indicates the occurrence of hydrogen donation.

Apart from the change in product distribution, the effect of tetralin as a liquefaction solvent compared to using no solvent seems to be limited for paraffin-to-olefin ratio. At high temperature (400 °C) a shift is seen for the reaction in tetralin, reducing the amount of olefins while increasing the amount of aromatics. The effect of catalyst is similar to the experiments with isopropanol, with zinc and cobalt catalyst reducing the amount of paraffins in the product. Zinc shows greater cracking potential at 350 °C, while both catalysts perform similarly at the other temperatures. The effect of catalyst is also increased by temperature, with less paraffinic and more olefinic product from the reaction at 400 °C. This effect is likely caused by the

insoluble catalysts covering reaction sites, promoting pyrolysis catalyzed by zinc or cobalt rather than liquefaction. In this case, no hydrogen donation can occur before the liquid product has been formed, limiting the usefulness of the solvent.

Results from the analysis of liquid products after reaction in decalin are presented in **Figure 60 - Figure 65**.

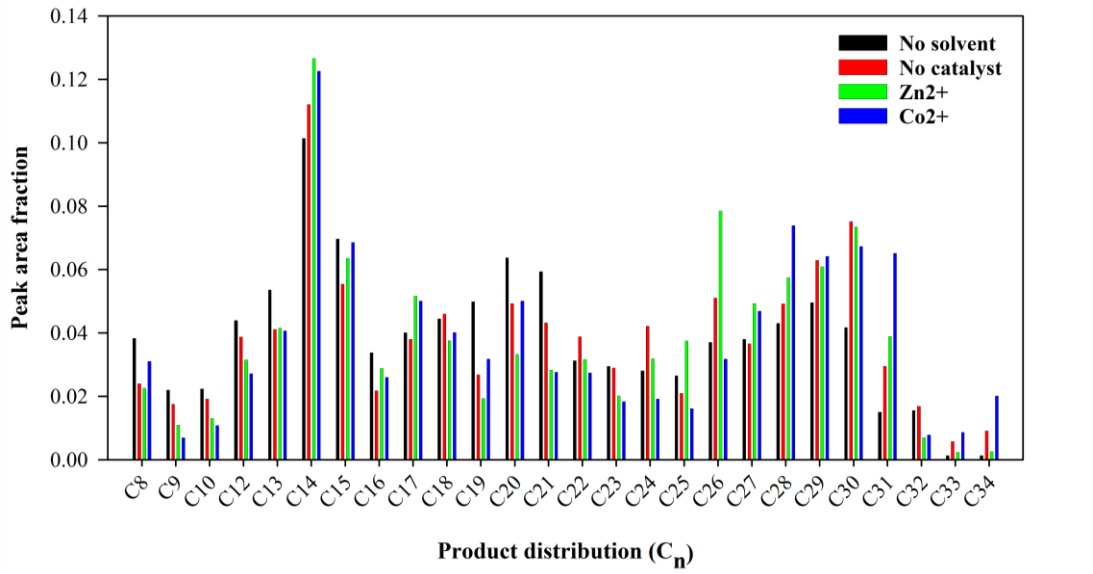

Figure 60 Liquid product distribution after reaction in decalin at 300 °C for the different catalysts used, compared to no solvent or catalyst.

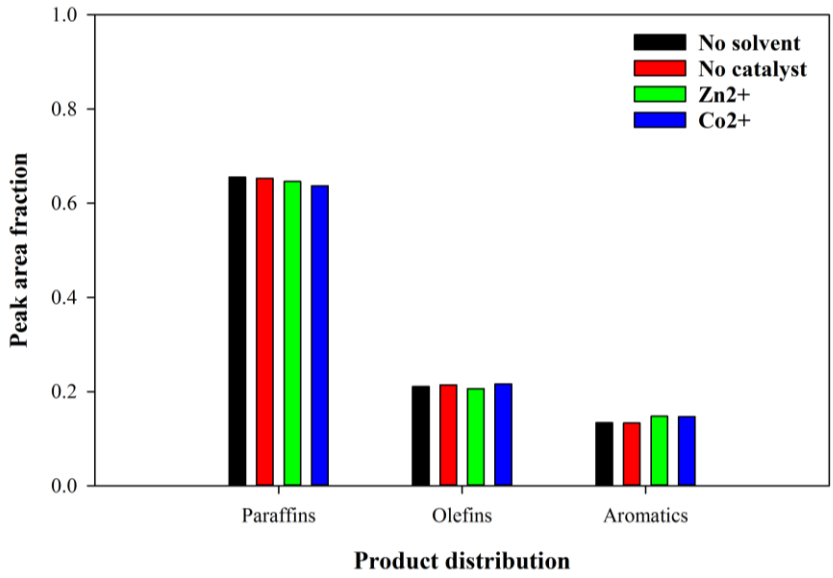

Figure 61 Paraffin, olefin and aromatics ratio of liquid product after reaction in decalin at 300°C for the different catalysts used, compared to no solvent or catalyst.

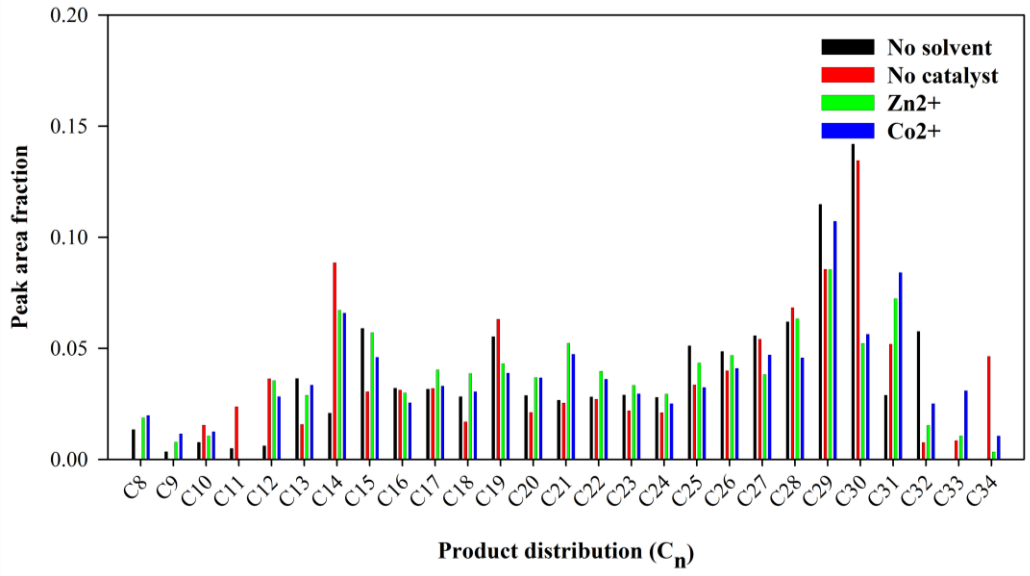

Figure 62 Liquid product distribution after reaction in decalin at 350 °C for the different catalysts used, compared to no solvent or catalyst.

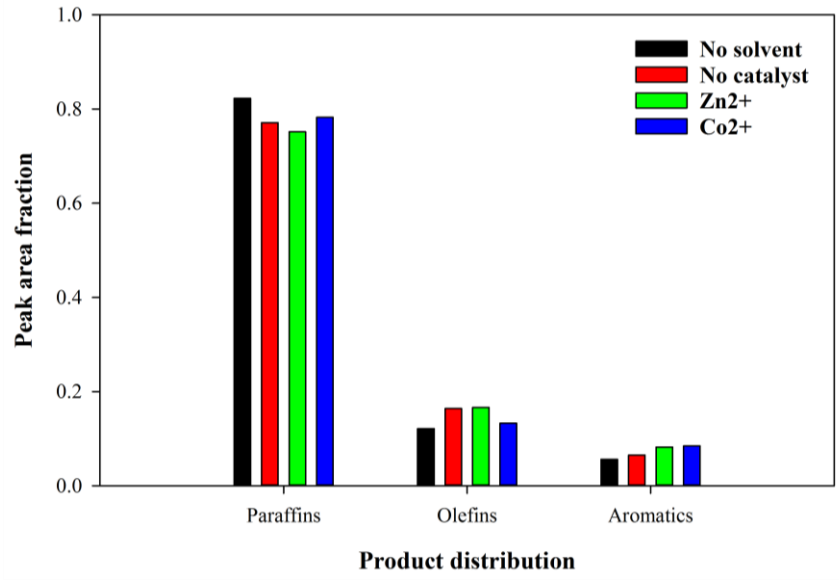

Figure 63 Paraffin, olefin and aromatics ratio of liquid product after reaction in decalin at 350°C for the different catalysts used, compared to no solvent or catalyst.

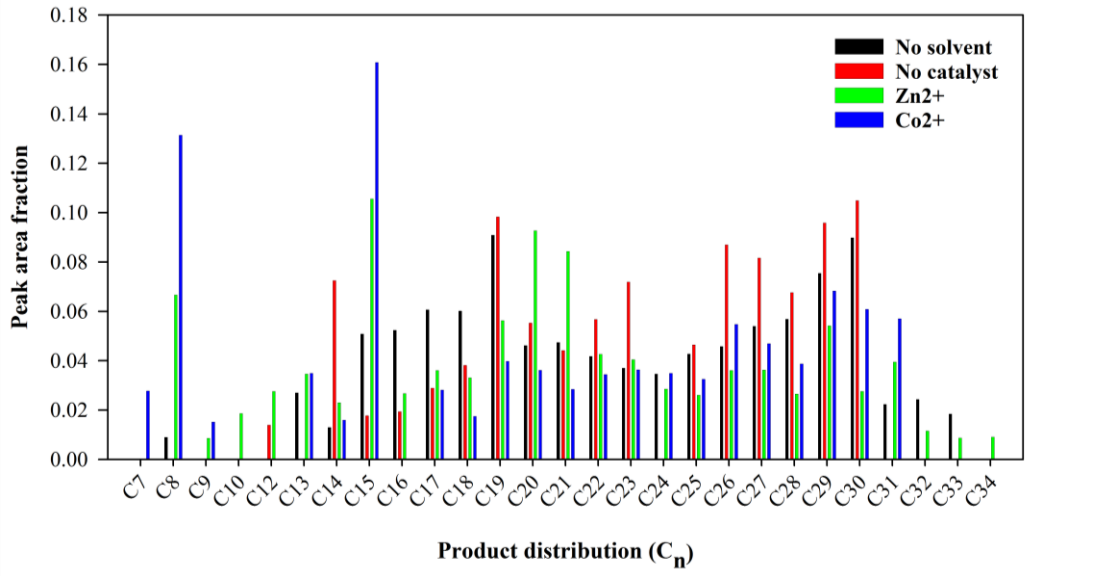

Figure 64 Liquid product distribution after reaction in decalin at 400 °C for the different catalysts used, compared to no solvent or catalyst.

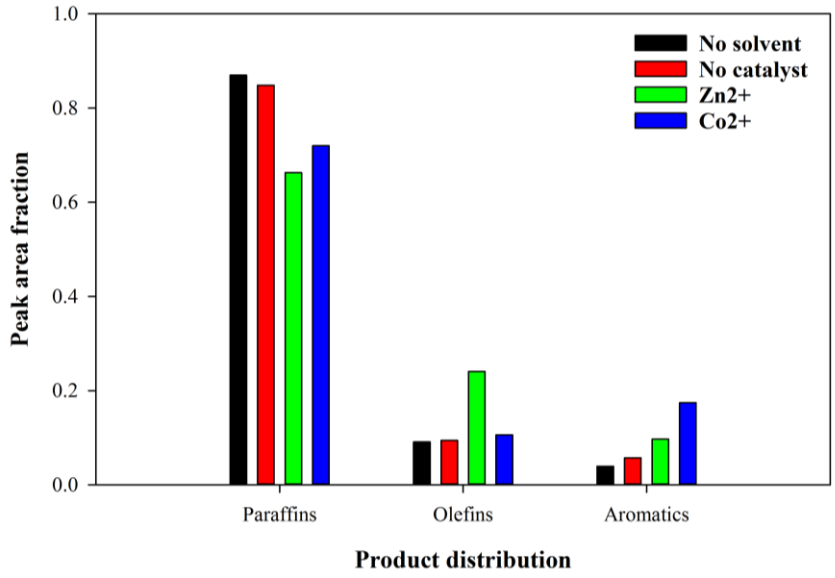

Figure 65 Paraffin, olefin and aromatics ratio of liquid product after reaction in decalin at 400°C for the different catalysts used, compared to no solvent or catalyst.

Effect of reaction temperature on product distribution, in **Figure 60**, **Figure 62** and **Figure 64**, is not noticeable. Decalin does not appear to alter product distribution much, whereas tetralin promoted some degree of cracking. This supports the theory of solvent-assisted hydrogen transfer, where radicals formed from the solvent can cause cleavage of strong bonds, as explained in **2.5.1 Liquefaction mechanism**. The metal ion catalysts again display a cracking

effect similar to that seen in tetralin, reducing the amount of larger fractions while increasing the amount of smaller fractions, particularly at 400 °C.

Paraffin-to-olefin-to-aromatic ratios displayed in **Figure 61**, **Figure 63** and **Figure 65** show an increase in paraffins with increasing temperature for both the experiment without solvent as well as the experiment with decalin. The trend displayed for the liquid product from reaction in decalin is more similar to that seen without any solvent than that seen for tetralin.

The effect of decalin as a liquefaction solvent compared to using no solvent seems to be limited for paraffin-to-olefin ratio. Product from reactions both without any solvent and in decalin appear to be similar. The effect of catalyst is similar to the experiments with tetralin, with zinc and cobalt catalyst reducing the amount of paraffins in the product; however, to a much smaller degree. Zinc shows greater cracking potential than cobalt at 400 °C, with cobalt increasing aromatics content while zinc increases olefinic content.

As a summary, increased liquefaction temperatures promote cracking reactions to a lesser degree in isopropanol solvent and to a greater degree in tetralin solvent. No significant effect by temperature on product distribution could be seen for the reactions in decalin and without solvent. Metal ions as catalyst promoted cracking for all solvents and had a detrimental effect on the paraffin-to-olefin ratio for all solvents tested; however, less of an impact was seen when using decalin as a solvent. Potassium hydroxide in isopropanol solvent displayed promising results, increasing the amount of paraffins in the liquid product while reducing the amount of olefins.

4.5.5 Optimization of liquefaction conditions

By combining the conversion results obtained by TGA with the product distribution results obtained by Py-GC/MS, liquefaction conditions can be optimized. Of particular interest is a comparison between liquefaction and pyrolysis (the reactions without solvent).

Solid conversion when using a liquefaction solvent is almost doubled compared to the conversion obtained without solvent. In tetralin the solid conversion is increased from 11.30 % to 24.89 %, from 28.76 % to 59.50 % and from 49.65 % to 85.55 % at 300 °C, 350 °C and 400 °C, respectively. A smaller, yet significant increase is also observed in decalin. The differences in paraffin-to-olefin ratios observed between tetralin and decalin and no solvent are not significant enough to outweigh the increase in solid conversion. Liquefaction is therefore considered superior to pyrolysis for the analyzed conditions. Comparison with isopropanol is

also similar, with an increase in solid conversion from 11.30 % without solvent to 23.52 % in isopropanol at 300 °C, and no significant difference in paraffin-to-olefin ratio.

While solid conversion for isopropanol is low due to the low reaction temperature, the performance without catalyst is similar to that of tetralin. With the addition of catalyst (Co^{2+} and KOH) at 300 °C, the solid conversion in isopropanol surpasses that of tetralin, being 44.17 % with Co^{2+} and 35.45 % with KOH (up from 24.89 % in tetralin). Cobalt as a catalyst increases cracking, resulting in a liquid product with poorer paraffin-to-olefin ratio; however, KOH improves paraffin-to-olefin ratio compared to the reaction without catalyst. Isopropanol is therefore a viable solvent for low-temperature reactions, particularly with KOH as a catalyst. At 330 °C, the maximum temperature for reaction in isopropanol, adding KOH as a catalyst increased solid conversion to match that of tetralin at 350 °C while having appreciably better paraffin-to-olefin ratio. The use of zinc catalyst in isopropanol at 330 °C improved solid conversion significantly to 76.11 %, matching that of decalin without catalyst at 400 °C. While paraffin-to-olefin ratio is inferior to that achieved with KOH, the high solid conversion at a low temperature suggests that zinc catalyst in isopropanol may be viable.

Comparison between decalin and tetralin shows that tetralin achieves the higher solid conversion, with 85.55 % for tetralin and 76.45 % for decalin, while decalin achieves the best paraffin-to-olefin ratio. Further investigation of product distribution; however, shows that liquid product from reaction in tetralin has a higher concentration of shorter-chained hydrocarbons. This indicates that tetralin is a better hydrogen-donor solvent, and may also be facilitating bond cleavage. While decalin performed better than tetralin for paraffin-to-olefin ratio when catalyst was added, the poor overall performance of impregnated catalyst samples makes it difficult to draw a conclusion for solvent performance in combination with catalyst.

As a summary, tetralin is considered the optimal solvent, due to it achieving the highest solid conversion while maintaining a decent paraffin-to-olefin ratio. Impregnated catalyst performance with tetralin proved detrimental to solid conversion and paraffin-to-olefin ratio. Isopropanol performs similarly to tetralin at low temperatures. Despite being thermochemically limited to a reaction temperature of 330 °C, the addition of soluble catalyst improved solid conversion significantly. Zinc catalyst proved most effective at increasing solid conversion while KOH improved paraffin-to-olefin ratio.

5. Conclusions

This study has performed analyses on the effect of catalysts for conversion of kerogen. Some of the primary results are summarized in this chapter.

Through EGA analysis, it was found that metal chloride catalysts can reduce the temperature at which pyrolysis occurs for kerogen. Zinc proved superior among the catalysts tested, while iron, nickel, cobalt and copper also displayed promising effects.

Catalyst loading of zinc was optimized based on T_{max} shift during EGA, and was found to be 10 wt%. The T_{max} shift at this catalyst loading was 35 °C compared to decarbonated kerogen without added catalyst.

Quantitative analysis of zinc catalyzed pyrolysis was performed by Py-GC/MS and compared to similar analyses of original oil shale and decarbonated kerogen, and a cracking effect was observed. The resulting product was highly olefinic at 65.7 % olefins and liquefaction was chosen as an alternative process to improve paraffin ratio in the product, using isopropanol, tetralin and decalin as hydrogen-donor solvents.

SEM-EDS showed agglomeration of the soluble zinc chloride catalyst after reaction in isopropanol. Impregnated zinc catalyst displayed good dispersion even after reaction in tetralin, indicating a support effect by the mineral matrix of the oil shale.

XRF and TGA of the liquid product proved centrifuge insufficient to separate the solid and liquid phase, as contamination by solid residue was found in significant quantities in the liquid product.

A combination of TGA of the solid residue to analyze solid conversion and Py-GC/MS for quantitative analysis of the liquid product was performed to analyze performance of the liquefaction processes. Tetralin proved most effective, achieving a solid conversion of 85.55 % at 400 °C reaction temperature and 75.0 % paraffins in the liquid product.

Soluble catalysts proved more effective than impregnated catalysts, and the combination of isopropanol and zinc catalyst achieved 76.11 % solid conversion at 330 °C reaction temperature and 54.9 % paraffins in the liquid product. Potassium hydroxide in isopropanol also performed appreciably, achieving 60.76 % solid conversion at 330 °C reaction temperature; however, this catalyst produced a liquid product with the highest obtained paraffin ratio of 79.4 %.

6. Perspectives

For future studies, isopropanol with zinc and potassium hydroxide catalyst could be further investigated and possibly optimized. It is also suggested that further analyses of isopropanol solvent be performed using a reactor capable of withstanding the pressures of reaction.

Attempts should be made to run further testing with oil soluble catalyst precursors in tetralin. A third option could be investigated using dispersed solid-phase catalyst (such as finely crushed pyrite). Analyses could also be performed using iron-, palladium- and molybdenum-based catalysts.

Different conditions should also be tested, investigating increased reaction times, different solvent-to-OM ratios and higher initial pressures.

Addition of an initial hydrogen pressure should also be investigated, due to its potential to improve solid conversion and oil yield[29].

New methods to analyze liquid product composition for the more volatile compounds (C_3-C_7) should also be investigated.

References

1. BP (2016), *BP energy outlook 2035.* Available from: http://www.bp.com/en/global/corporate/energy-economics/energy-outlook-2035.html [Downloaded 23. May 2016]
2. BP (2015), *BP Statistical Review of World Energy June 2015*. Available from: http://www.bp.com/en/global/corporate/energy-economics/statistical-review-of-world-energy.html [Downloaded 23. May 2016]
3. Bartis, J. T., LaTourrette, T., Dixon, L., Peterson, D. J. and Cecchine, G. (2005) *Oil Shale Development in the United States: Prospects and Policy Issues*, RAND Corporation, Santa Monica, 68 pp.
4. Bloomberg (2016), *Energy & Oil* [online]. Available from: http://www.bloomberg.com/energy [Downloaded 23. May 2016]
5. Speight, J. G. (2012), *Shale Oil Production Processes*, Gulf Professional Publishing, Boston, 192 pp.
6. Enefit (2015), *Oil Shale* [online]. Source: Enefit. Available from: https://www.enefit.com/oil-shale [Downloaded 5. November 2015]
7. Institute for Energy Resource (2015), *Oil Shale* [online]. Source: Institute for Energy Resource. Available from: http://instituteforenergyresearch.org/topics/encyclopedia/oil-shale/ [Downloaded 5. November 2015]
8. Enefit (2015), Enefit Outotec Technology [online]. Source: Enefit. Available from: https://www.enefit.com/en/technology [Downloaded 5. November 2015]
9. Brown, S. D., Sirkecioglu, O. and Snape, C. E. (1997), Speciation of the Organic Sulfur Forms in a Recent Sediment and Type I and II-S Kerogens by High-Pressure Temperature-Programmed Reduction, *Energy & Fuels*, **11**, 532-538.
10. Vandenbroucke, M. and Largeau, C. (2007), Kerogen origin, evolution and structure, *Organic Geochemistry*, **38**, 719-833.
11. McCarthy, K., Rojas, K., Niemann, M., Palmowski, D., Peters, K. and Stankiewicz, A. (2011), Basic Petroleum Geochemistry for Source Rock Evaluation, *Oilfield Review*, **23**(2), 32-43.
12. Orendt, A.M., Pimienta, I. S. O., Badu, S. R., Solum, M. S., Pugmire, R. J., Facelli, J. C. (2013), Three-Dimensional Structure of the Siskin Green River Oil Shale Kerogen

Model: A Comparison between Calculated and Observed Properties, *Energy & Fuels*, **27**(2), 702-710.

13. Yeboah, I. (2015), Characterization and Thermal/Catalytic Upgrading of Kerogen in a Green River Oil Shale, NTNU, Norway.
14. Marceau, E., Carrier, X. and Che, M. (2009), Impregnation and Drying. de Jong, K.P. (Ed.), *Synhesis of Solid Catalysts*, Wiley-VCH Verlag GmbH & Co. KGaA, Weinheim, p. 59-82.
15. Ertl, G., Knözinger, H. and Weitkamp, J. (eds) (1999), Deposition of Active Component. *Preparation of Solid Catalysts*, Wiley-VCH Verlag GmbH, Weinheim, p. 315-371.
16. Frontier Laboratories (2015), *Evolved Gas Analysis* [online]. Source: Frontier Laboratories. Available from: http://www.frontier-lab.com/english/evolved-gas-analysis/ [Downloaded 10. November 2015]
17. Basu, P. (2013), *Biomass gasification, pyrolysis and torrefaction: practical design and theory*, 2nd ed., Academic Press, Amsterdam, 530 pp.
18. Padua, G. W. and Wang, Q. (2012), *Nanotechnology Research Methods for Foods and Bioproducts*, 1st ed., John Wiley & Sons, Inc., p. 103-126.
19. Purdue University (2016), *Scanning Electron Microscope* [online]. Source: Purdue Universities. Available from: https://www.purdue.edu/ehps/rem/rs/sem.htm [Downloaded 20. May 2016]
20. Crompton, T.R. (2013), *Thermal Methods of Polymer Analysis*, Smithers Rapra Technology, p. 37-51.
21. Coats, A. W. and Redfern, J. P. (1963), Thermogravimetric Analysis, *Analyst*, **88**, 906-924.
22. O'neill, M. J. and Watson, E. S. (1966), *U.S. Patent No. 3263484.* Washington, DC: U.S. Patent and Trademark Office.
23. Rigaku (2016), *X-ray fluorescence* [online]. Source: Rigaku. Available from: http://www.rigaku.com/en/techniques/xrf [Downloaded 21. May 2016]
24. Beckhoff, B., Kanngießer, B., Langhoff, N., Wedell, R. and Wolff, H. (2006), *Handbook of Practical X-Ray Fluorescence Analysis*, Springer-Verlag Berlin Heidelberg, Germany, 863 pp.
25. Kaneko, T., Derbyshire, F., Eiichiro, M., Gray, D., Tamura, M. and Li, K. (2012), Coal Liquefaction. In *Ullmann's Encyclopedia of Industrial Chemistry* (p. 1-83). Wiley-VCH Verlag GmbH & Co. KGaA, Weinheim.

26. Johannes, I., Tiikma, L., Luik, H., Tamvelius, H. and Krasulina, J. (2012), Catalytic Thermal Liquefaction of Oil Shale in Tetralin, *ISRN Chemical Engineering*, 11 pp.
27. Pajak, J. and Socha, L. (2002), Effects of pressure on the rate of hydrogen transfer from tetralin to different rank coals, *Fuel Processing Technology*, **77-78**, 131-136.
28. Robinson, W. E. and Cummins, J. J. (1960), Composition of low-temperature thermal extracts from Colorado oil shale, *Journal of Chemical and Engineering Data*, **5**(1), 74-80.
29. Vasilakos, N. P. and Austgen, D. M. (1985), Hydrogen-Donor Solvents in Biomass Liquefaction, *Ind. Eng. Chem. Process Des. Dev.,* **24**, 304-311.
30. Ross, D. S., and Blessing, J. E. (1979), Alcohols as H-donor media in coal conversion. 1. Base-promoted H-donation to coal by isopropyl alcohol, *Fuel*, **58**, 433-437.
31. Ross, D. S., and Blessing, J. E. (1979), Alcohols as H-donor media in coal conversion. 2. Base-promoted H-donation to coal by methyl alcohol, *Fuel*, **58**, 438-442.
32. Carlson, C. S., Langer, A. W., Stewart, J. and Hill, R. M. (1958), Thermal Hydrogenation: Transfer of Hydrogen from Tetralin to Cracked Residua, *Industrial and Engineering Chemistry*, **50**, 1067-1070.

Appendix

A) Calculation of catalyst loading

$$Mass\ of\ metal\ ion = \frac{\%\ loading}{(1 - \%\ loading)} * mass\ of\ kerogen$$

$$Mass\ of\ precursor = \frac{molecular\ weight\ of\ precursor}{molecular\ weight\ of\ metal\ ion} * mass\ of\ metal\ ion$$

B) TGA-DSC and MS for solid conversion comparison of solvents

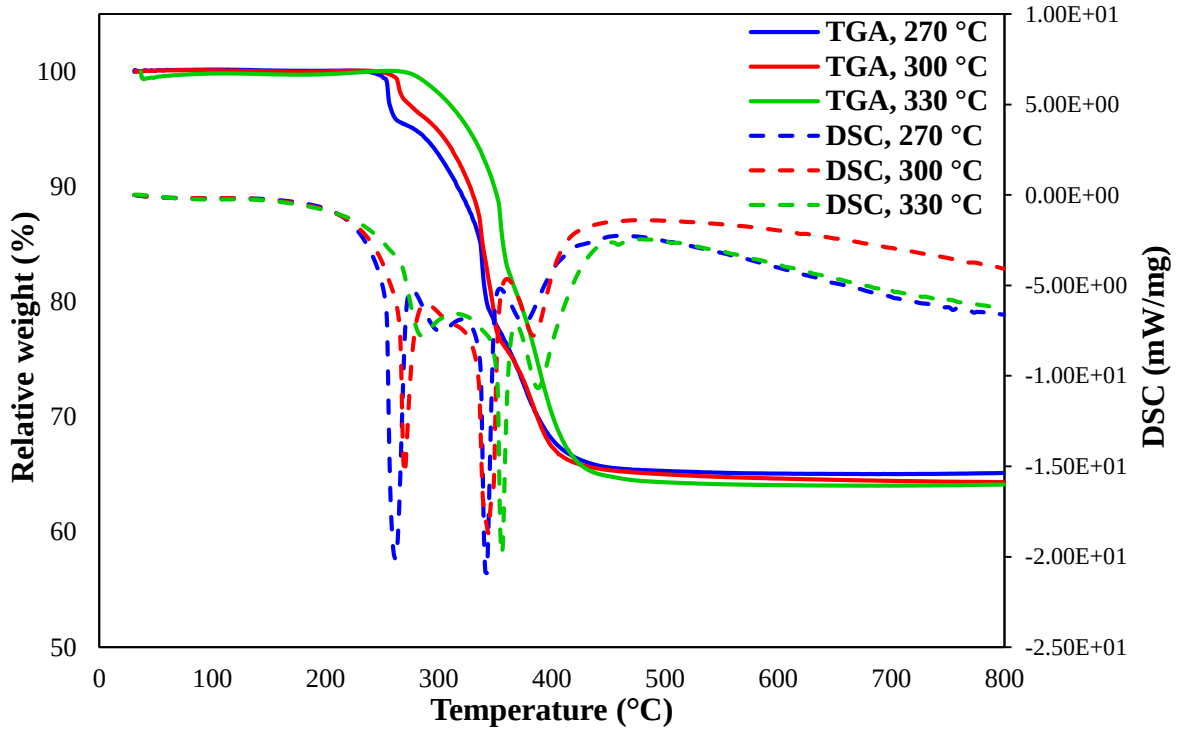

Figure B. 1 TGA-DSC for solid residue after reaction in isopropanol.

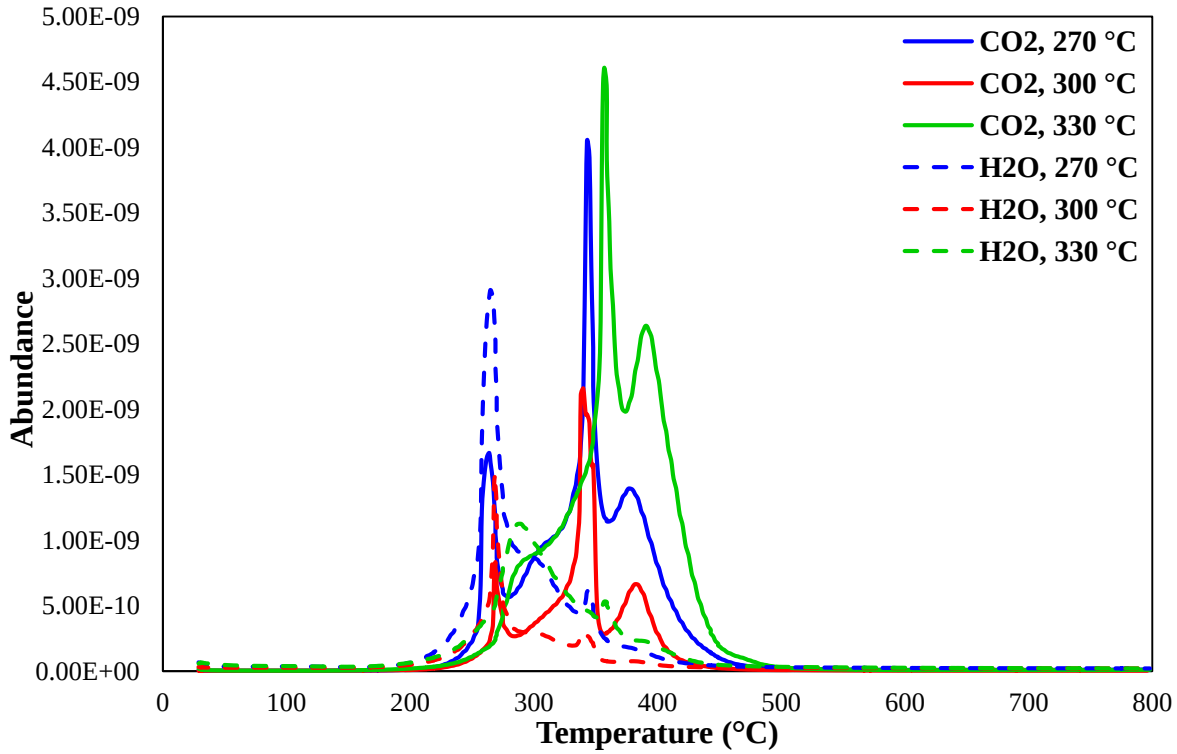

Figure B. 2 MS for solid residue after reaction in isopropanol.

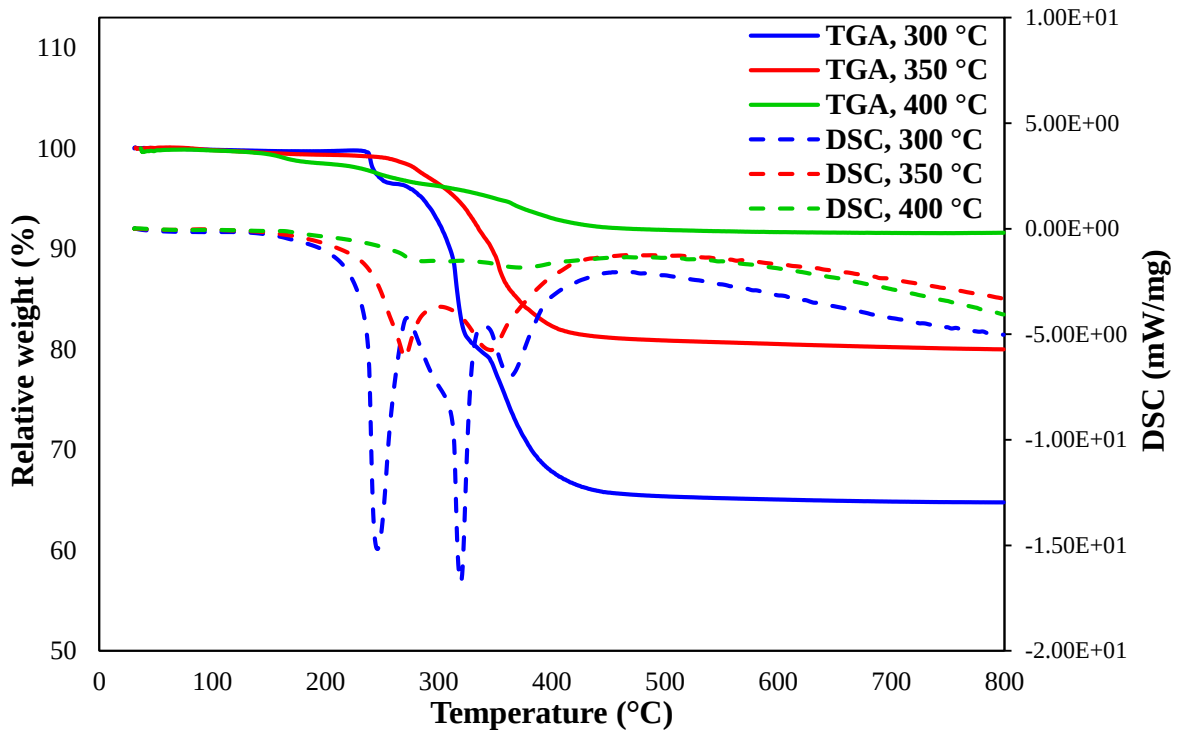

Figure B. 3 TGA-DSC for solid residue after reaction in tetralin.

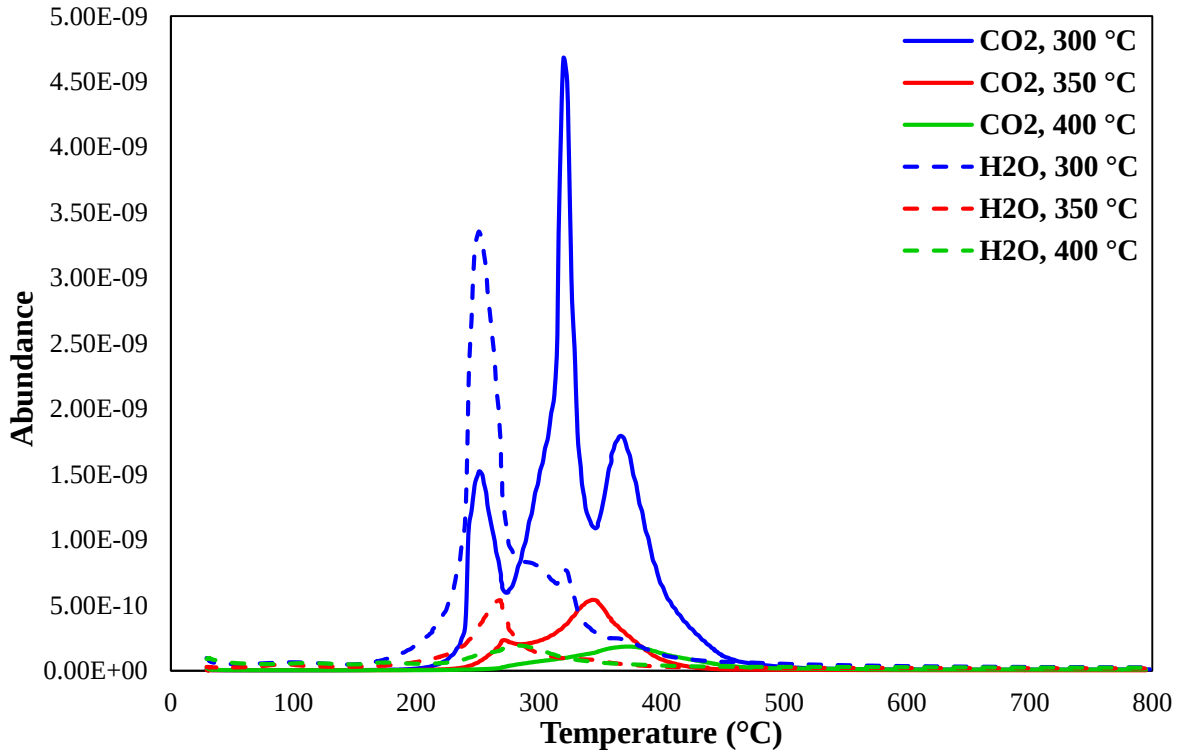

Figure B. 4 MS for solid residue after reaction in tetralin.

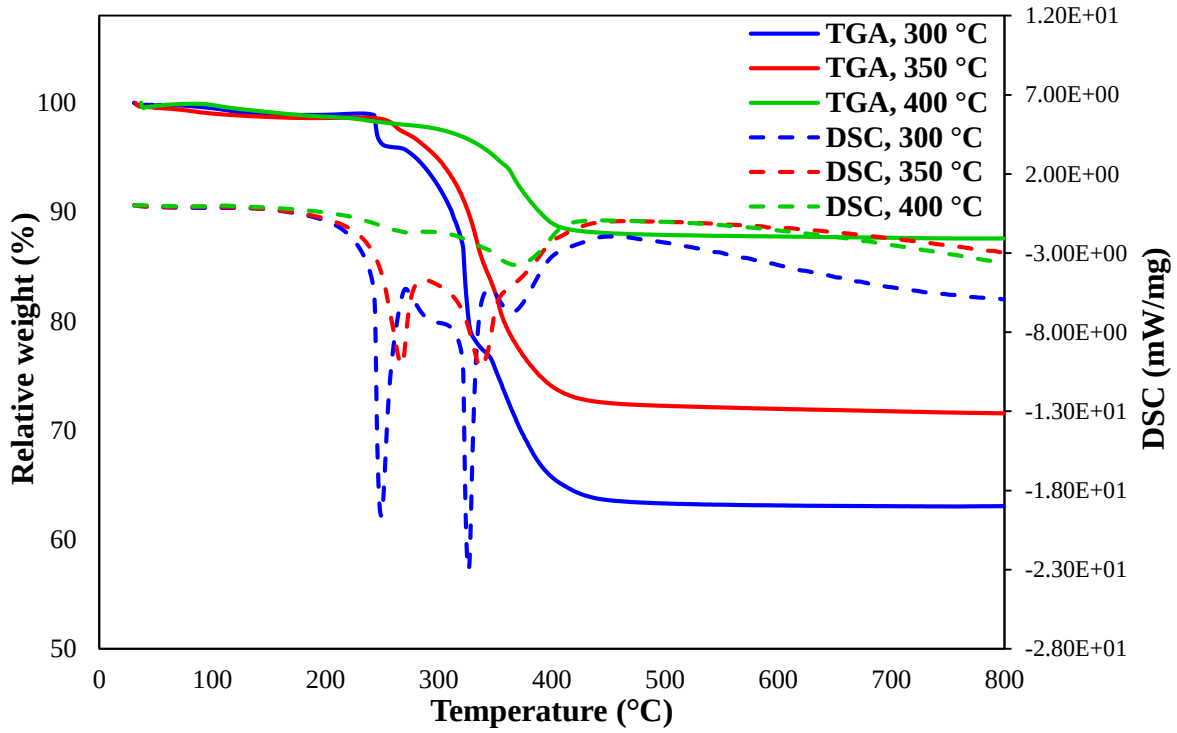

Figure B. 5 TGA-DSC for solid residue after reaction in decalin.

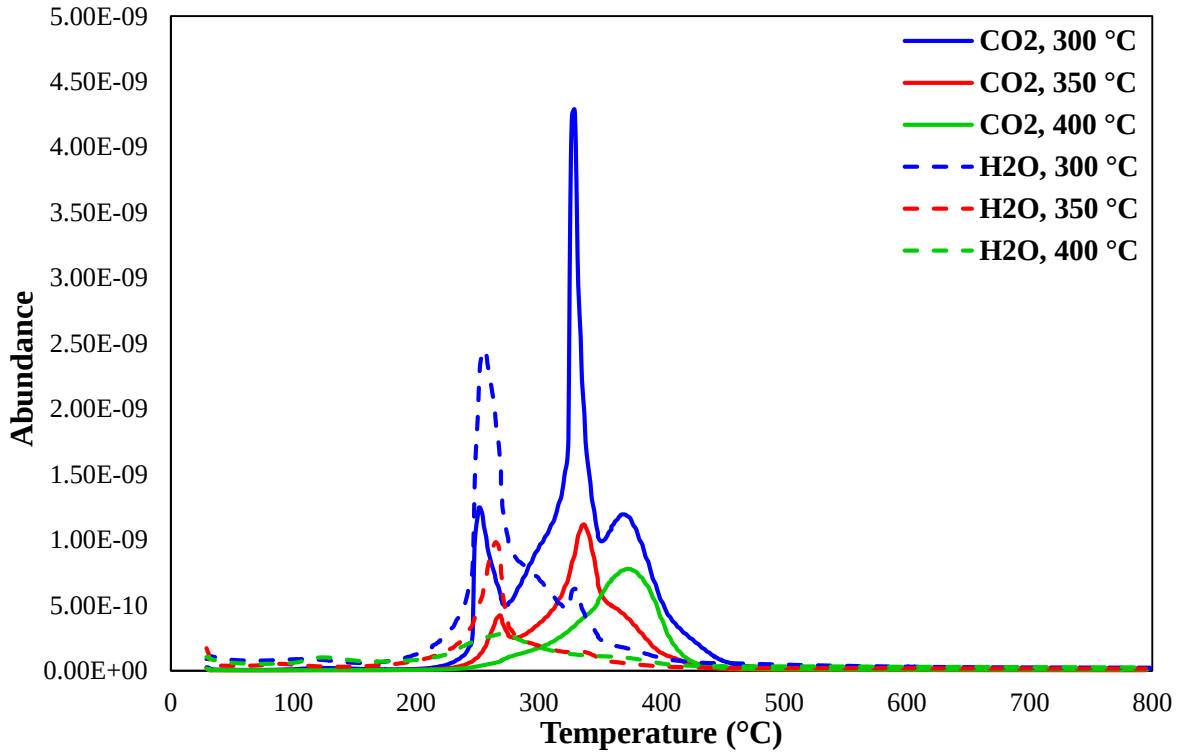

Figure B. 6 MS for solid residue after reaction in decalin.

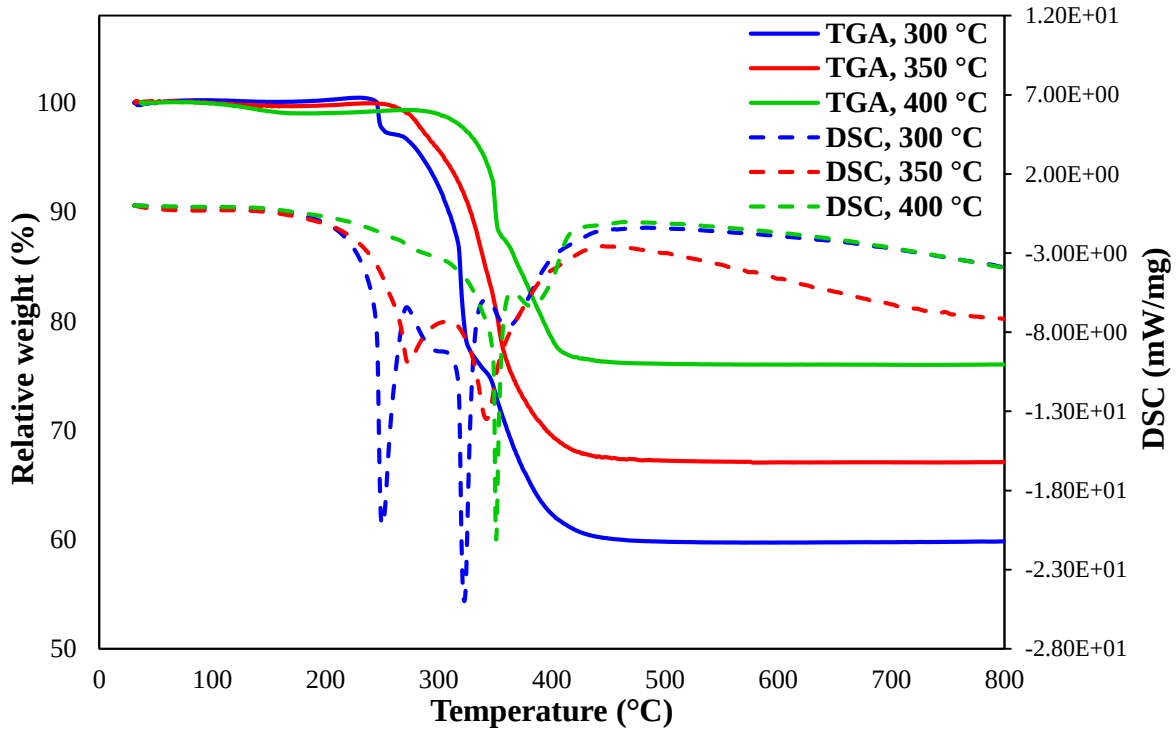

Figure B. 7 TGA-DSC for solid residue after reaction without solvent.

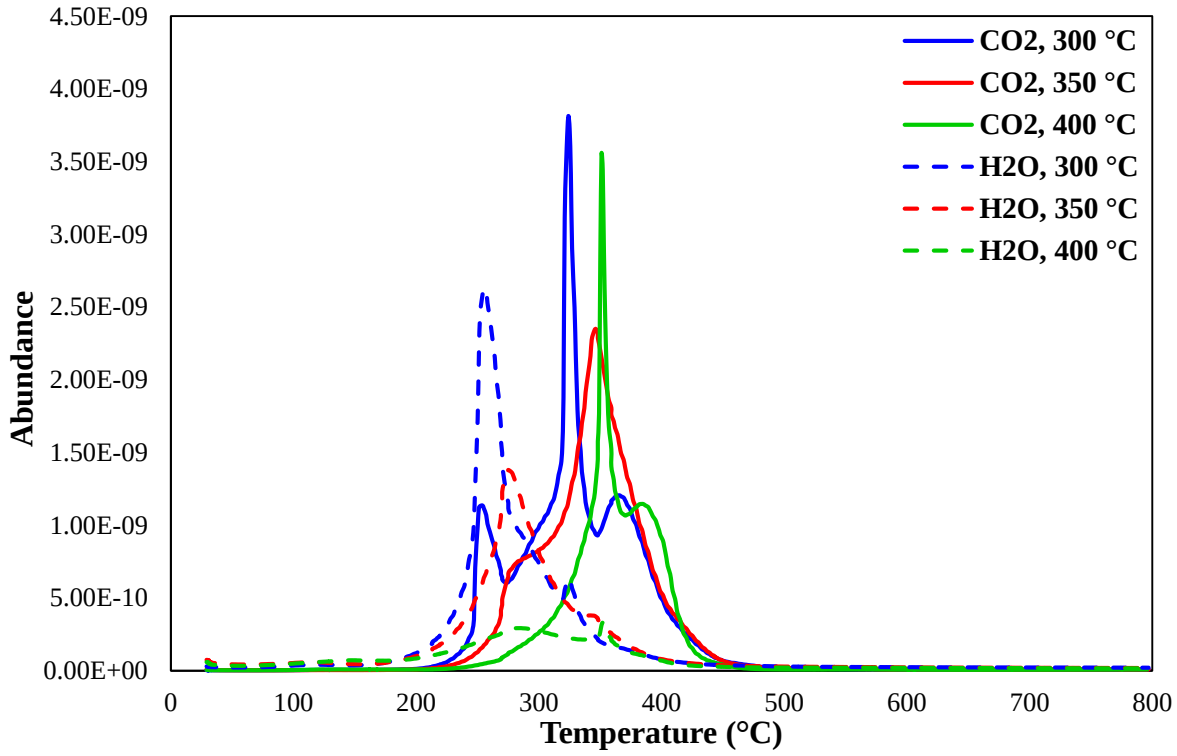

Figure B. 8 MS for solid residue after reaction without solvent.

C) TGA-DSC and MS for solid conversion comparison of catalysts

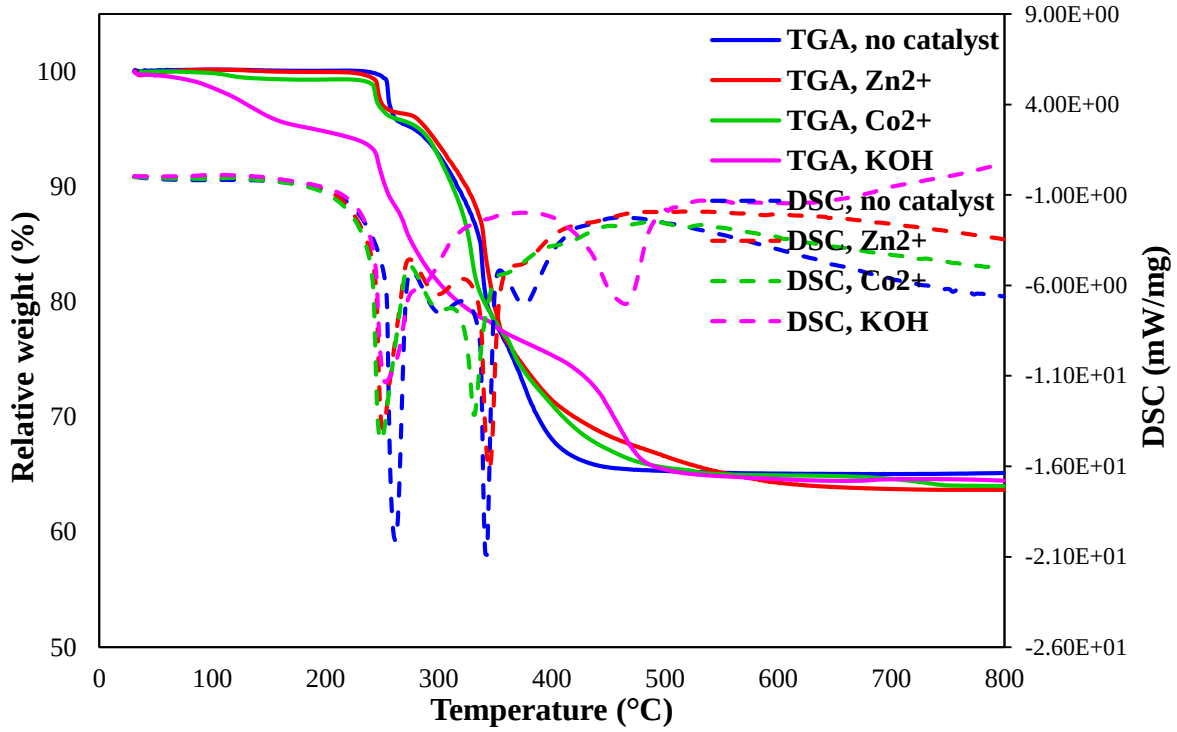

Figure C. 1 TGA-DSC for solid residue after reaction in isopropanol at 270 °C.

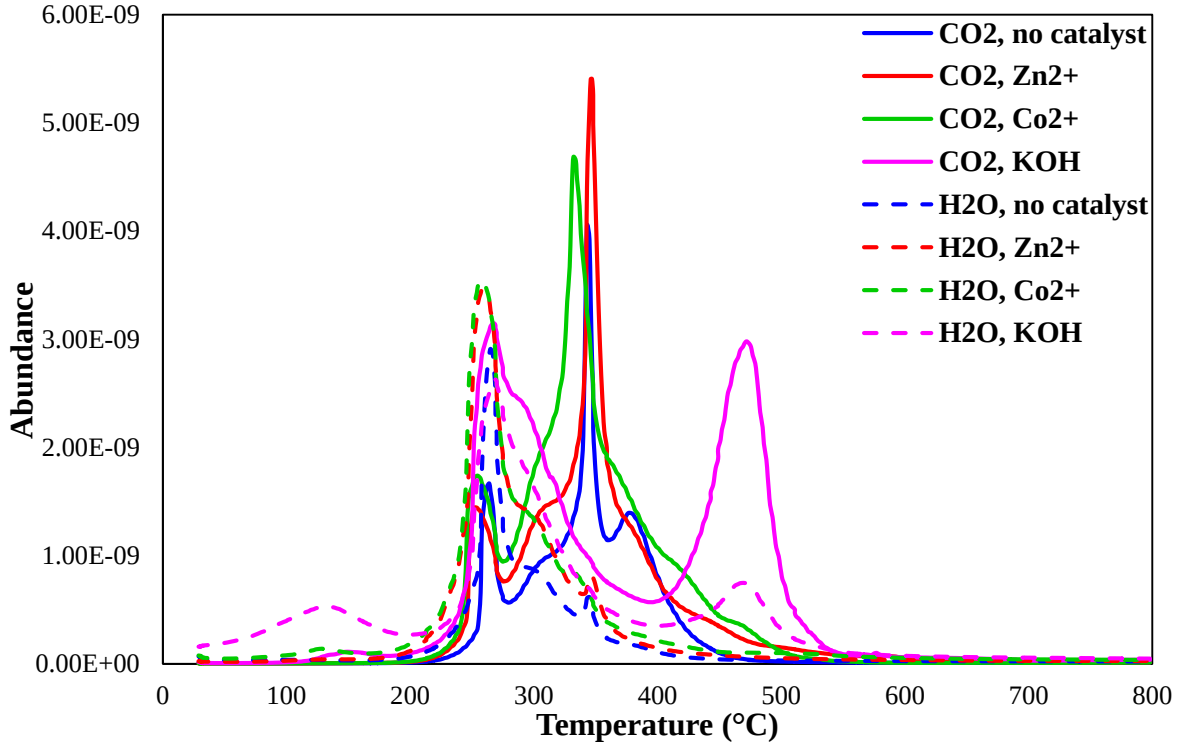

Figure C. 2 MS for solid residue after reaction in isopropanol at 270 °C.

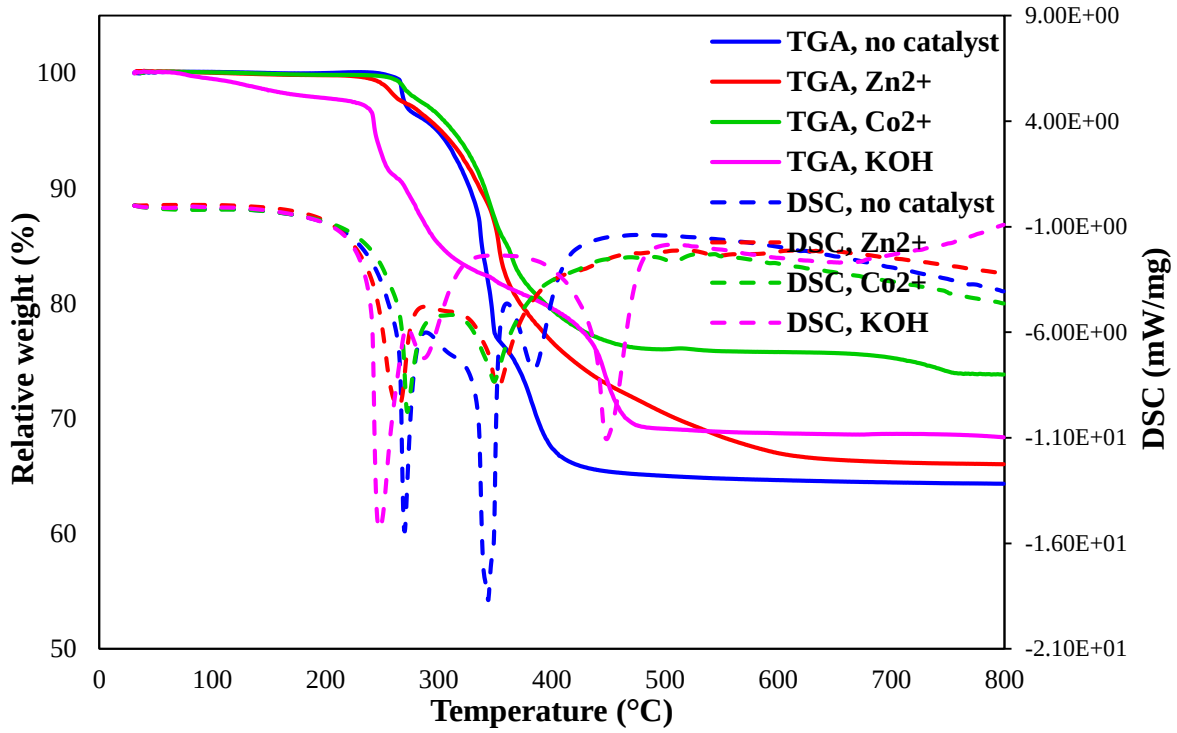

Figure C. 3 TGA-DSC for solid residue after reaction in isopropanol at 300 °C.

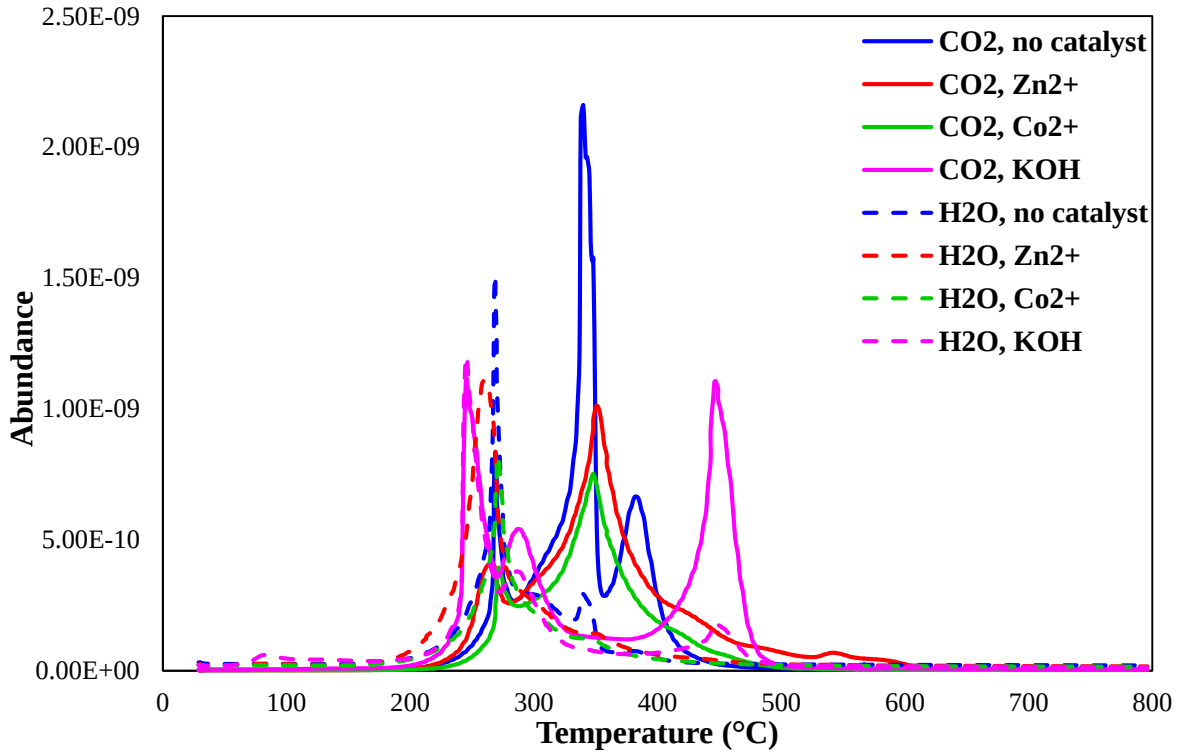

Figure C. 4 MS for solid residue after reaction in isopropanol at 300 °C.

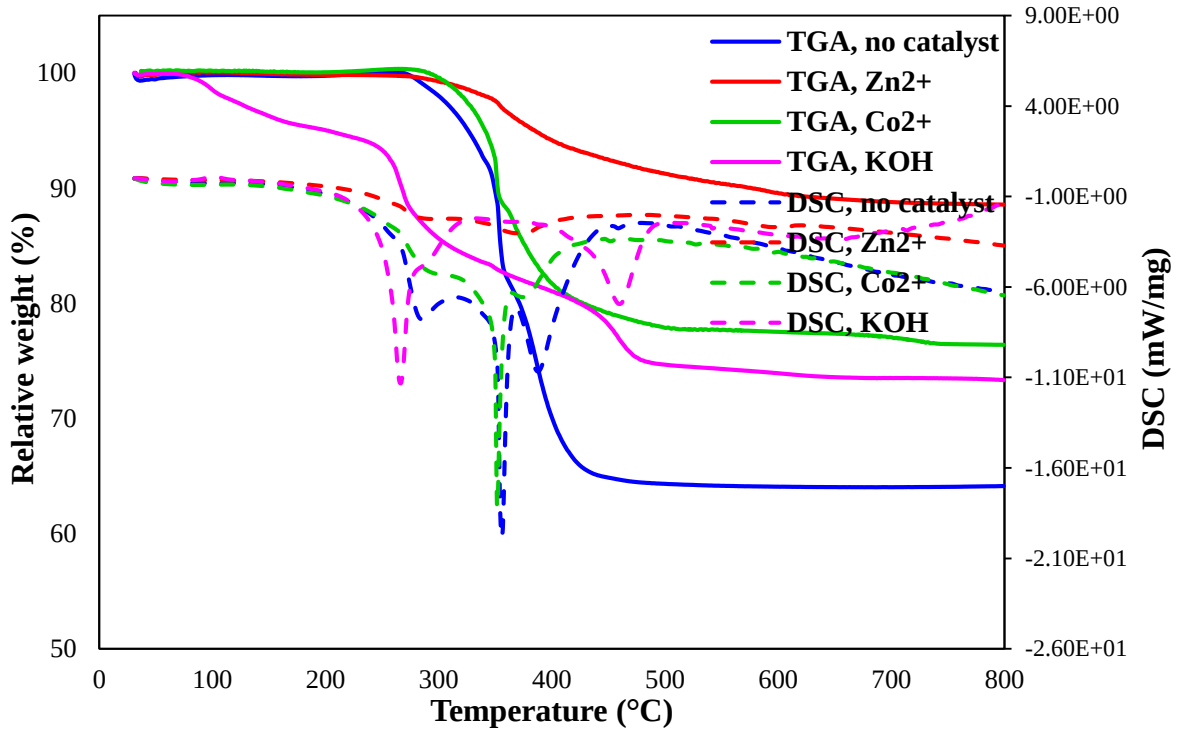

Figure C. 5 TGA-DSC for solid residue after reaction in isopropanol at 330 °C.

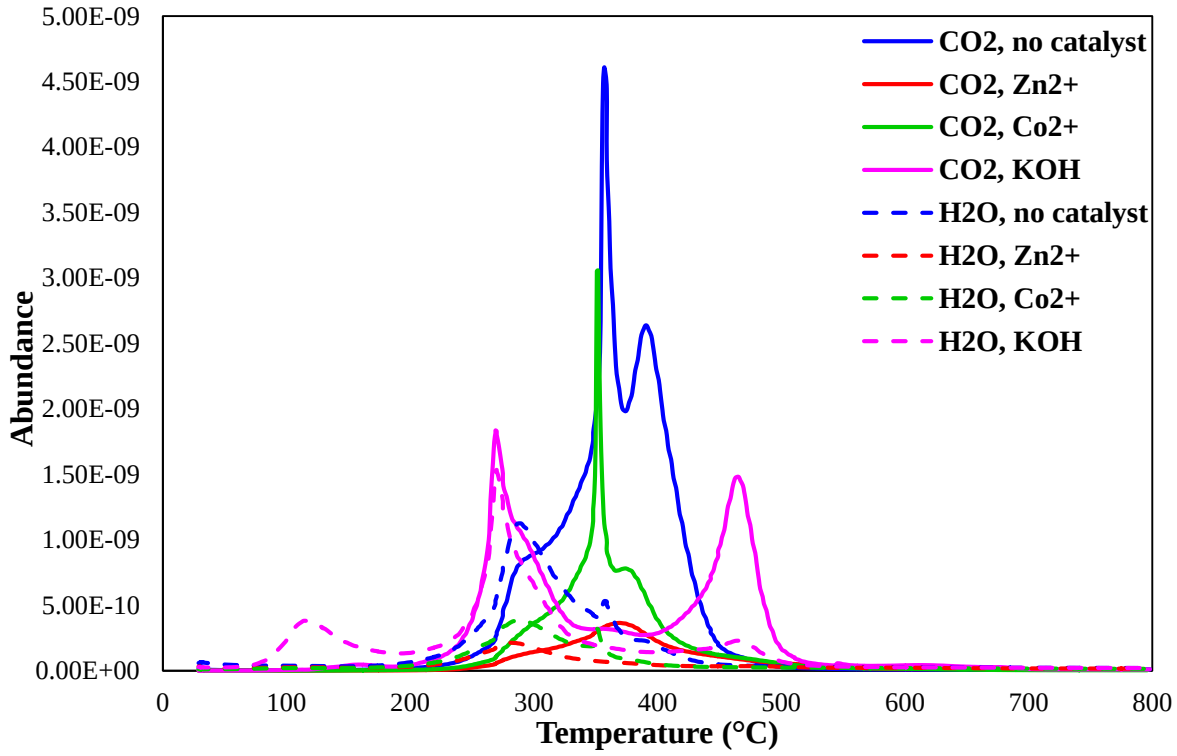

Figure C. 6 MS for solid residue after reaction in isopropanol at 330 °C.

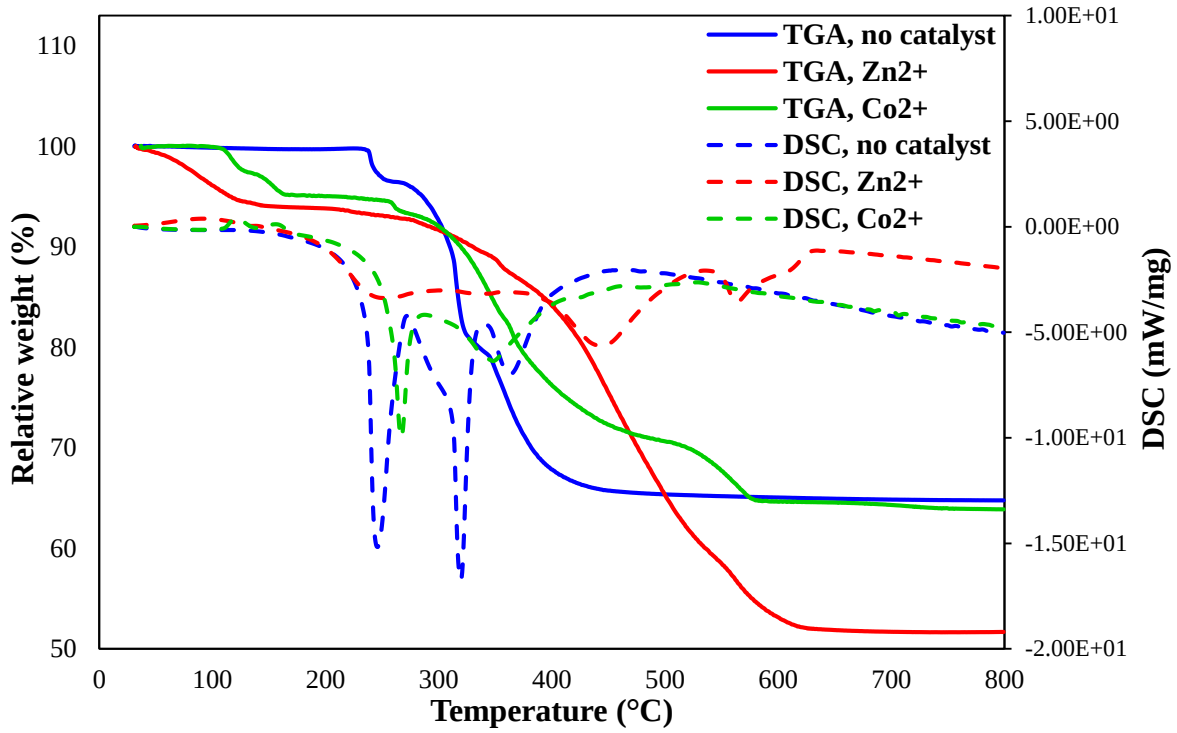

Figure C. 7 TGA-DSC for solid residue after reaction in tetralin at 300 °C.

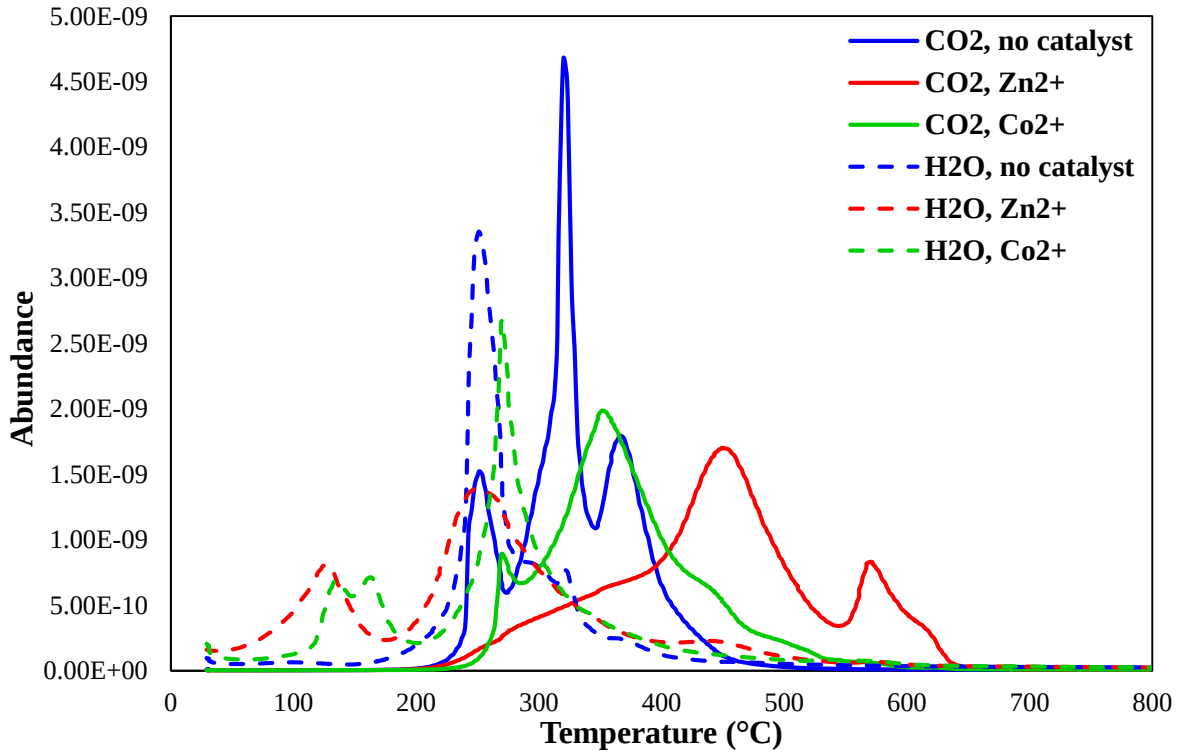

Figure C. 8 MS for solid residue after reaction in tetralin at 300 °C.

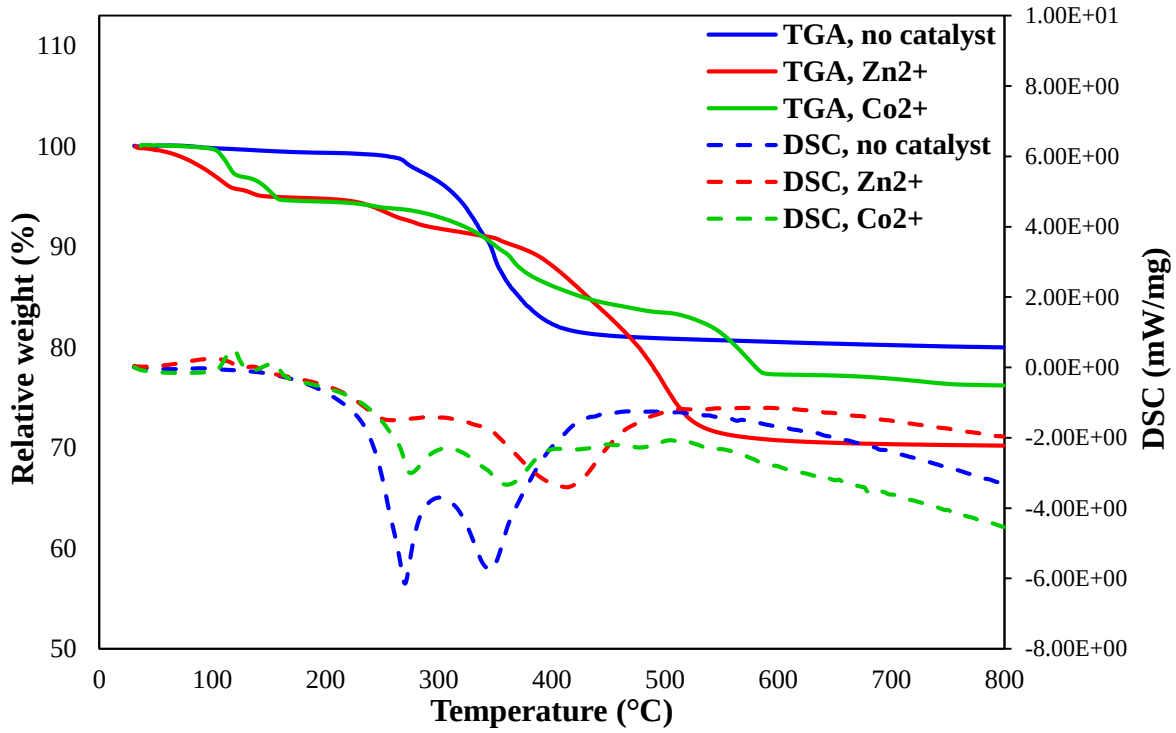

Figure C. 9 TGA-DSC for solid residue after reaction in tetralin at 350 °C.

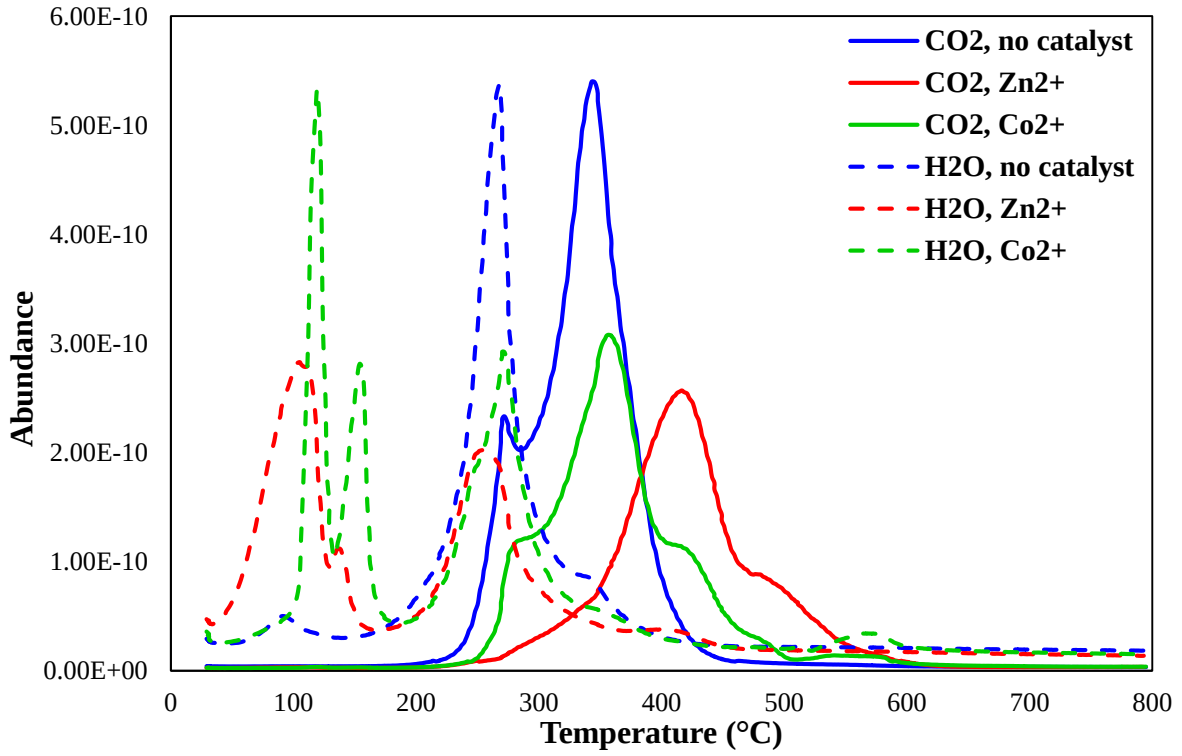

Figure C. 10 MS for solid residue after reaction in tetralin at 350 °C.

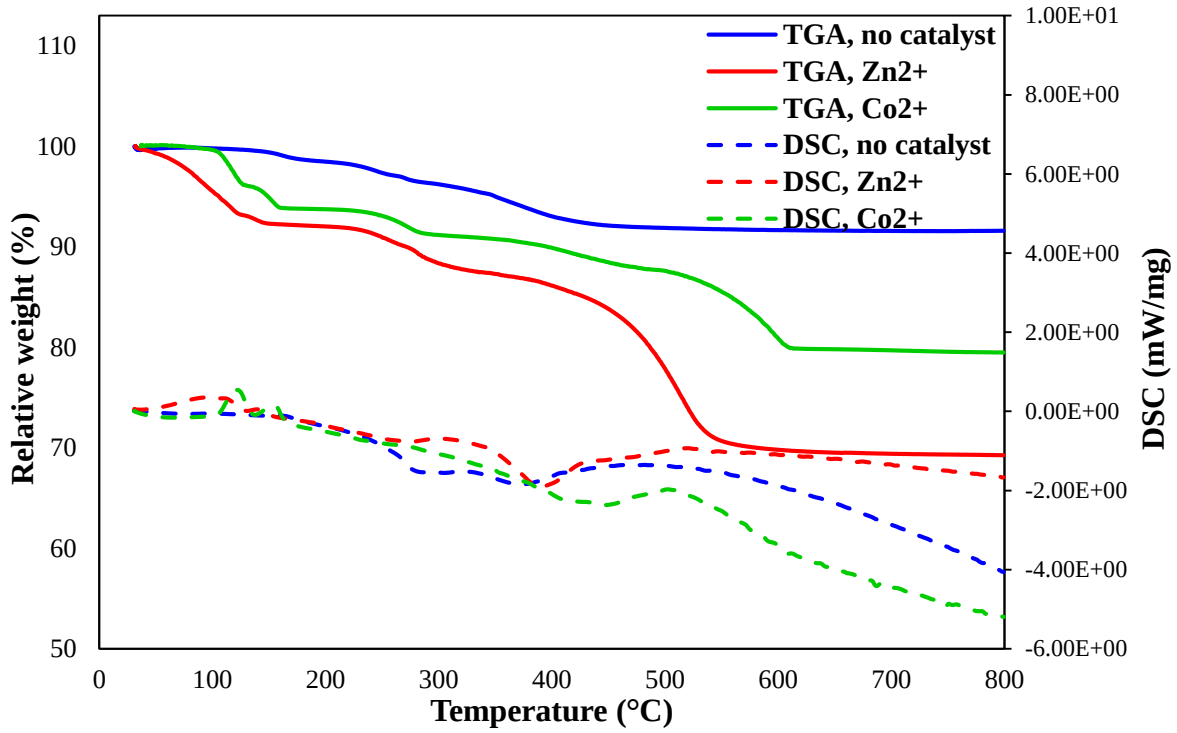

Figure C. 11 TGA-DSC for solid residue after reaction in tetralin at 400 °C.

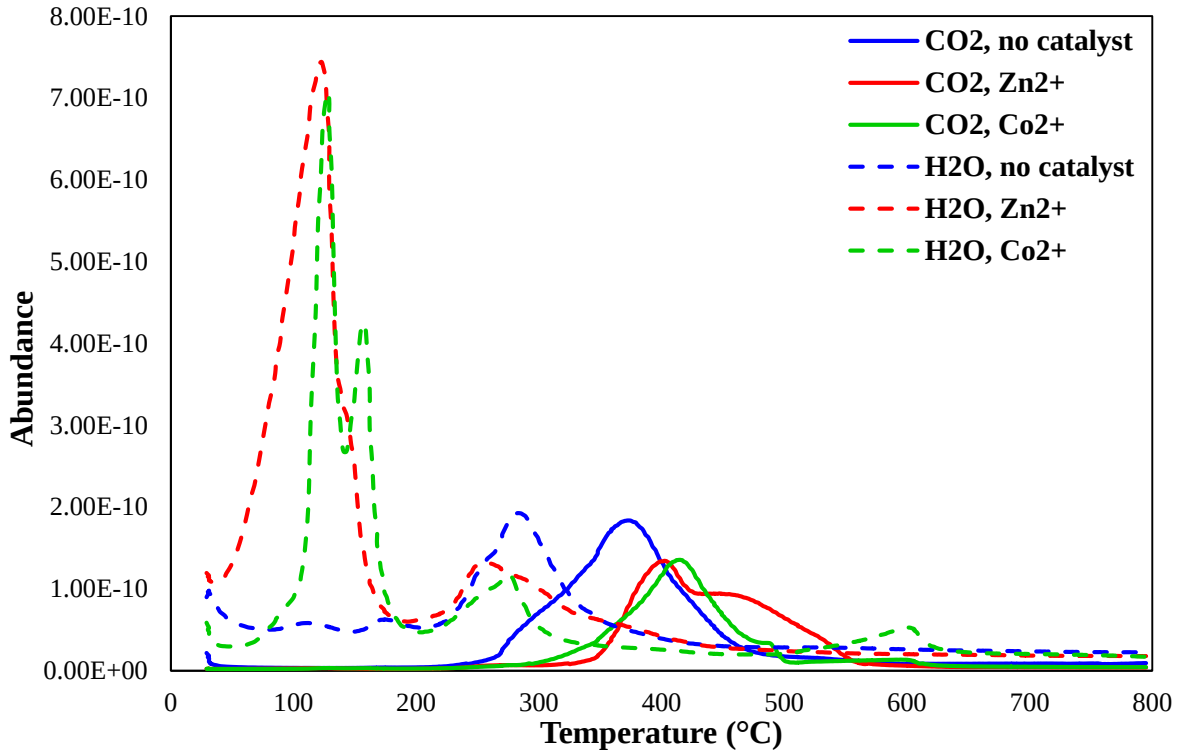

Figure C. 12 MS for solid residue after reaction in tetralin at 400 °C.

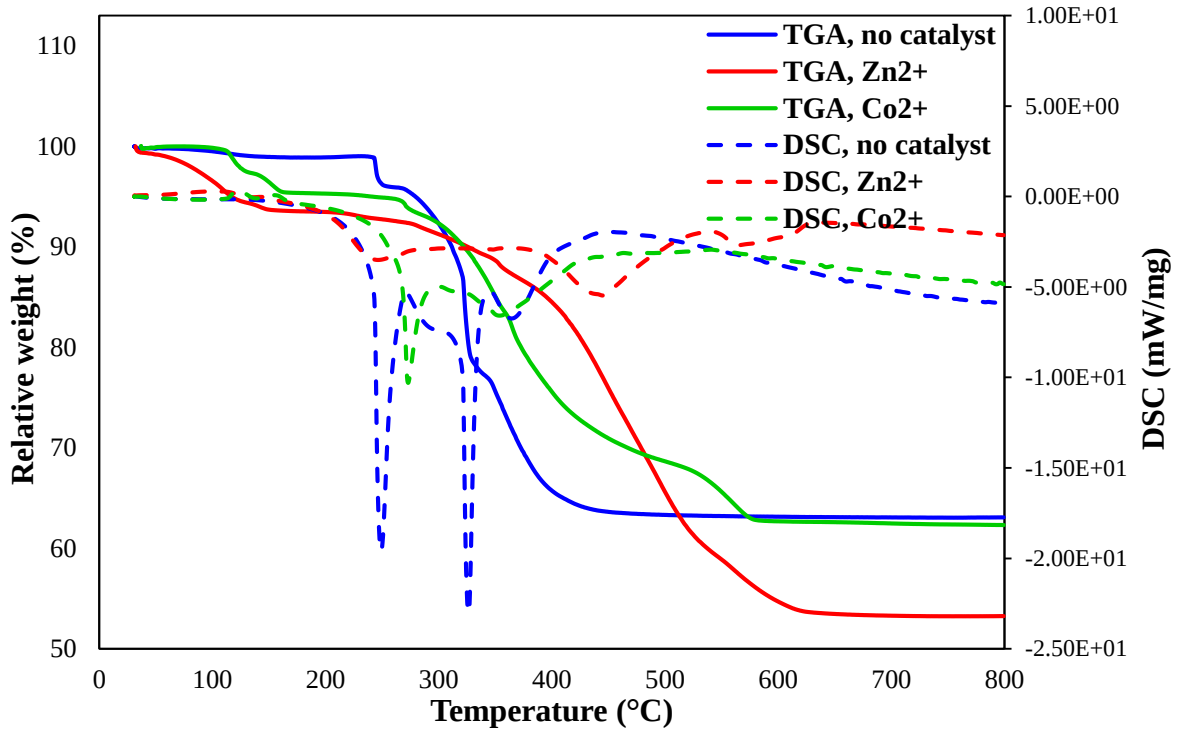

Figure C. 13 TGA-DSC for solid residue after reaction in decalin at 300 °C.

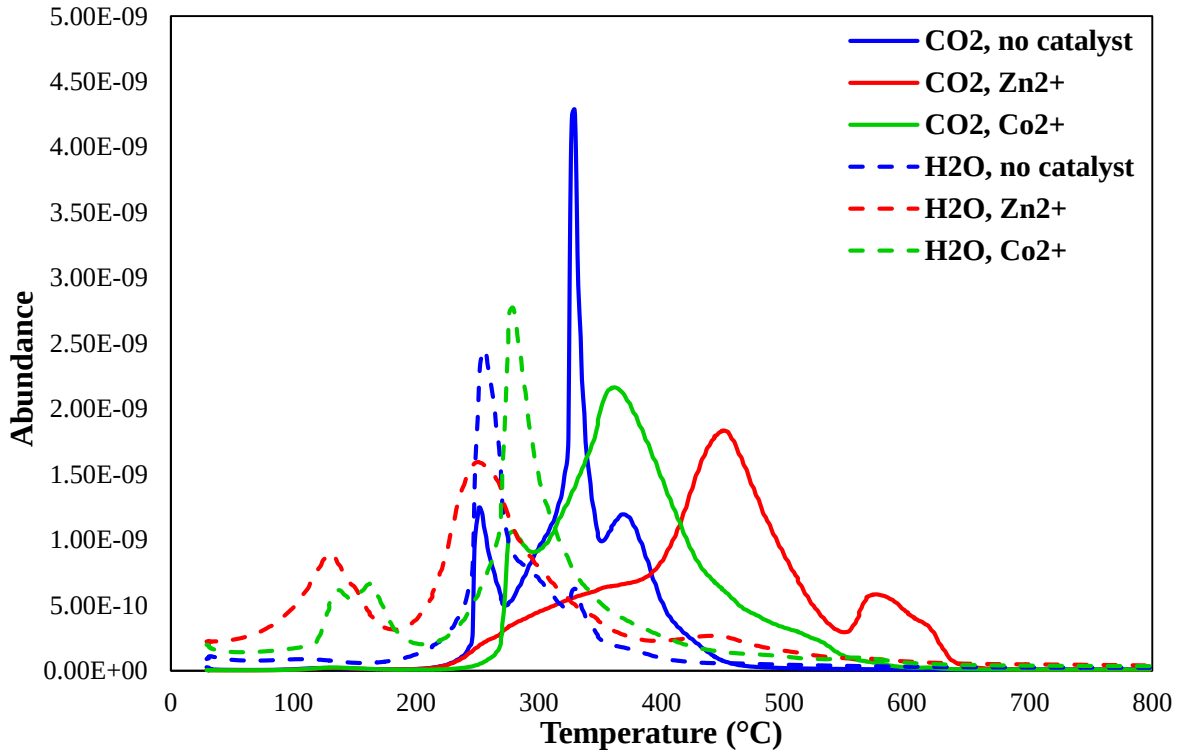

Figure C. 14 MS for solid residue after reaction in decalin at 300 °C.

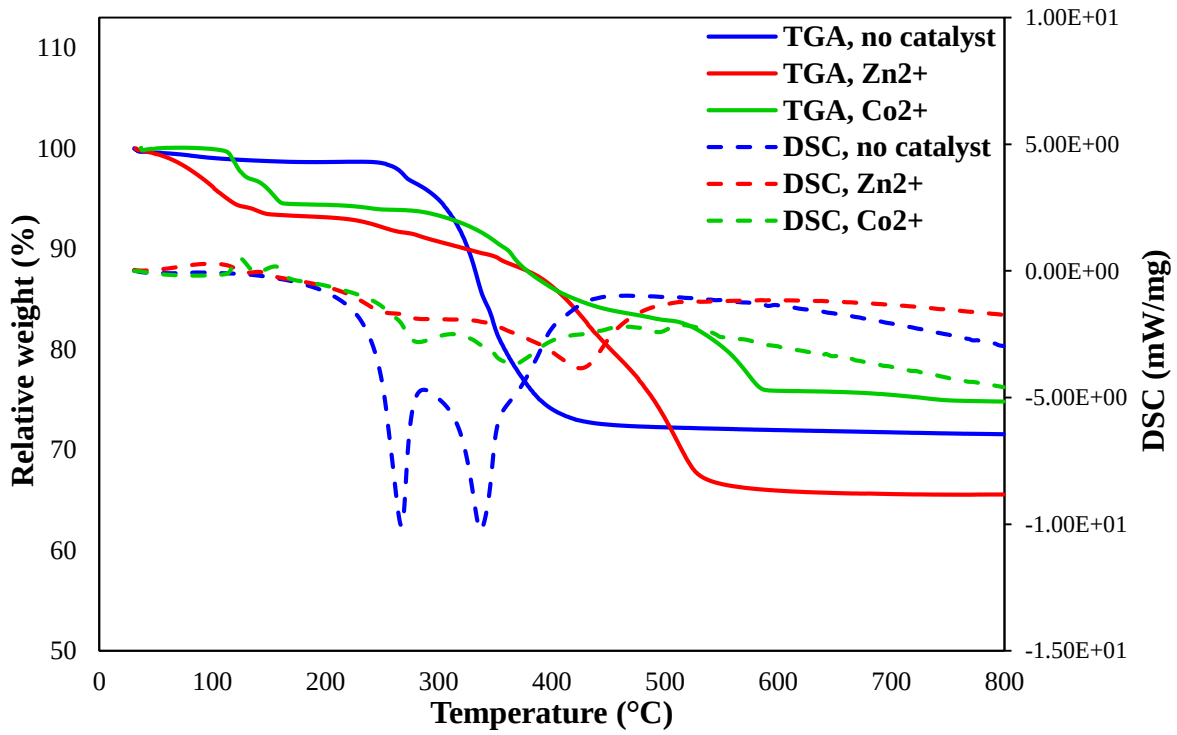

Figure C. 15 TGA-DSC for solid residue after reaction in decalin at 350 °C.

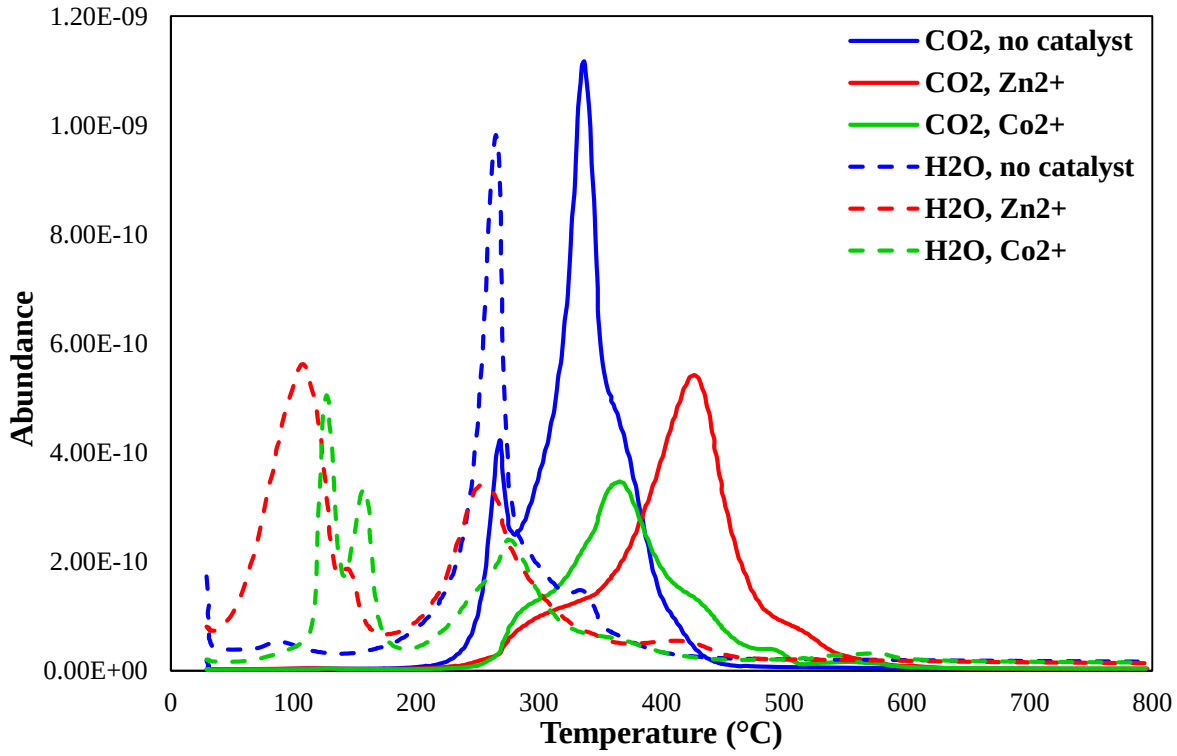

Figure C. 16 MS for solid residue after reaction in decalin at 350 °C.

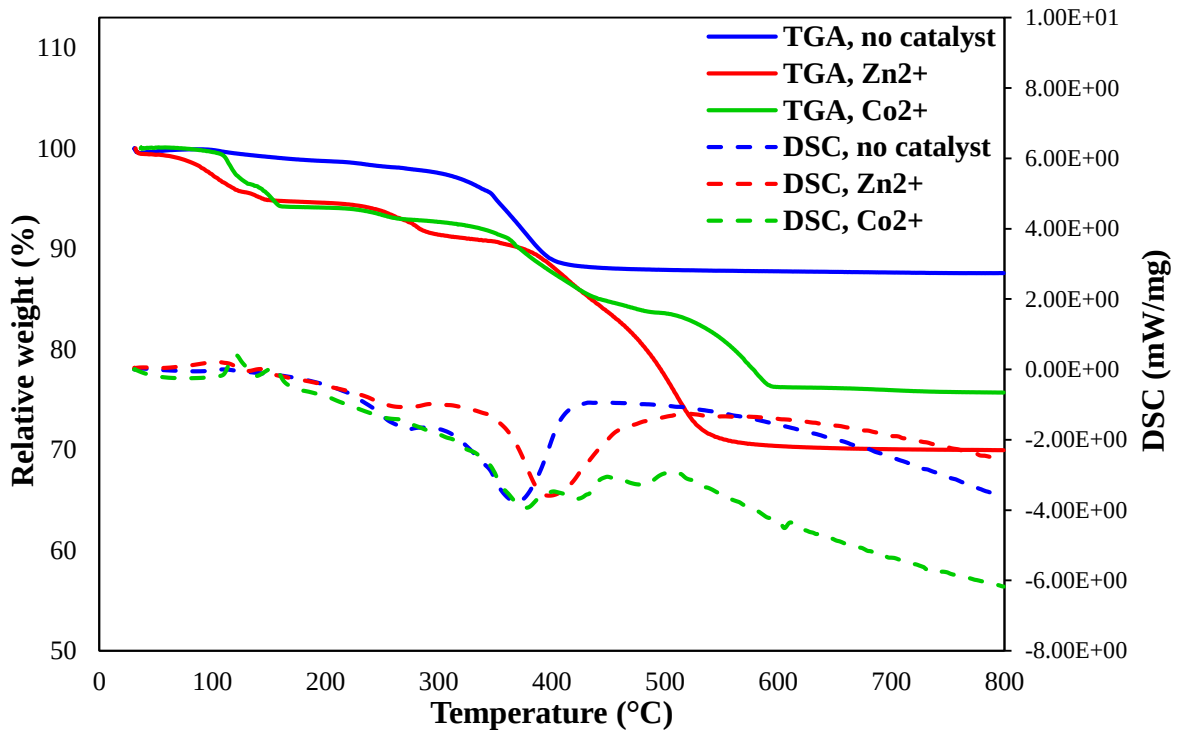

Figure C. 17 TGA-DSC for solid residue after reaction in decalin at 400 °C.

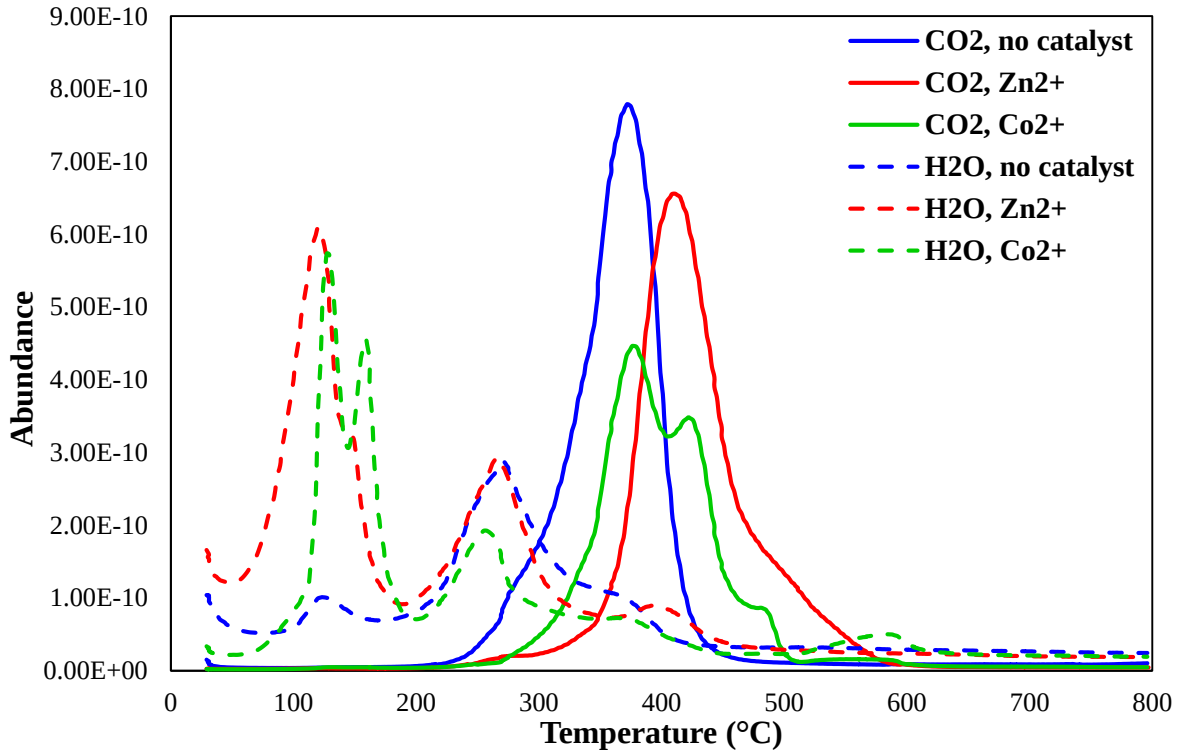

Figure C. 18 MS for solid residue after reaction in decalin at 400 °C.